



**Integrated Cooperative SWIPT THz-NOMA and Secure DLTs
for Efficient 6G Communications**

*A Thesis Submitted to the Department of Electronic and Electrical
Engineering / Brunel University London in Fulfillment of the
Requirement for the Degree of Doctor of Philosophy (Ph.D.)*

By

Haider W. Olewi

Supervised By

Prof. Hamed Al-Raweshidy

July 2024

Dedication

To the almighty Allah, for his comprehensive care, and to the special one, who supported me, with due respect.

Acknowledgment

My heartfelt gratitude and appreciation to Prof. Hamed Al-Raweshidy for his helpful guidance and unlimited support along with my Ph.D. journey.

ABSTRACT

This thesis concentrated on advancing the performance of 6G communications and networks, evaluating efficiency, reliability, resource management, cost-effectiveness, energy consumption, user fairness, and security. Key enabling technologies and intelligent techniques, including terahertz (THz) frequency bands, nonorthogonal multiple access (NOMA), energy harvesting, cooperative networking (decode-and-forward relaying), and artificial intelligence were explored to achieve the targeted objectives. Cooperative simultaneous wireless information and power transfer (SWIPT) in THz-NOMA (and hybrid-NOMA) were integrated to overcome challenges in THz communications. Besides, the proposed deep learning-based 6G channel estimation (CE) model established a robust system against intelligent attacks associated with intelligent systems.

The research highlighted the significant improvements achieved by these technologies, showcasing a 70% enhancement in wireless transmission performance for 6G communications compared to existing systems. The proposed cooperative SWIPT THz-NOMA system demonstrated noteworthy improvements in energy efficiency (EE), spectral efficiency (SE), and other critical metrics. Utilizing the proposed technologies resulted in a remarkable improvement over conventional cooperative networking.

Additionally, the investigation extended to exploring cooperative SWIPT THz multiple-input multiple-output (MIMO) NOMA, introducing path-selection mechanisms and reliable transmission strategies. That outperformed the basic THz-NOMA and provided more enhancement in terms of SE and EE. The entire study emphasized a simpler design, reduced transceiver hardware (which accordingly reduced energy consumption, complexity, and cost), and improved reliability compared to previous work.

Furthermore, this work addressed the imperfections in successive interference cancellation (SIC) in 6G NOMA-based communications, proposing an optimized two-user pairing scheme with SWIPT and cooperative hybrid-NOMA (H-NOMA) in THz communications. It presented a system performance improvement of 75% in SE and EE compared to conventional NOMA and orthogonal multiple access techniques.

Moreover, the work focused on upgrading 5G communication systems to be 6G-compatible and meet the 6G stringent requirements of emerging technologies/applications. It addressed challenges in THz transmission, improving wireless connectivity, resource availability, processing, robustness, and capacity. It evaluated the best pairing strategy in H-NOMA, investigating all the possible SWIPT pairs with the available line-of-sight users to optimize the best pair/performance.

Finally, the last part addressed CE vulnerability to adversarial attacks in 6G systems. The proposed deep autoencoder-based 6G CE model demonstrated robustness against adversarial attacks, providing a promising solution for securing 6G networks. System security and accuracy were validated through simulations, presenting an added value to the field.

List of Publications

Published Papers:

- Journal Papers:

1. H. W. Oleiwi and H. Al-Raweshidy, "Cooperative SWIPT THz-NOMA / 6G Performance Analysis," *Electronics*, Vol. 11, No. 6, pp. 873, March 2022.
2. H. W. Oleiwi, N. Saeed, and H. Al-Raweshidy, "Cooperative SWIPT MIMO-NOMA for Reliable THz 6G Communications", *Network*, Vol. 2, Issue 2, pp. 257–269, 2022.
3. H. W. Oleiwi and H. Al-Raweshidy, "SWIPT-Pairing Mechanism for Channel-Aware Cooperative H-NOMA in 6G Terahertz Communications," *Sensors*, Vol. 22, No. 16, pp. 6200, Aug. 2022.
4. H. W. Oleiwi, D. N. Mhawi, and H. Al-Raweshidy, "MLTs-ADCNs: Machine Learning Techniques for Anomaly Detection in Communication Networks," *IEEE Access*, Vol. 10, pp. 91006–91017, Aug. 2022.
5. H. W. Oleiwi, D. N. Mhawi, and H. Al-Raweshidy, "A Meta-Model to Predict and Detect Malicious Activities in 6G-Structured Wireless Communication Networks," *Electronics*, Vol. 12, No. 3, pp. 643, Jan. 2023.

- Conference Papers:

6. H. W. Oleiwi, N. Saeed, and H. Al-Raweshidy, "Cooperative SWIPT-Hybrid-NOMA pairing scheme considering SIC imperfection for THz communications," In *Proceedings of IEEE 4th Global Power, Energy, and Communication Conference (GPECOM)*, Cappadocia, Turkey, 2022.
7. H. W. Oleiwi and H. Al-Raweshidy, "Cooperative Hybrid-NOMA / Dynamic SWIPT-Pairing Mechanism for 6G THz Communications," In *Proceedings of IEEE 5th Global Power, Energy, and Communication Conference (GPECOM)*, Cappadocia, Turkey, 2023.
8. H. W. Oleiwi, D. N. Mhawi, and H. Al-Raweshidy, "Secure Deep Autoencoder-based 6G Channel Estimation to Detect/Mitigate Adversarial Attacks," In *Proceedings of IEEE 5th Global Power, Energy, and Communication Conference (GPECOM)*, Cappadocia, Turkey, 2023.

Submitted Papers:

- Journal Papers:

9. H. W. Oleiwi, D. N. Mhawi, and H. Al-Raweshidy, "Utilizing Deep Autoencoders for Anomaly Detection in 6G Network Traffic," *IEEE Open Journal of the Computer Society*, Submitted, 2024.

Contents

ABSTRACT.....	III
Chapter 1: Introduction	1
1.1. Introduction.....	1
1.2. General Introduction.....	1
1.2.1. Cooperative SWIPT THz-NOMA/6G Performance Analysis.....	1
1.2.2. Cooperative SWIPT MIMO-NOMA for Reliable THz 6G Communications ..	2
1.2.3. Cooperative SWIPT-Hybrid-NOMA Pairing Scheme Considering SIC imperfection for THz Communications	2
1.2.4. SWIPT-Pairing Mechanism for Channel-Aware Cooperative H-NOMA in 6G Terahertz Communications.....	3
1.2.5. Secure Deep Autoencoder-based 6G Channel Estimation to Detect/Mitigate Adversarial Attacks.....	3
1.3. Limitations and Critical Requirements	3
1.4. Motivation.....	4
1.5. Aim and Objectives.....	5
1.6. Contributions.....	6
1.7. Thesis Organization	8
Chapter 2: Literature Review	9
2.1. General Introduction	9
2.2. Literature Overview	9
2.2.1. Supporting Technologies.....	9
2.2.2. Cooperative SWIPT THz-NOMA/6G Performance Analysis.....	11
2.2.3. Cooperative SWIPT MIMO-NOMA for Reliable THz 6G Communications	15
2.2.4. Cooperative SWIPT-Hybrid-NOMA Pairing Scheme Considering SIC imperfection for THz Communications	17
2.2.5. SWIPT-Pairing Mechanism for Channel-Aware Cooperative H-NOMA in 6G Terahertz Communications.....	21
2.2.6. Secure Deep Autoencoder-based 6G Channel Estimation to Detect/Mitigate Adversarial Attacks.....	24
2.3. Related Work	28
Chapter 3: Cooperative SWIPT THz-NOMA/6G Performance Analysis.....	33
3.1. Introduction.....	33
3.2. System Model	33
3.3. Simulation Scenarios	39
3.4. Simulation Results	39
3.4.1. DF Relay vs. IRS.....	40

3.4.2.	System Numerical Analysis and Simulation	41
3.4.2.1.	Sum-Throughput against Transmit Power	42
3.4.2.2.	Users' OP against Transmit Power	42
3.4.3.	System Simulation	42
3.4.3.1.	Average Achievable Rate against Transmit Power	43
3.4.3.2.	OP against Transmit Power	43
3.4.3.3.	Instantaneous Rates	44
3.4.4.	Scenario1 vs. Scenario2	45
3.4.5.	Average Achievable Rate against Transmit Power	45
3.4.6.	OP against Transmit Power	46
3.4.6.1.	Instantaneous Achievable Rates	47
3.5.	Summary	48
Chapter 4: Cooperative SWIPT MIMO-NOMA for Reliable THz 6G Communications		
.....		49
4.1.	Introduction	49
4.2.	System Model Design	49
4.3.	Implementation	54
4.4.	Simulation Results	54
4.4.1.	System Validity Analysis	55
4.4.1.1.	Sum Throughput Versus Transmit Power	56
4.4.1.2.	Users' OP versus Transmit Power	56
4.4.2.	System Simulation	56
4.4.2.1.	Achievable Users' Rates versus Transmit Power	56
4.4.2.2.	OP versus Transmit Power	57
4.4.2.3.	Achievable Sum Rates versus Transmit Power	58
4.5.	Summary	59
Chapter 5: A Cooperative SWIPT-Hybrid-NOMA Pairing Scheme considering SIC		
imperfection for THz Communications		60
5.1.	Introduction	60
5.2.	System Model	60
5.3.	Implementation	64
5.3.1	NOMA Users' Capacities	64
5.3.2	H-NOMA Vs. Other multiple-access schemes	64
5.4.	Simulation Results	65
5.4.1	NOMA Users' Capacities	66

.5.4.2	H-NOMA Vs. Other multiple-access schemes	66
5.5.	Summary.....	68
Chapter 6: SWIPT-Pairing Mechanism for Channel-Aware Cooperative H-NOMA in		
6G Terahertz Communications		
6.1.	Introduction.....	69
6.2.	Methodology	69
6.2.1.	The Best Hybrid-NOMA Strategy:	70
6.2.2.	Near-Far pairing (N-F)	70
6.2.3.	Near-Near, Far-Far pairing (N-N, F-F)	71
6.2.4.	The Best SWIPT-Pairing Mechanism.....	71
6.2.5.	Optimal SWIPT-Pairing	76
6.3.	Implementation Environment.....	76
6.4.	Results and Discussion.....	77
6.4.1.	H-NOMA, NOMA, and OMA Performance Comparison	78
6.4.2.	Proposal Simulation.....	78
6.4.2.1.	Average Rate Versus Transmission Power	79
6.4.2.2.	OP Versus Transmission Power	80
6.4.2.3.	Instantaneous-Rate Versus Channel-Realization.....	80
6.5.	Optimal SWIPT-Pairing Mechanism.....	81
6.5.1.	Average Rate Versus Transmission Power.....	82
6.5.2.	OP Versus Transmission Power	82
6.5.3.	Instantaneous Achievable Rate Versus Channel Realization	83
6.6.	System Numerical Analysis and Simulation.....	83
6.6.1.	Sum Throughput Versus Transmission Power	84
6.6.2.	User OP Versus Transmission Power	84
6.7.	Summary.....	85
Chapter 7: A Secure Deep Autoencoder-based 6G Channel Estimation to		
Detect/Mitigate Adversarial Attacks		
7.1.	Introduction.....	86
7.2.	Methodology	86
7.2.1.	Dataset Descriptions and Scenario.....	87
7.2.2.	Programming Deep Autoencoder-Based Channel Estimation.....	88
7.3.	Implementation Environment.....	92
7.4.	Results, Evaluation, and Discussion	92
7.4.1.	Performance Results and Evaluation	92

7.4.2. MSE for Training and Testing Datasets.....	94
7.5. Summary.....	96
Chapter 8: Conclusion, Challenges, and Recommendations for Future Work	97
8.1. Introduction.....	97
8.2. Conclusions.....	97
8.3. Challenges.....	98
8.4. Recommendations for Future Work	99
REFERENCES.....	101
<i>Figure 2.1 SWIPT with cooperative NOMA.</i>	15
<i>Figure 2.2 Relay-based transmission strategy</i>	17
<i>Figure 2.3 SIC procedure in NOMA Rx.</i>	20
<i>Figure 2.4 SWIPT with DF-relayed NOMA.</i>	24
<i>Figure 3.1 Model of cooperative SWIPT THz-NOMA.</i>	34
<i>Figure 3.3 Throughput vs. transmit power.</i>	42
<i>Figure 3.4 OP vs. transmit power.</i>	42
<i>Figure 3.5 Achievable rate vs. transmit power.</i>	43
<i>Figure 3.6 OP vs. transmit power.</i>	44
<i>Figure 3.7 Instantaneous rate vs. channel realization.</i>	45
<i>Figure 3.8 Achievable rate vs. transmit power.</i>	46
<i>Figure 3.9 OP vs. transmit power.</i>	47
<i>Figure 3.10 OP vs. transmit power.</i>	48
<i>Figure 4.1 Cooperative SWIPT MIMO-NOMA in THz model.</i>	50
<i>Figure 4.2 Throughput vs. transmit power.</i>	56
<i>Figure 4.3 OP vs. Transmit Power.</i>	56
<i>Figure 4.4 Rates vs. transmit power.</i>	57
<i>Figure 4.5 OP vs. transmit power.</i>	58
<i>Figure 4.6 Sum rates vs. transmit power.</i>	58
<i>Figure 5.1 SWIPT-paired H-NOMA system.</i>	61
<i>Figure 5.2 Hybrid-NOMA strategies.</i>	61
<i>Figure 5.3 NOMA Users' Capacities Vs SNR.</i>	66
<i>Figure 5.4 System SE Vs. SNR of H-NOMA strategies, NOMA, and OMA.</i>	67
<i>Figure 5.5 Main system model.</i>	69
<i>Figure 6.1 Hybrid-NOMA pairing strategy.</i>	70
<i>Figure 6.2 Cooperative SWIPT hybrid THz NOMA model.</i>	73
<i>Figure 6.3 H-NOMA techniques vs. NOMA/OMA.</i>	78
<i>Figure 6.4 Average rate versus transmission power.</i>	79
<i>Figure 6.5 OP versus transmission power.</i>	80
<i>Figure 6.6 Instantaneous rate versus channel realization.</i>	81
<i>Figure 6.7 Average rate versus transmission power.</i>	82
<i>Figure 6.8 OP versus transmission power.</i>	83
<i>Figure 6.9 Instantaneous rate versus channel realization.</i>	83
<i>Figure 6.10 Sum throughput versus transmission power</i>	84
<i>Figure 6.11 User OP versus transmission power.</i>	84
<i>Figure 6.12 The General Structure of DAE-Based CE.</i>	86
<i>Figure 7.2 The DAE-Based CE.</i>	89
<i>Figure 7.3 Demonstrates the training and testing dataset's MSE with epochs 1000.</i>	94

Figure 7.4 Malicious distance with real and predicted MSE for each attack. 95

Table 3.1 Simulation parameters. 40
 Table 4.2 Simulation parameters. 55
 Table 6.1 Simulation parameters. 77
 Table 6.2 H-NOMA strategies. 77
 Table 7.1 Original dataset description. 87
 Table 7.2 CE parameters. 87
 Table 7.3 DAE parameters. 89
 Table 7.4 Experimental test results of DAE-based CE for AA. 93
 Table 7.5 Demonstrates the details about all the AA. 95

List of Symbols

Symbols	Description
σ^2	Variance
A	Number of antennas
$a(f)$	Absorption coefficient
c	Speed of light
d	Source-to-destination distance
dsn	BS-to-NU transmission distance
f	Frequency
$F-F$	Far-Far
FU	Far user
G	Antenna-gain
H	A vector of Rayleigh channels for k -number of users
$h_2, h_3, \text{ and } h_4$	Rayleigh fading channels of user2, user3, and user4
h_{nf}	NU-FU Rayleigh fading channel
H_{sn}	BS-to-NU Rayleigh fading channel
K	Constant
$N-N$	Near-Near
NU	Near user
P	Transmit power
R	Relaying user
w_{eh}	Thermal noise
W_n	AWGN
a_f	Power coefficient of the far user
a_n	Power coefficient of the near user
δ	A very small value of 10^{-6}
ζ	Electronic circuits' energy harvesting efficiency
η	THz source-to-destination losses
ψ	The energy harvesting power fraction
x_f	Signal of the far user
x_n	Signal of the near user

List of Abbreviations

Abbreviate	Description
<i>AA</i>	adversarial attacks
<i>AI</i>	artificial intelligence
<i>AWGN</i>	additive white Gaussian noise
<i>CE</i>	channel estimation
<i>DAE</i>	deep autoencoder
<i>DF</i>	decode-and-forward
<i>EE</i>	energy efficiency
<i>EH</i>	energy harvesting
<i>FU</i>	far user
<i>H-NOMA</i>	hybrid-NOMA
<i>IoE</i>	Internet of everything
<i>IRS</i>	intelligent reflecting surfaces
<i>LOS</i>	line-of-sight
<i>MIMO</i>	multiple-input multiple-output
<i>NLOS</i>	non-line-of-sight
<i>NOMA</i>	nonorthogonal multiple access
<i>NU</i>	near user
<i>OMA</i>	orthogonal multiple access
<i>OP</i>	outage probability
<i>PDF</i>	probability density function
<i>SE</i>	spectral efficiency
<i>SIC</i>	successive interference cancellation
<i>SWIPT</i>	simultaneous wireless information and power transfer
<i>TDMA</i>	Time Division Multiple Access
<i>THz</i>	Terahertz
<i>UDHNs</i>	ultra-dense heterogeneous networks

Chapter 1: Introduction

1.1. Introduction

This chapter presents the general introductions of all the topics and techniques used in this thesis. Further, it addresses the thesis motivation, aims and objectives, contributions, and thesis organization.

1.2. General Introduction

The introduction encompasses several key themes related to non-orthogonal multiple access (NOMA)-based cooperative simultaneous wireless information and power transfer (SWIPT) in Terahertz (THz) communications, and the security of 6G networks against Adversarial Attacks (AA). Cooperative networks were studied with several use cases and scenarios, where the main benefits were fully demonstrated, addressing the disadvantages of using that technique with wireless communication systems. Similarly, for other technologies of this work, that is, energy harvesting (EH), NOMA, and THz communications. Each technology is considered either separately or by integrating some of them to achieve a particular impact on the wireless communication field. The disadvantages of using any of the mentioned technologies were discussed thoroughly, showing the weak points, limitations, and the shortage of performance throughout the research attempts. They are briefly overviewed as follows:

1.2.1. Cooperative SWIPT THz-NOMA/6G Performance Analysis

The first contribution of the thesis explores cooperative SWIPT in THz communications, specifically employing THz-NOMA. The proposed system aims to address challenges inherent to THz communications by enhancing energy efficiency (EE) and spectral efficiency (SE) through

THz and NOMA technologies. By utilizing THz frequencies, the system targets improvements in connectivity, resource management, SE, reliability, scalability, simplicity, and user fairness. Results indicate an improvement in EE and SE compared to recent cooperative networks, demonstrating the effectiveness of utilizing decode-and-forward (DF) relays over intelligent reflecting surfaces (IRS) for particular scenarios.

1.2.2. Cooperative SWIPT MIMO-NOMA for Reliable THz 6G Communications

This section focuses on Cooperative SWIPT in THz Multiple-Input Multiple-Output (MIMO) NOMA for improved wireless connectivity, resource management, scalability, and user fairness. The system optimizes current wireless communication systems by employing MIMO-NOMA technology and THz frequencies. The proposed system exhibits substantial improvements in EE, SE, reliability, and outage probability (OP), outperforming conventional cooperative networks multiple times. The use of a simplified design and DF relaying further reduces transceiver hardware, enhancing transmission rates and reliability.

1.2.3. Cooperative SWIPT-Hybrid-NOMA Pairing Scheme Considering SIC imperfection for THz Communications

This part introduces a pairing scheme that considers the imperfections in NOMA successive interference cancelation (SIC) for THz communication networks. It focuses on enhancing overall performance, including wireless connectivity, resource management, scalability, and user fairness. The proposed scheme outperforms conventional NOMA and OMA (i.e., Time Division Multiple Access (TDMA)), offering improvements in SE and EE. The system's simplicity contributes to reduced hardware, complexity, and cost, without the need for resource-demanding techniques.

1.2.4. SWIPT-Pairing Mechanism for Channel-Aware Cooperative H-NOMA in 6G Terahertz Communications

This part suggests integrating cooperative SWIPT and hybrid-NOMA (H-NOMA) in THz frequencies for compatibility with emergent technologies and applications. The proposed SWIPT-pairing mechanism demonstrates significant improvements in SE and EE, enhancing various system specifications. The optimized H-NOMA pairing scheme for cell users results in a reduction of transceiver hardware and computational complexity, improving reliability and transmission rates without relying on complex technologies.

1.2.5. Secure Deep Autoencoder-based 6G Channel Estimation to Detect/Mitigate Adversarial Attacks

This last contribution in this thesis focuses on the critical role of channel estimation (CE) security in 6G wireless communications and the vulnerability to AA. The proposed deep autoencoder (DAE)-based CE model aims to detect and prevent such attacks, showcasing its accuracy and security through simulations. The model offers a promising solution for secure CE, demonstrating robustness against AA and providing a valuable contribution to enhancing the security of 6G networks.

In summary, the introduction emphasizes the application of cooperative SWIPT in NOMA-based THz communications across various scenarios, addressing challenges, optimizing system performance, and enhancing security in the context of 6G wireless communication networks.

1.3. Limitations and Critical Requirements

The research investigates the multifaceted challenges faced by 5G systems in accommodating emerging applications, emphasizing the essential need for ubiquitous connectivity in the new era's context, e.g., the internet of everything (IoE). The study explores the critical requirement for adequate bandwidth to support candidate technologies, highlighting the

shortage, sensitivity, and limitation of THz transmission. Additionally, it delves into the demanding task of CE in THz communications, particularly under mobility scenarios. Furthermore, the thesis examines the intricate design considerations associated with ultra-massive MIMO-based transceiver antenna arrays. It addresses the scarcity of cell capacity to efficiently connect the growing number of IoE-associated devices and explores innovative cellular network architectures and densification strategies. The research also scrutinizes the challenges related to energy and hardware dissipation, as well as the computational and procedural complexities inherent in 5G systems.

The investigation extends to encompass security concerns, with a specific focus on the unique challenges presented by the multiple hops of ultra-densified networks' communications. By comprehensively analyzing the issues of intelligent attacks (i.e., AA) associated with intelligent systems, i.e., machine learning-based systems, the research aims to contribute valuable insights that can inform the development of robust and adaptive solutions to enhance the capabilities of 6G systems, confronting the evolving technological landscapes.

1.4. Motivation

The imperative needs for efficient 6G and future communication systems urge the necessity for an exceptional leap into a new paradigm to cope with the stringent requirements of emergent technologies and thereby fulfill the demand of the new realm users/gadgets. To provide decent services, 6G and green communications require advanced key enablers, e.g., energy-aware ubiquitous communications, flexible infrastructure, security robustness, and spectrally sufficient reliable THz transmission. The proposed work demonstrates the significance of accommodating, integrating, and utilizing the foreseen candidate technologies to make use of their advantages aggregately on the one hand and avoid their inevitable

shortages/limitations, on the other hand, to improve their functionalities and advance the performance of wireless communications. Besides, the research spots light on the envisaged deficiency of the nominated technologies to deploy apart, e.g., THz shortage/susceptibility to blockage, NOMA complexity/insufficiency, the burdens of cooperative networking, resources (hardware, power, and cost) dissipating techniques, and vulnerability of ML-based systems against intelligent attacks (i.e., AA).

This thesis provides an insightful diagnosis for the discussed issues and introduces efficient solutions for each studied part to upgrade communications and networks of the new era, towards empowerment, adaptability, and trustworthiness.

1.5. Aim and Objectives

Introducing a reliable/robust 6G-based communication system with powerful capabilities (for open areas or any location where IRS, fixed relays, unmanned aerial vehicles (UAVs), or other non-line-of-sight (NLOS) transmission assistance can/cannot be deployed) to cope with the emerging technologies requirements, meet the stringent requirements and achieve the targets. It integrates the 6G candidate technologies to fully utilize their characteristics for sufficient performance, including:

- 1) Establishing a Sufficient, Trustworthy, and Sustainable Energy 6G-based communication system with efficient/reliable networks.
- 2) Enabling cooperative EH-driven THz transmission for Fronthaul and Backhaul links, enabling Synergy/Integration with other EM frequencies. Overcoming THz communications shortages and Challenges, e.g., operation/processing in highly mobile systems, susceptibility to blockage, small coverage area, lack of propagation models, the need for high-fidelity hardware, and co-existence/synergy with frequency bands.

- 3) Increasing Reliability, SE, EE, Capacity, resource management, scalability, and user fairness.
- 4) Reducing Complexity, Energy consumption, and cost-effectiveness. Developing Automated Intelligent systems/processes.
- 5) Improving System performance and Security, by Providing AI-based Efficient, Robust, and Secure Systems.

1.6. Contributions

The thesis studied the use of DF relaying rather than complex and costly intelligent reflecting surfaces (IRS) for cooperative networking to achieve the same objective of reliable connectivity with NLOS transmission path in THz frequencies for open terrestrial areas, such as rural areas, countryside, or any area where we cannot deploy IRS (assuming the existence of an obstacle blocking the transmission path) or for low-rate communication use cases in a new potential system. The main contributions of this thesis are:

1. Investigating system performance when applying the EH SWIPT technique to improve THz transmission, SE, EE, and other important metrics. Proposing a simple and cost-effective design of SISO high-directional antenna with the system to simplify THz-NOMA networks and not MIMO (this design reduces decoding complexity at Rx where it does not require extra SE with THz and NOMA) and to reduce bulky hardware (i.e., DF relaying instead of IRS), computational complexity, power consumption, and cost. On the other hand, a MIMO-based system was introduced to achieve further reliability as an added value to the proposed system. The proposal utilizes existing mobile user equipment (not a fixed device) for signal relaying to gain an extra served user. It achieves a synergic coexistence with the expected mobile

6G infrastructure. Hence, this proposed system can be upgraded based on the implementation preferences.

2. Enhancing the NOMA SIC procedure, preventing propagating errors, complexity, and SE degradation due to the burden of the additional operations by proposing a two-user clustering. Further, analyzing the introduced scalable system and simulated performance while setting moderate and flexible parameters (i.e., distances, transmission power, frequency, BW, and simple modulation scheme as it does not need to use a complex modulation to improve SE). Moreover, demonstrating the importance of selecting the nearest relaying user to the BS based on the technologies' concepts. This system is upgradeable based on trade-offs among systematic priorities.
3. Developing a path-selection mechanism for the potential NOMA-based far users to enhance system performance and reliability, by solving the SIC-dependent detection problem, decreasing the cluster's users (SIC operations), and reducing computational and procedural complexities. The work utilizes the practical application of H-NOMA to the proposal for the utmost benefit of this scheme over single-carrier NOMA shortages. Further, evaluating the best pairing strategy in H-NOMA to attain the best possible system performance, investigating all the possible SWIPT pairs with the available LOS users to specify the best pair that provides the best performance, and developing a dynamic mechanism to select the best SWIPT-pairing user out of all available users to guarantee fast and accurate dynamism.
4. Presenting an efficient DAE-based 6G CE model with a secure transmission protocol using deep learning training data with epsilon values ranging from 0.5 to 3.0 that uses transmitted signal parameters for learning, avoiding overfitting, and detecting intelligent AA.

1.7. Thesis Organization

The remainder of this thesis is structured as follows:

1. **Chapter Two** introduces the literature overview and related work.
2. **Chapter Three** indicates Cooperative SWIPT THz-NOMA/6G Performance Analysis.
3. **Chapter Four** indicates Cooperative SWIPT MIMO-NOMA for Reliable THz 6G Communications.
4. **Chapter Five** indicates the Cooperative SWIPT-Hybrid-NOMA Pairing Scheme considering SIC imperfection for THz Communications.
5. **Chapter Six** indicates the SWIPT-Pairing Mechanism for Channel-Aware Cooperative H-NOMA in 6G THz Communications.
6. **Chapter Seven** indicates Secure Deep Autoencoder-based 6G Channel Estimation to Detect/Mitigate Adversarial Attacks.
7. **Chapter Eight** summarizes the Conclusion and Future work with Recommendations.

Chapter 2: Literature Review

2.1. General Introduction

This chapter provides an overview of the applied techniques/methods, the relevant studies to the work, and a discussion of related work. The following sections detail the key approaches and their applications in the context of this research.

2.2. Literature Overview

This section demonstrates the overview of all the techniques as follows:

2.2.1. Supporting Technologies

❖ Spectral Efficiency:

In wireless communications, SE represents the communication systems' efficiency in transmitting data using a certain BW, determining the effectiveness of that frequency's utilization. SE measures the ability of data transmission of the utilized BW [1].

In all wireless communications/networks, SE depends on several factors, e.g., BW utilization/optimization, Shannon's theory criteria, modulation/multiple access techniques, and number of antennas. However, achieving the best possible SE (avoiding SE degradation) requires managing effective factors, e.g., interference, complexity, and power dissipation to overcome the emerging challenges and to enhance system efficiency and reliability [2].

❖ Energy Efficiency:

In wireless communications, EE represents the use (i.e., energy optimization) of the lowest power to achieve a particular target/output [3], [4]. It could be achieved by utilizing the edge of technologies depending

on several factors concerning reducing the dissipation in energy and accordingly improving cost-effectiveness, environment, and sustainability. However, achieving the best possible EE requires managing effective factors, e.g., initial cost, Behavioral Barriers, and Technical Limitations to overcome emerging challenges and to enhance system efficiency and reliability [5].

❖ **Energy Harvesting:**

In a wireless communication context, EH is a process by which the device's surrounding electromagnetic energy (radiofrequency signals) is captured and converted into usable power to reuse for retransmission [6]. It provides communication user equipment with operational power with/without conventional energy sources, utilizing the captured power to do further tasks. EH can be applied to gadgets, e.g., IoE, wireless sensor networks, and mobile infrastructures' devices for the new era of wireless communications [7]. However, achieving the optimal EH process requires mitigating the accompanying challenges, e.g., low-power output, energy-conversion efficiency/losses, and managing the energy storage/stability to overcome the limitations and enhance EH feasibility and efficiency [8].

❖ **Simultaneous Wireless Information and Power Transfer (SWIPT):**

In the ever-increasing wireless communication devices, SWIPT represents EH technology by transmitting data and power wirelessly and simultaneously via one transmission channel to another device [9]. It is considered a key-enabling technique to assist the new generations of 6G and beyond communication equipment, networks, and the huge number of associated devices in terms of energy and information transfer [10]. SWIPT was earlier motivated by the essential requirement for green

communications to reduce reliance on traditional power sources and enable self/wireless-powered communications [10], [11].

It works at the transmitter (Tx) device that already captures energy from the surrounding environment to be reused for transmitting data and power in one signal using the required electronic circuitry. Whereas, at the receiver (Rx) side, a power-splitting (or time/frequency-based) protocol splits the combination signal into EH and data decoding to enable energizing the device and decoding its intended data. However, there are challenging issues that require to be considered to make use of this significant technology, e.g., EH/information power fractions balance, efficiency, optimization, channel condition, and complexity [12].

2.2.2. Cooperative SWIPT THz-NOMA/6G Performance Analysis

The tremendous growth of service-demanding smart devices, e.g., global coverage, unprecedented technologies, and intelligent applications accompany the rapid leap in wireless communications. Necessary data transfer with ubiquitous coverage led to revolutionary research efforts. EE and SE are sharp criteria that measure the compatibility of any proposed system [13]–[15]. Their improvement is essential to meet the stringent requirements of various applications, such as data-hungry and energy-demanding applications, due to 6G's increasing demands with its key-enabling technologies. EE is considered a crucial designing metric in wireless communications, particularly in 6G and beyond with their upgraded infrastructures, such as cell-free and ultra-dense heterogeneous networks (UDHNs) with distributed BSs, access points, and relays due to their number of antennas, equipment, and power-consuming electronic (and photonic) elements, connecting billions of devices, i.e., IoE [16], [17]. The EE of 6G operations is compulsory for energy savings, green communications [18], and feasibility in 6G network requirements such as

quality of service (QoS) and processing [19], [20]. THz communication [21] is a cornerstone that will play a pivotal role in the next generations. SE depends mainly on available channel BW following Shannon's theorem [22]. THz has attracted the great attention of many researchers as the hottest topic in the paradigm shift of 6G due to its unique advantages as the last uninvestigated band of electromagnetic frequencies. It is in the middle of millimeter Wave (mmWave) and infrared bands between (0.1–10) THz [23]. It is considered the system's backbone of the next era due to its ability to enable various applications. THz communication has extremely high frequencies, ultra-wide BW, superfast data transfer, extensive throughput, extremely low latency, and very good directivity due to its very short wavelength (3 – 0.03) mm [24]. Locating the boundary between mmWave and optical bands motivated researchers to explore these bands' capability to support THz communications as THz outperforms the two bands at specific points. Electronic, photonic, and plasmonic technologies are expected to evolve the manufacturing of THz transceivers [25]. THz communication logically complements mmWave and optical bands by providing alternative signals as a replacement to optical paths in some use cases, such as the connections of backhaul, kiosk to nodes, data center racks, and intra-device links, in addition to THz integration with fiber networks [26]. Hence, the disadvantage of noticeable water vapor absorption and path loss spikes that divide the THz spectrum into several spectral windows, as stated in IEEE Std. 802.15.3d–2017; however, these windows are being extensively explored, considering them to support 6G services with some exemptions where some 6G services will not be compatible with the new frequency bands [27]. The demand for IoE ignites an emergent necessity to connect everything to everything. The current systems have limitations restricting any upgrades or improvements to meet these requirements. Developing decent techniques to be integrated

is mandatory to build a modern communication system to satisfy the new requirements such as ultra-massive connectivity, very high SE, very low latency, very high data rate, ultra-high reliability, user fairness, unprecedented applications support, EE, and cost-effectiveness [28].

2.2.2.1. Background

Power domain NOMA [29] is one of the famous candidates to evolve 6G systems. It can improve the SE of mobile communication systems, outperforming conventional OMA schemes in terms of SE, capacity, resource allocation, user fairness, connectivity, and latency [30]. This research mainly concentrates on single-input single-output (SISO)-NOMA (despite the gains of MIMO systems) because MIMO-NOMA systems are practically complicated to implement. NOMA mechanism allows various users' signals to superimpose at Tx and then to be distinguished and filtered by using successive interference cancelation (SIC) operation at Rx that effectively enlarges the data transfer capacity that depends mainly on the BW; however, interference is discarded by the SIC implementation, and the noise is filtered [31]. The two operations are conducted at the Rx side. With the NOMA concept, the channel capacity is calculated as $C = BW \times \log_2(1 + S/(N + I))$, where C is the channel capacity, BW is the bandwidth, S is the signal power, N is the noise power, and I is the interference of other users' signals. NOMA multiplexing is performed in the power domain, allocating different power coefficients to the users per their channel conditions (i.e., strong or weak). All users' signals are superimposed in Tx. Demultiplexing of NOMA signals is conducted by applying SIC at Rx [32]. Grouping or clustering the served users is essential in THz-NOMA communications to improve SE and mitigate complexity as the LOS is the main transmission link. For the SISO-NOMA scheme, BS/users with single antenna equipment rely on the simultaneous channel state information (CSI), where the users are sorted to allow decent SIC decoding

at Rx. The larger the channel gain difference, the more sufficient NOMA is gained [33]. User clustering may be impractical with many users; therefore, it is aimed to develop low-complexity solutions to avoid the clustering problem [34]–[36]. SIC is not only CSI-based but also QoS-based or hybrid-based. CSI acquisition at Tx and Rx is a great challenge for all modulation schemes [37].

Hence, a simple binary phase-shift keying (BPSK) is used in the proposed system with its advantages compared with other formats. Research efforts are exploring all the possible means, including NOMA-assisted cooperative systems, to tackle the problems of distance shortages and power losses in THz communications. Cooperative networking with its relaying categories offers multiple advantages such as reliability and capacity with better coverage area, enhancing overall performance [38]. When applied to cooperative networks, the SE of NOMA can be reasonably improved to support extra (blocked, weak, or cell-edge) users in the short-distance THz transmission, significantly when deploying EH with NOMA-based cooperative networks [39]. It represents the main topic of this work in THz communications. Hence, DF relaying is used because NOMA is adopted in this system [40]. Relaying user implies a copy of the far (weak) user's signal (to decode and remove it before decoding the intended strong user's signal in NOMA) included in the superposed signal received by that user. It reasonably utilizes that to achieve the objective of relaying as an additional advantage, which is better than using an extra relaying device with extra costly power-consuming complexity. The repetitive use of cooperative networks causes the drainage of the relaying user's battery, leading to system failure because THz-NOMA requires high computational SIC procedures at the Rx [29]. Thus, research efforts aim to overcome the challenge of moving toward green communications [18], [41] by applying the EH technique. Energy and information are sent to

other destinations by exploiting the energy of radiofrequency (RF) signals that exist everywhere around most devices [42]. EH enables devices to harvest that energy by using simple RF circuits. It can then utilize that harvested power to use it again with the targeted transmissions to send the desired signals without applying an extra burden to the relaying user's battery. Relaying user divides the received signal's power into EH and information decoding through EH power splitting, allowing the implementation of energy harvesting and information decoding at the same time, leading to the principle of SWIPT [43]. SWIPT qualifies the near-relaying user to capture power from the transmitted signal from the source and uses that energy to relay information to the far user [44], as shown in Figure 2.1; this improves the system throughput and OP accordingly.

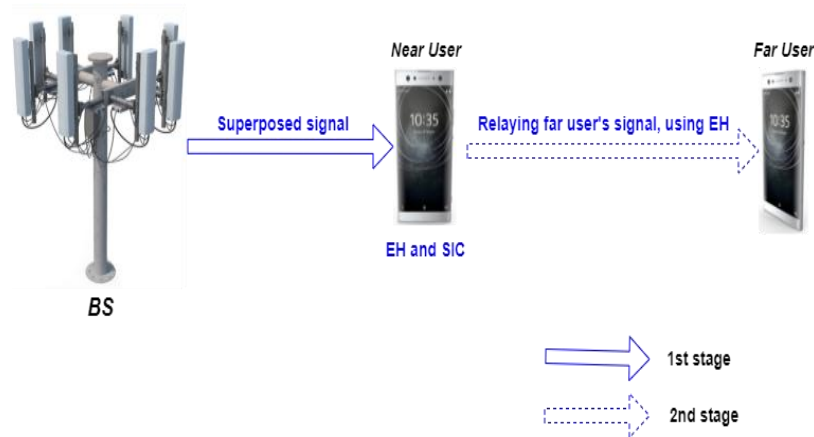


Figure 2.1 SWIPT with cooperative NOMA.

2.2.3. Cooperative SWIPT MIMO-NOMA for Reliable THz 6G Communications

The wireless communication field has witnessed a rapid rise with a significant expansion of smart gadgets, new technologies, and modern applications. The critical requirement for fast data transport combined with the global ubiquity of services has resulted in ground-breaking research [19], [20], [41], [45]. It is critically required to enhance EE and SE to fulfill the strict requirements of diverse emerging applications, adapting to the upgrades of the next era and eliminating power consumption of the

required equipment [34], [46]–[50]. The efficient use of energy has become an inevitable demand in the next generation of 6G to support its practicability and satisfy its needs [51]. THz communication [52] will have a significant impact on future generations. According to Shannon's Equation, SE is determined based on BW availability. THz represents the unexplored electromagnetic (EM) gap between EM and optical bands; it has piqued the interest of the research community toward 6G because of its favored benefits. THz is regarded as an essential pier for 6G due to its capacity and capabilities to build an adequate system, supporting a wide range of applications due to its very short wavelength (λ) of 3000–30 μm and other features, e.g., very high frequencies, ultra-wide BW, very high data rates, enormous throughput, very low latency, and excellent directivity. THz has encouraged researchers to investigate its capabilities to enable THz communications as it outperforms the two adjacent frequency bands in some ways. The need for fully connected systems has arisen as a result of IoE requirements. There are restrictions to 5G systems that prevent any additions or enhancements to satisfy these needs.

It is aimed to improve wireless connectivity, resource management, scalability, and user fairness, as well as to enhance the overall performance of 6G wireless communications and reliability. Hence, the current wireless communication systems are optimized by utilizing MIMO-NOMA technology and THz frequencies, exploring the performance and gains obtained.

2.2.3.1. Background

To address the challenges of THz communications, researchers are looking into all options, highlighting MIMO-NOMA-assisted cooperative networks. It provides several benefits, including increased reliability and capacity, as well as a larger coverage area, all of which improve overall

performance, i.e., implementing energy harvesting (EH) with cooperative NOMA [45].

Cooperative networking has been previously investigated utilizing a variety of cases and situations; the major benefits were demonstrated while the drawbacks of adopting this strategy were addressed. Other technologies of this study, i.e., EH, NOMA, and THz, were discussed separately or in combination to attain a specific influence on the field. The drawbacks of employing those technologies were thoroughly explored, including the flaws, restrictions, and lack of performance. In [53] and [47], despite the consideration of the IRS as an edge of technology to improve source-to-destination transmission in particular cases of interrupted communication path, it must outperform the usage of relaying regarding complexity, energy, and cost. Briefly, when comparing the IRS to the older DF relay, the general impression of this work stated that a supreme data rate is necessary to outperform the DF relay regarding transmit power minimization and EE maximization. Furthermore, IRS and other signal-relaying (fixed) devices require additional hardware. Figure 2.2 demonstrates the relay-based transmission strategy.

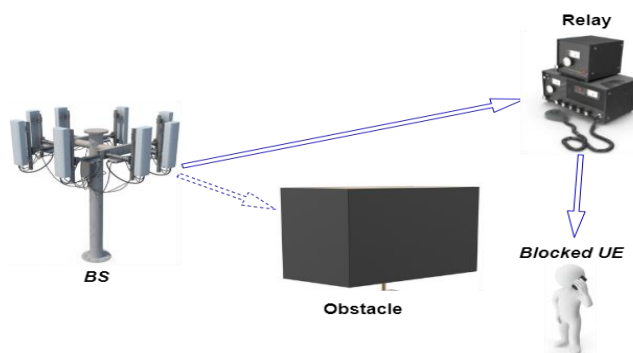


Figure 2.2 Relay-based transmission strategy.

2.2.4. Cooperative SWIPT-Hybrid-NOMA Pairing Scheme Considering SIC imperfection for THz Communications

The massive increase of users, devices, and data traffic nowadays necessitates integrated wireless communication systems and technologies

to adapt to the emerging requirements of 6G various applications, considering the achievement of the required levels of EE, SE, and other evaluating metrics [41], [51], [52], [54]. When it comes to NOMA studies, SIC has commonly been considered to be implemented perfectly, where procedural errors might occur. Furthermore, it is extremely important to minimize the number of users per cluster as users' CSI acquisition has a high impact on SIC implementation [55]. Due to the expected additional hardware and power consumption, EE is essentially considered a crucial factor in the next era of wireless communications (6G and beyond), especially with ubiquitous coverage of the massive number of devices i.e., IoE [46]–[49], [56]. Moreover, energy-efficient systems are critical in 6G communications to meet green communications criteria [49]. The existing systems have noticeable constraints to support the new needs, to this end, integrating promising techniques is recommended to build a capable wireless system that provides the supreme targeted levels of connectivity, SE, latency, data rate, reliability, user fairness, EE, and cost-effectiveness. Recent studies have nominated NOMA to be part of 6G systems, as it outperforms the previous OMA schemes, providing better SE, capacity, user fairness, connectivity, and latency, however, decoding complexity must be considered alongside system planning [37], [57], [58]. NOMA technique performs superposition coding at Tx, merging users' signals, and then manipulating SIC at Rx to remove any interference with the user's signal. The work concentrates specifically on the impact of imperfect SIC on SIC-dependent NOMA-based systems using a simplified scheme of SWIPT-paired clustered users equipped with SISO H-NOMA. NOMA dedicates power fractions to users per their CSI, target rates, or other metrics, combining all the signals in the power domain. Users' clustering depends on certain parameters of users to reduce procedural complexity,

significantly with THz-NOMA communications, e.g., setting main CSI as a reference to other users within a cluster [59].

This modified system and its metrics have not yet been investigated with THz aspects, considering SIC imperfection. This work contributes to solving the SIC-dependent detection problem by proposing EH-based low-cost scalable simplified system self-powered/double-regulated mobile DF relaying, lower power-consuming elements/procedures equipped with SISO instead of MIMO to minimize SIC-based decoding complexity at Rx while enhancing EE. Further, the presented work applies a SWIPT-pairing strategy to the proposed system to achieve the best performance by integrating the promising technologies and decreasing the cluster's users (SIC operations) that is reducing computational and procedural complexities.

2.2.4.1. Background

In the SISO-NOMA scheme, the base station (BS) and nodes are equipped with one antenna, considering simultaneous CSI to specify users' sequence for successful SIC at Rx. As a multi-user detection (MUD), SIC is critically required for signal detection [60]. It is worth noticing that the smaller number of cluster users the simpler SIC implementation is achieved, Figure 2.3 explains the SIC procedure for an n th number of iterations at Rx where it occurs upon receiving a superposed signal from numerous users with varying amounts of power. The signal strength of the SIC receiver is ranked ascendingly, however, error propagation is an issue [61].

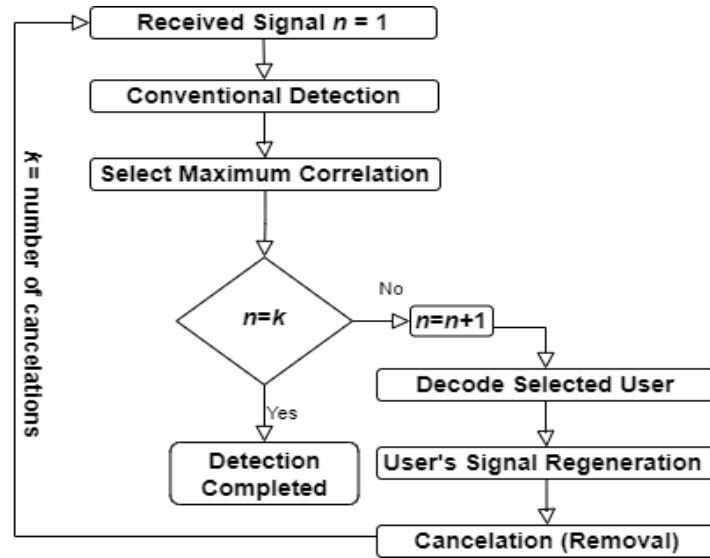


Figure 2.3 SIC procedure in NOMA Rx.

H-NOMA scheme supports a variety of services more than single carrier (SC)-NOMA and OMA as a combination of these two schemes, taking full advantage of them. It is presented to overcome system constraints e.g., the potential SIC complexity with the interference of the massive number of users of SC-NOMA and the resources limitation of OMA [62]. Due to THz characteristics, researchers proposed many advanced schemes such as cooperative-NOMA. It was suggested to integrate cooperative relaying with NOMA to overcome THz issues. Cooperative-NOMA provides signal diversity, reliable connectivity, expanded coverage area, and improved SE consequently supporting users with weak (or zero) SNR in THz communication. Thus, integrating the EH technique with cooperative NOMA delivers a prestigious enhancement to THz communications [35]. Cooperative networking leads to battery exhaustion of the relaying user's device (due to high computational SIC at Rx), thus, it is reasonably required to adopt the EH technique [63], [64]. Using EH the relaying user harvests the surrounding RF energy for retransmission. The EH power splitting protocol enables relaying users to split the power of the received signal into power harvesting and data

decoding fractions to manipulate energy harvesting and information decoding simultaneously i.e., SWIPT. SWIPT improves system capacity, diversity, and reliability [65]. Recently, NOMA-based/integrated systems research considered SIC to be implemented perfectly, which is an impractical assumption as SIC errors occur and propagate to other signals' detection successively. THz-NOMA communications were investigated pointing out system performance and constraints by academic and industrial research.

Notably, the proposed system with its integrated 6G candidate technologies has not been previously utilized under the assumption of imperfect SIC in the state-of-the-art. Based on the authors' knowledge, it achieves multiple gains sufficiently making use of all the integrated edge of technologies.

2.2.5. SWIPT-Pairing Mechanism for Channel-Aware Cooperative H-NOMA in 6G Terahertz Communications

Current wireless communication systems lack the ability to meet the new requirements of the ever-updating next generations. This requires compulsory integration of the leading edge of promising technologies and intelligent applications to comply with distance-dependent THz constraints. It is essential to develop a suitable capable communication system to satisfy the expected features and demands, i.e., ubiquitous connectivity, supreme SE, minimal latency, huge data rate, system robustness, user fairness, supporting emergent applications, EE, SE, and cost-effectiveness. Revolutionary research across the world has identified THz frequencies as the future of wireless communications [66]–[68]. EE and SE are pivotal factors to assess and enhance communication systems to satisfy the emergent essential 6G applications [19], [20], [41], [45]. EE is an essential criterion in the next era of wireless communications and its overwhelmed infrastructure due to the rising power consumption of the

required elements to connect a huge number of devices supporting the principle of IoE [34], [46]–[49], [56]. Hence, EE in 6G communications is mandatory to save energy and meet the practicality of 6G communication networking [51]. SE depends on the availability of BW and working frequency. It is the backbone of the next wireless communications era given its valuable features as well as the various services that THz provides [52]. The new generation's ubiquitous coverage necessitates a revolutionary upgrade to the existing systems toward establishing robust and reliable wireless systems with extraordinary capabilities.

To this end, this work is motivated by the capability of integrating the evolutionary technologies and developing a channel-aware path selection mechanism, targeting the establishment of a reliable and scalable simplified system by the enhancement of BW-competitive 6G THz communications, and overcoming the constraints of the current resource-scarce systems. Moreover, this work optimized the existing communication systems by adopting H-NOMA, and THz with cooperative SWIPT technologies to comply with the intended goals, highlighting the attained gains.

2.2.5.1. Background

To meet the potential technical specifications, NOMA is a strong candidate to be integrated with the 6G paradigm [37]. It enables the evolution of SE, outperforming the earlier strategies of OMA in terms of SE, channel capacity, resource management, user fairness, massive connectivity, and lower latency. The main procedure of NOMA is to carry out superposition coding combining users' signals at Tx, where it must be realized and treated using SIC as a multi-user detection at Rx to discard any interference. It enlarges the channel capacity, which relies on channel BW. This work concentrates specifically on H-NOMA. Based on NOMA fundamentals, various power coefficients are allocated to the users based

on their CSI and multiplex in the power domain. To improve SE and eliminate complexity, user-clustering is important in THz-NOMA communications based on users' locations or other metrics. However, to reduce the complexity of clusters in some cases, only one main user's CSI might be set as a reference for the remaining number of users within the NOMA cluster [37]. In the SISO-NOMA scheme, both BS and users are equipped with a single antenna that relies on CSI for users' sorting, preparing them to implement better SIC at the receiving end. The larger the channel condition differences among users, the better NOMA performance is obtained [55]. H-NOMA is an integration of NOMA/OMA techniques. It is proposed to overcome the challenges or limitations that undermine the performance of those systems, e.g., the complexity and possibly interference due to the huge number of users. Due to the lack of transmission distance and the losses in THz communications, it is recommended to adopt NOMA-assisted cooperative networking to tackle those problems. Cooperative network relaying offers more reliability and capacity, enhancing the overall performance, especially when integrated with other modern technologies such as NOMA. NOMA's SE can be improved using cooperative networking for better support to the blocked users or users with a weak SNR with THz communication, especially with the merging EH technique with cooperative NOMA [35], which the work studies with THz frequencies. Reasonably, using cooperative networks will cause battery drainage of relaying of the user's device. In addition, the THz-NOMA system experiences the burden of high computations of SIC at Rx; therefore, to comply with that problem, it is logically recommended to apply the EH technique [63]. Applying EH will exploit RF signals' energy that surrounds most of the devices, e.g., energy belonging to other destinations. Utilizing EH enables the relaying user to harvest that energy to use it again to retransmit the targeted user's signal. In power splitting-

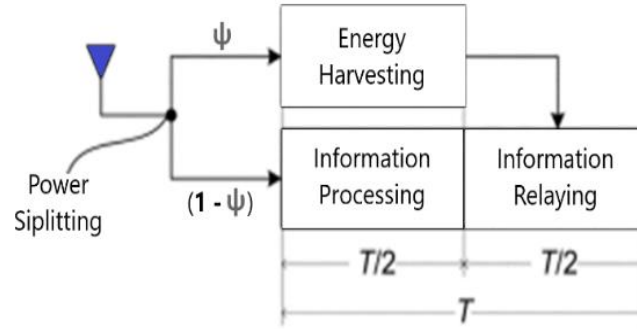


Figure 2.4 SWIPT with DF-relayed NOMA.

based EH, the relaying user splits the received signal's power into an EH partition (ψ) and an information-decoding partition ($1-\psi$) to carry out EH and information-decoding at the exact time, i.e., SWIPT [69], as demonstrated in Figure 2.4, SWIPT enhances system capacity, OP, and accordingly EE. It represents one of the potential technologies for physical layer optimization [70].

2.2.6. Secure Deep Autoencoder-based 6G Channel Estimation to Detect/Mitigate Adversarial Attacks

In wireless communications CE, the security, cost, and complexity measurements represent important metrics for evaluating systems' feasibility and practicability. The CE process is critical for successful communications [71], [72]. 6G CE represents a very complex operation compared to previous generations due to the upgraded infrastructure, features, applications, network traffic, technologies, and the number of associated gadgets/users connected ubiquitously to cope with the emerging IoE [68], [70], [73]. Cellular networks have grown significantly over the past few decades with developments in communications technologies that enable faster data rates, bigger cell/channel capacities, and lower latency. Such technologies' major objective is to make a variety of unique applications possible (e.g., online learning, telepresence, flying, driverless automobiles, smart cities/grids, and intelligent manufacturing) [66], [74]. The 6G emerging requirements and features accompany serious security

anxiety and increase network computational complexity. According to the jeopardizes of wireless communication networks to renewable various attacks, 6G-related researchers must focus on the necessity for novel AI-based security systems to satisfy the development of AA detection and mitigation for 6G wireless communication networks. It is critically required to confront the threats efficiently, abandoning the current incapable CE-targeted security systems that cannot adapt to the upgradable attacks [75], [76]. In risk-sensitive systems safety, detecting AA is a challenging issue as enormous traffic of suspicious activities is discovered every day. The impact of these complex attacks is increasing, introducing additional complications to the current attacks. Moreover, cybersecurity has become a prioritized essential topic in the modern scientific community. Moreover, cybersecurity has become a prioritized essential topic in the modern scientific community [77]–[79]. Therefore, monitoring and analyzing network traffic is essential to detect potential AA. The main risk in traditional and machine learning (ML)-based security systems is the insufficiency of distinguishing AA in 6G communication networks as AA manipulates signals or data in ways that are not detectable by traditional measures [67]. To this end, it is important to design 6G networks with security in mind and to implement best practices for securing the network against AA. This may involve developing new security measures that are specifically designed to detect and defend against AA. Deep Autoencoders (DAEs) are a type of NN that can be trained to learn a compressed representation of the input data, also known as the encoding, and then use this encoding to reconstruct the original input, also known as the decoding [80]–[88]. By training an AE on a set of received signals and their corresponding channel characteristics, the AE can learn to extract features that are relevant to CE. The encoding produced by the AE can then be used as a representation of the received signal, which can be fed into a CE to

estimate the channel characteristics [60], [62], [89]. This can be particularly useful in scenarios where the channel is highly complex or time-varying, as the AE can adapt to changes in the channel over time and provide more accurate estimates of the channel characteristics.

Hence, this work proposes a secure deep autoencoder (DAE)-based communication environment (i.e., CE) model to address the challenges of accurately detecting and preventing AA in 6G wireless communication networks with minimal complexity. This outperforming integrated DAE model with its performance has not been achieved previously.

Overall, the proposed secure DAE-based CE model offers a promising solution to enhance the security of 6G networks against AA with minimal complexity, paving the way for more advanced and effective security mechanisms.

2.2.6.1. Background

The CE process [89] is the first step in identifying the characteristics of the radio transmission channel through which the transmitted signal propagates from Tx to Rx. This prerequisite information (i.e., CSI) and it requires to be realized by Tx and Rx. The common assessment of CE methods (e.g., mean square error (MSE)) is achieved by a predefined reference (pilot) sequential signal sent with the transmitted signal and compared to the original pilot at Rx after undergoing influential (e.g., attenuation, distortion, and noise) effects while being transmitted. The traditional CE is poor, non-robust, complicated, and performs inaccurately because of the changeable non-linear channel characteristics and the information's high dimensionality. Its complexity increases with respect to the increase in the number of communication links [72]. Besides, 6G plans assume an upgraded mobile infrastructure, expanding the number of ubiquitously connected communication components and links to deploy ultra-densified networks using ultra-massive (UM)-MIMO. Providing

extremely high data rates (Terabits/Second) and extremely low latency with bigger cell/channel capacities is a fundamental objective of 6G networks. The incorporation of the edge of technologies, e.g., AI, UM-MIMO, and terahertz frequency bands is strongly nominated for 6G networks. The integration of the 6G key enabling technologies/networks provides the targeted performance THz, while very big arrays of antennas are designed at the Tx and Rx sides using UM-MIMO. This causes a considerable increase in energy dissipation, procedural/computational complexity, and hardware[72]. Therefore, 6G CE operations require adapting to the upgraded features and satisfying the growing demands of services to certain standards of data rates, cost-effectiveness, and spectral/energy efficiencies. To this end, AI was intended to be embedded in the new era's systems to optimize networks' functionalities and improve system performance. As a valuable candidate of 6G key enablers, AI plays a pivotal role in CE processes [90], [91]. DL-based CE is a promising approach for improving the accuracy and efficiency of CE in 6G wireless communication systems by learning the transmitted and the received signals. It has several advantages over traditional CE techniques. It is more adaptive to changing channel conditions in real time. Additionally, DL-based CE can be performed more efficiently than traditional CE techniques, reducing system computational complexity [92]. AA are typically associated with AI systems and accordingly 6G communication networks by manipulating perturbed input data. They are constructed to deliberately deceive and mislead them into making the wrong prediction or decision. AA in 6G manipulate signals or data in ways that are not detectable and could potentially bypass traditional and existing security measures. They mimic legitimate traffic but contain malicious content or commands [93].

Remarkably, CE is considered an essential topic for academics' cybersecurity research in wireless communication networks resulting in several articles published in recent years. However, CE jeopardizes AA vulnerabilities that degrade 6G system efficiency despite applying ML against these attacks. Therefore, this work introduces a DAE-based CE.

2.3. Related Work

This section reviews existing research on NOMA-based cooperative SWIPT technologies, specifically focusing on THz communication in the context of 6G networks. The discussed related work covers various aspects such as performance analysis, NOMA-based schemes, transmission aid techniques, user clustering, pairing mechanisms, and security considerations. Each of them provides a concise overview of the key findings from the relevant literature as follows:

- ❖ Tataria et al., 2021 [26], the authors presented some significant points as drawbacks or difficulties against designing and deploying the IRS technique for supporting 6G infrastructure, that is, controlling the alignment of beams for instantaneous beam steering, interference control, energy efficiency degradation, and the challenges that accompany IRS deployment, such as (1) the design and control joint communications of active and passive components, for instance, extra operations and analyses needed, which is about improving the PHY coverage and hardware effects on the performance, in addition to the total cost of renting a space to deploy it and the continuous maintenance needed. (2) Effect of potential full or partial failures due to environmental or accidental factors, such as temperature, rain, and wind. (3) IRS standardization before system deployment and the interactivity of IRS with the radio traffic instant changes to attain efficient signaling. (4)

Computational and procedural complexity as additional transmission steps.

- ❖ The authors Zhang *et al.*, 2020 [94] studied clustering, precoding, and power optimization. They developed an artificial intelligence (AI)-based algorithm to present a clustering technique for THz MIMO-NOMA designs. This methodology comes at the cost of the required running time of the huge dataset, as well as the updated dataset acquisition needed.
- ❖ Saad *et al.*, 2021 in [95], a MIMO spatial multiplexing technique was introduced, featuring a novel index modulation range. The innovation extended to the exploration of MIMO technology at sub-THz frequencies, aimed at unlocking the potential for ultra-high data rate applications while ensuring a remarkable SE. Nevertheless, it is noteworthy that NOMA was not considered during the investigation, and the outcomes fell short of expectations when evaluated against comparative metrics. Future research may benefit from incorporating NOMA to further enhance the performance and broaden the scope of this technique.
- ❖ On the other hand, for data rate maximization, an investigation was conducted by Elkhartbotly *et al.*, 2020 [96]. It Addressed the power allocation challenge within NOMA-based cooperative MIMO systems, particularly when implementing half-duplex and full-duplex modes in THz communications, remaining an ongoing concern. The current state of research indicated that the achieved results fall short of the anticipated targets set forth by the proposed system in this study. This emphasized the need for a more robust and refined approach to power allocation in order to bridge the existing gap between system performance and the envisioned objectives. Future investigations and optimizations in this area are crucial to unlocking the full potential of NOMA-based

cooperative MIMO systems in the dynamic landscape of THz communications.

- ❖ For instance, Nazar *et al.*, 2021 [97] developed a closed form for the bit error rate (BER) in the network represented a significant stride, contributing to the enhancement of OP. However, it is noteworthy that although strides were made in BER, the improvements in SE and EE were not realized with optimal efficiency. Future research endeavors should focus on refining strategies to concurrently optimize SE and EE, ensuring a more comprehensive advancement in the overall network performance.
- ❖ Khan *et al.*, 2021 study delved into optimizing transmission power and reflection coefficient as crucial elements to enhance the overall sum rate. However, it is worth noticing that the improvements achieved were not as efficient as anticipated. Future research endeavors should concentrate on refining these optimization strategies for a more effective enhancement of the sum rate [98].
- ❖ Whereas, (Khan, Javed, et al., 2022) [99], the exploration involved the application of an optimization method aimed at improving the system's EE, albeit with less-than-optimal results. Future investigations should focus on refining and fine-tuning these optimization techniques to achieve a more efficient enhancement of EE.
- ❖ Ahmed *et al.*, 2022 employed multi-cell NOMA networks, the primary goal was to enhance EE. However, the efficiency of this enhancement fell short of expectations. Future endeavors should concentrate on refining strategies to more effectively boost EE in multi-cell NOMA networks [100].
- ❖ In the study conducted by Khan, Lagunas, *et al.*, in 2022 [101], the central objective was the improvement of SE. However, it is noteworthy that the efficiency of this enhancement did not meet expectations. Future

research efforts should aim at refining methodologies to boost SE more efficiently.

- ❖ Do and An, 2018 utilized THz frequencies in [65], despite using IRS to improve the transmission between Tx and Rx, it was supposed to outperform the cooperative networks by all the means, simplicity, EE, and cost, not only optimizing reflectors but also to consider all other criteria, e.g., to minimize power consumption and to maximize EE.
- ❖ Letaief *et al.*, 2019 [102], the authors conduct a comprehensive review of AI-empowered wireless networks, delving into the role of AI in the deployment and optimization of next-generation architectures, particularly in operational aspects. This review highlights the utilization of AI-based models for training Tx, Rx, and channel as an auto-encoder, facilitating mutual optimization between Tx and Rx. The study also predicts distinctions between next-generation and current networks, spanning network infrastructures, wireless access technologies, computing, application types, and more.
- ❖ Additionally, Ozpoyraz *et al.*, 2022 [72] focused on deep learning (DL)-based solutions in next-generation networks, concentrating on physical layer applications in cellular networks, including massive MIMO, reconfigurable intelligent surface (RIS), and multi-carrier (MC) waveform. Emphasis was placed on the positive impact of AI-based solutions on enhancing network performance with more complexity and delay.
- ❖ Jin *et al.*, 2019, 2020 in [103], [104] proposed a robust CE framework using fast and flexible denoising convolutional neural networks (FFDNet) and deep convolutional neural networks (CNNs) for mmWave MIMO. These proposed methods exhibit versatility across a wide range of signal-to-noise ratio (SNR) levels, providing superior accuracy for channel estimators with high delay and complexity. DL-based algorithms

significantly contribute to overall system performance in next-generation wireless networks.

- ❖ Addressing security concerns related to AI-based algorithms, several research groups within the wireless research community scrutinized the potential issue of model poisoning (Kuzlu, Fair, and Guler, 2021) [105].
- ❖ Porambage *et al.*, 2021; and Siriwardhana *et al.*, 2021 in [106], [107] delivered a comprehensive review of next-generation wireless networks, encompassing opportunities and challenges related to security and privacy. The authors proposed solutions tailored to the next generation's networks and highlighted studies presenting robust frameworks for accurately detecting AA.
- ❖ Notably, Li *et al.*, 2020 [108] introduced "DeSVig," a decentralized swift vigilance framework, as a method to detect AA for industrial AI systems (IAISs). According to the results of this work, the framework can detect adversarial attacks, such as DeepFool and FGSM, however, it was inefficient in terms of accuracy and delay.

Chapter 3: Cooperative SWIPT THz-NOMA/6G

Performance Analysis

3.1. Introduction

This chapter provides a comprehensive explanation of the verification process for Cooperative SWIPT THz-NOMA / 6G Performance Analysis. It begins with outlining the system models, followed by a discussion of the simulation scenarios, and concludes with an in-depth analysis of the simulation results.

3.2. System Model

The proposed simple system in Figure 3.1 can work in a terrestrial open space use case, where THz-NOMA smallest single-cell downlink transmission with a cluster of two paired users is considered. The BS implements superposition to send signals to the two users simultaneously near user (NU) and far user (FU) by using SISO with a high-directional antenna. An obstacle is located in the path between BS and FU, causing extreme shadowing. Thus, FU is not capable of detecting its blocked or weak signal; however, NU has a strong connection with BS. Under NOMA fundamentals, firstly, FU's signal must be decoded by NU before performing SIC to remove it and consequently decode NU's data. Thus, NU already has a copy of the FU's information. Accordingly, the NU can assist FU's connection by playing the role of DF relay; however, the NU battery's energy does not suffice to relay the information to the FU. For that purpose, NU is proposed to perform the power-splitting protocol of EH (i.e., SWIPT) to capture power from BS and radiofrequency energy surrounding NU. The entire transmission process is performed in two stages. In the first stage, NU receives the transmitted signal from BS.

An amount of NU's received power will be captured using the power-splitting process, whereas the left power will be exploited to decode data. In the next stage, NU uses the captured power to relay the FU's information to the FU.

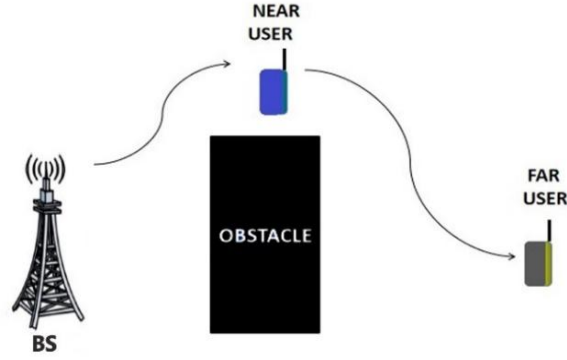


Figure 3.1 Model of cooperative SWIPT THz-NOMA

The proposed channel model in this work of all scenarios is Rayleigh fading channel with zero mean and variance = Transmission Distance^{-THz total losses}, whereas the transmission noise is additive white Gaussian noise (AWGN) with zero mean and variance = σ^2 . The Gaussian distributed probability density function (PDF) of z-point is expressed as:

$$f_{(z,\sigma)} = \frac{1}{\sqrt{2\pi\sigma^2}} \exp\left(-\frac{z^2}{2\sigma^2}\right) \quad (3.1)$$

The signal model of cooperative SWIPT NOMA considers atmospheric attenuation and molecular absorption, and the path loss of NLOS is more than that of the LOS path. The NLOS effect can be abandoned if the LOS path dominates. Hence, in the assumed open-space transmission medium, the THz total losses (η) are set to be extremely high. The channel gain for a kth number of users can be calculated as:

$$h_k = \sqrt{A} \sqrt{\frac{1}{\eta}} G \quad (3.2)$$

Where A is the number of antennas for SISO, G is the antennas' gain, and η is the THz total losses between source and destination, given by:

$$\eta = \left(\frac{4\pi f d}{c}\right)^2 e^{a(f)d} \quad (3.3)$$

Where f is the THz frequency, d is the source-to-destination distance, $a(f)$ is the absorption coefficient of the transmission medium, and c is the speed of light.

The closed forms based on the proposed scenario are derived as follows: Phase 1: The transmitted superposed signal by Tx is expressed as

$$X = \sqrt{P}(\sqrt{\alpha n} xn + \sqrt{\alpha f} xf) \quad (3.4)$$

Where P is the transmission power, αn is the NU's power, αf is the FU's power, xn is the NU's power signal, and xf is the FU's power signal. The FU cannot receive the signal due to full shadowing. The NU's received signal is expressed as:

$$yn = \sqrt{P}(\sqrt{\alpha n} Xn + \sqrt{\alpha f} xf)Hsn + Wn \quad (3.5)$$

Where Hsn is the BS-NU Rayleigh fading coefficient with zero mean and variance = $dsn^{-\eta}$, dsn is the BS-NU distance, and Wn is the AWGN with zero mean and variance = σ^2 . From yn , NU harvests a fraction of power called the EH coefficient (denoted as ψ). The remaining power fraction $(1 - \psi)$ is the information decoding power. Accordingly, when energy is harvested, the information decoding signal is:

$$\begin{aligned} YD &= (\sqrt{(1-\psi)})Yn + Weh \\ &= (\sqrt{(1-\psi)})\sqrt{P}(\sqrt{\alpha n} Xn + \sqrt{\alpha f} Xf) + (\sqrt{(1-\psi)})Wn + Weh \end{aligned} \quad (3.6)$$

where weh is the thermal noise of EH electronic components (mean = 0 and variance = σ^2). Mathematically, the harvested power of Wn could be ignored, and yD will be represented as:

$$yD = (\sqrt{(1-\psi)})\sqrt{P}(\sqrt{\alpha n} xn + \sqrt{\alpha f} Xf) + Weh \quad (3.7)$$

From yD, NU decodes Xf directly. NU achievable rate for FU's information decoding is:

$$R_{nf} = \frac{1}{2} \log_2 \left(1 + \frac{(1-\psi)P \alpha_f |h_{sn}|^2}{(1-\psi)P \alpha_n |h_{sn}|^2 + \sigma^2} \right) \quad (3.8)$$

By performing SIC, NU achievable rate for NU's data decoding is:

$$R_{nf} = \frac{1}{2} \log_2 \left(1 + \frac{(1-\psi)P \alpha_n |h_{sn}|^2}{\sigma^2} \right) \quad (3.9)$$

Harvested power: ψ is the EH coefficient captured in the first stage. The harvested energy is expressed as:

$$PH = P |h_{sn}|^2 \zeta \psi \quad (3.10)$$

Where ζ is the circuitry EH efficiency.

Phase 2: In the second stage, NU relays the information that is intended for the FU by using the harvested energy (PH). Thus, the transmitted signal by the NU is:

$$\sqrt{PH} \tilde{X}f \quad (3.11)$$

The received signal at the FU is:

$$\sqrt{PH} \tilde{X}f h_{nf} + Wf \quad (3.12)$$

where h_{nf} is the Rayleigh fading channel between NU and FU. The achievable rate at the FU is:

$$R_f = \frac{1}{2} \log_2 \left(1 + \frac{PH |h_{sn}|^2}{\sigma^2} \right) \quad (3.13)$$

NU must decode the FU's data in the first stage to derive an expression for evaluating the optimal value of the power-splitting coefficient ψ . It will then be able to relay the FU's information appropriately. To achieve that, the condition: $R_{nf} > R_f^*$ is set.

where R_f^* is the FU's target rate. This condition assumes that NU's achievable rate for FU's information decoding must surpass FU's target rate. R_{nf} in Equation (3.9) in the assumed constraint above is substituted to derive ψ .

$$\frac{1}{2} \log_2 \left(1 + \frac{(1-\psi)P \alpha f |h_{sn}|^2}{(1-\psi)P \alpha n |h_{sn}|^2 + \sigma^2} \right) > R_f^* \quad (3.14)$$

$$\log_2 \left(1 + \frac{(1-\psi)P \alpha f |h_{sn}|^2}{(1-\psi)P \alpha n |h_{sn}|^2 + \sigma^2} \right) > 2R_f^* \quad (3.15)$$

$$\frac{(1-\psi)P \alpha f |h_{sn}|^2}{(1-\psi)P \alpha n |h_{sn}|^2 + \sigma^2} > 2^{2R_f^*} - 1 \quad (3.16)$$

denoting $2^{2R_f^*} - 1$ by τf , which is FU's target SINR.

$$\frac{(1-\psi)P \alpha f |h_{sn}|^2}{(1-\psi)P \alpha n |h_{sn}|^2 + \sigma^2} > \tau f \quad (3.17)$$

$$(1-\psi)P \alpha f |h_{sn}|^2 > \tau f (1-\psi)P \alpha n |h_{sn}|^2 + \tau f \sigma^2 \quad (3.18)$$

$$(1-\psi)P \alpha f |h_{sn}|^2 - \tau f (1-\psi)P \alpha n |h_{sn}|^2 > \tau f \sigma^2 \quad (3.19)$$

$$(1-\psi)P |h_{sn}|^2 (\alpha f - \tau f \alpha n) > \tau f \sigma^2 \quad (3.20)$$

$$\psi < 1 - \frac{\tau f \sigma^2}{P |h_{sn}|^2 (\alpha f - \tau f \alpha n)} \quad (3.21)$$

To make sure that ψ is less than that value, the above Equation is reformed to be:

$$\psi = 1 - \frac{\tau f \sigma^2}{P |h_{sn}|^2 (\alpha f - \tau f \alpha n)} - \delta \quad (3.22)$$

Where δ is a tiny number (i.e., 10^{-6}) This value of ψ assures the required power for information decoding to achieve the FU's target rate.

Outage Probability:

The OP for each user is the probability of falling the user's instantaneous data rate below the target. Assuming R_n^* and R_f^* (bits/s/Hz) are NU's and FU's target rates, respectively.

FU will be in an outage if its achievable rate R_f in (3.13) is less than the target rate, which is mathematically expressed as:

$$PFU = Pr(R_f < R_{f*}) \quad (3.23)$$

NU must decode the FU's signal and its own precisely. The target rates for NU and FU must reach the NU's target rate. With SIC operation, if the target rate of either NU or FU in (3.9) and (3.13) does not reach NU's target rate, then NU will be in an outage, which is mathematically expressed as:

$$PNU = Pr(R_{NF} < R_{f*}) + Pr(R_{NF} > R_{f*}, R_n < R_{n*}) \quad (3.24)$$

By adopting the first mode principle that is stated in the physical layer section in [109], which is the THz single-carrier. This principle was proposed for high data rate connections, targeting BW-dependent applications, such as wireless backhaul/backhaul links, fronthaul/backhaul links, and data center links [110], based on the availability of spectral windows within THz frequencies (252.72–321.84) GHz. The available spectrum is divided into various channels (approved at the World Radio Conference 2019 [WRC-2019]) due to atmospheric and other effects where every individual channel has its own characteristics [110]. In total, 69 overlapping channels and 8 supported BWs (2.16–69 GHz) were found as multiples of 16 GHz. The widest entire channel (69.12) or the multiple smaller channels might be allocated depending on the application requirements, hardware limits, transmission conditions, and compatibility with the system. Among various modulation schemes that THz-SC PHY supports, BPSK is adopted as the simplest scheme, although BPSK and QPSK modulations are compulsory. It is required to balance the range of distances and the system performance per the use case, application, and deployment, i.e., range–rate trade-off policy.

3.3. Simulation Scenarios

The simulation scenarios are as follows (based on IEEE standard parameters [111]): The first simulation was to demonstrate the validity of using DF relaying rather than IRS for the same purpose to gain the mentioned benefits, and the values of all parameters can be found in [69]. The subsequent simulation was compared with the mathematical analysis and then simulated the work's main scenarios. Scenario1: Cooperative SWIPT THz- NOMA using equal distance for two stages (BS-NU and NU-FU) with moderate parameters' values of frequency, BW, power, and distance to compare it with the previous work. Scenario2: same system with an enlarging distance of each stage apart (BS-NU, NU-FU) changing parameters' values for distance adapting reason to compare the two cases with the main Scenario 1 to study the effect of distancing and changed parameters. For the two scenarios, set: (1) Transmission power, frequency, BW, and distance to be adjustable. (2) A simple target of 1 Gbps as a reference point for comparison. (3) Power (30 dBm) is used with Scenario 1 to cover more distance in case of having longer FU's distance (it could be 20 dBm or less). Accordingly, 42 dBm power is set with Scenario 2 while enlarging distances. (4) High path loss exponent assumed $\eta = 4$ as a worst-case scenario (while it could be less, such as urban or the best UDHNs case). The absorption coefficient can be found in [96]. The simulation results are based on the MATLAB program.

3.4. Simulation Results

In this section, numerical analysis and simulation were implemented to validate the optimized achievable rates and OP. Table 3.1 denotes the simulation parameters.

Table 3.1 Simulation parameters.

Parameters	Scenario1	Scenario2
Frequency	311.04 GHz	287.28 GHz
Bandwidth	12.96 GHz	69.12 GHz
Transmission power	30 dBm	42 dBm
Transmission distance	Phase1 = 10 m Phase2 = 10 m	(1) Phase1 = 15 m, Phase2 = 10 m (2) Phase1 = 10 m, Phase2 = 15 m
NU power coefficient		0.2 of total power
FU power coefficient		0.8 of total power
Antenna gain		25 dB
Path loss exponent		4
Target data rate		1 Gbps
EH conversion efficiency		0.7

As mentioned previously, the simulation results validate the derived closed forms of the proposed optimized system. These results are compared with that of previous work, whereas the same system is compared with the suggested Scenario 2, changing the metrics of the two cases. The system performance was investigated depending on some parameters that THz communication yields. The proposed mechanism should enable the blocked node to maintain ongoing communication while being shadowed by BS. The next sections explore the capability of this simple and scalable system to manage the THz transmission shortage, showing how this can improve SE, EE, reliability, and overall performance.

3.4.1. DF Relay vs. IRS

This section presents the simulation of DF relay-assisted source-to-destination connection versus IRS-assisted connection (as shown in Figure 3.2) to validate the reason behind using such a technique, utilizing its advantages compared with IRS based on the scenario shown in Figure 3.2 using the SISO technique.

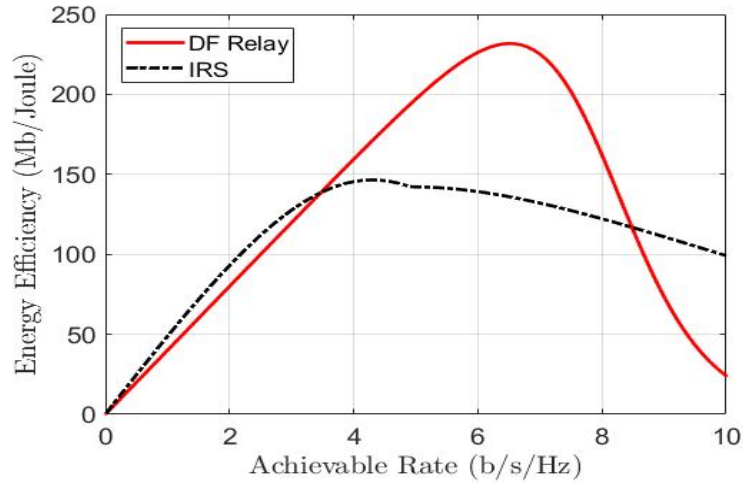


Figure 3.2 EE of DF Relay vs. IRS.

According to the comparison in Figure 3.2 [53], [69], DF relaying outperforms the new IRS technology (despite its unique advantages) in specific cases, whereas IRS needs a huge number of bulky power-consuming reconfigurable elements to be competitive because of the obtained low channel gain due to the two transmission stages it propagates from source to destination throughout reflection (e.g., IRS needs a place to be deployed in, with continuous maintenance); however, in DF relaying, the signal is transmitted twice with different channel gains. The EE of using DF relay with THz-NOMA, including EH, demonstrates the validity of this system even for very high-rate communications.

3.4.2. System Numerical Analysis and Simulation

In this section, mathematical analysis and simulation of the main system model are manipulated, exploring the system performance in terms of sum-throughput and OP based on the parameters of Scenario1 mentioned in Sections 4 and 5 (with 20 dBm transmit power) to validate this optimized system model analysis, achieving the intended objectives.

Figures 3.3 and 3.4 show a notable matching of analytical and simulation results, affirming the precision of analysis and proving the

validity of the proposed system model, gaining the novelty of added values (detailed next section).

3.4.2.1. Sum-Throughput against Transmit Power

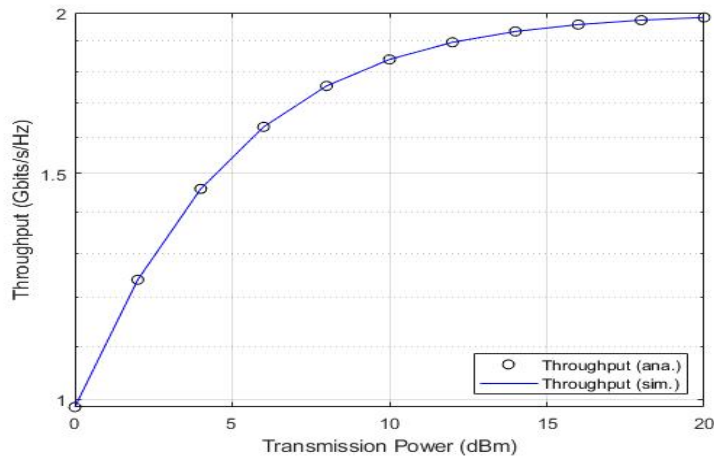


Figure 3.3 Throughput vs. transmit power.

3.4.2.2. Users' OP against Transmit Power

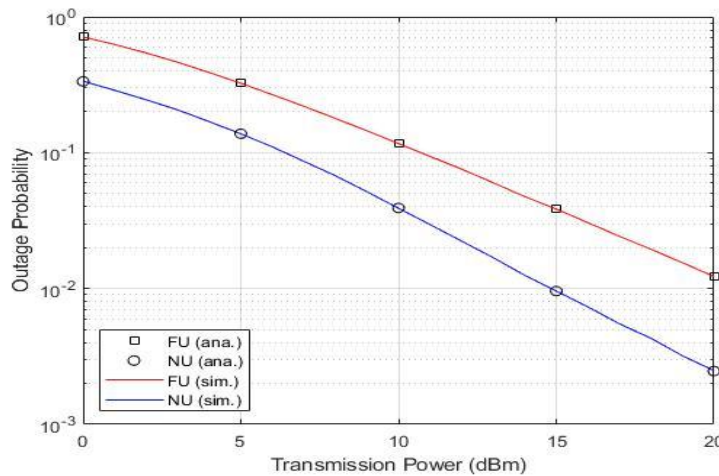


Figure 3.4 OP vs. transmit power.

3.4.3. System Simulation

This section presents the simulation of the main system model for every single user in three subsections to study the system performance based on the parameters of Scenario1 mentioned in Sections 4 and 5 to compare it with similar recent work and to demonstrate how the proposed system presents a valuable enhancement to the wireless communication field using the promising technologies.

3.4.3.1. Average Achievable Rate against Transmit Power

Figure 3.5 depicts the performance of users in accordance with allocated power. The NU is saturated at 1 Gbps/Hz due to the EH mechanism that uses only the required power to reach the targeted rate and capture all the remaining power, and the FU data rate keeps increasing (does not affect NU stability) by using the harvested power; however, the overused power of the FU can be exploited for more EH operations.

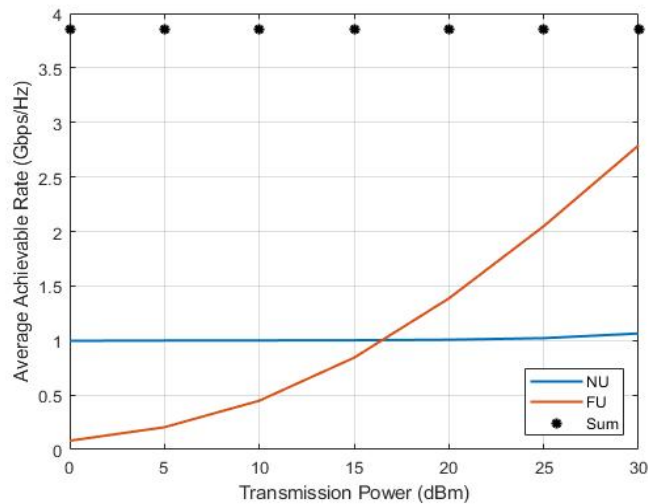


Figure 3.5 Achievable rate vs. transmit power.

3.4.3.2. OP against Transmit Power

As shown in Figure 3.6, the FU experiences a much greater outage than NU despite the larger (average) data rate in Figure 3.5 compared with NU, which is the normal performance according to their different conditions.

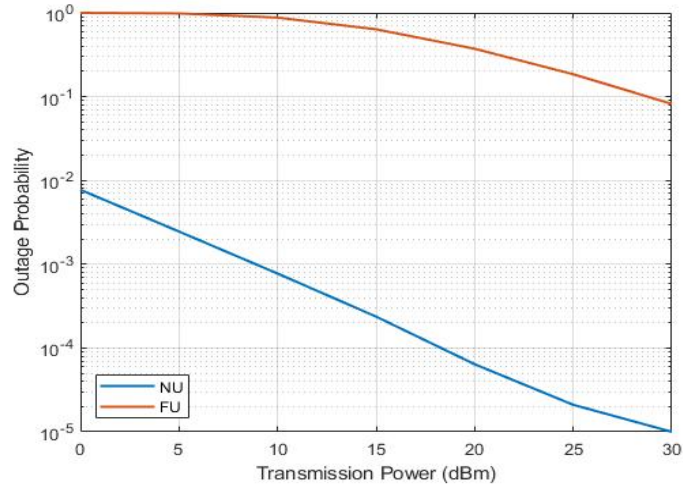


Figure 3.6 OP vs. transmit power.

3.4.3.3. Instantaneous Rates

To study users' performance accurately, instantaneous rates under channel realization are carried out.

In Figure 3.7, the FU still does not have better stability than the NU despite the higher data rate, and the FU instantaneous rate is pivoted around the same value it reached in Figure 3.5 with a few spikes beneath the target rate. This condition explains the reasonable difference in outage performance between the two users.

In a brief comparison, the proposed system outperforms that of [96] in terms of simplicity, cost-effectiveness, computational complexity, SE, and EE. The system in [96] reaches the reference point (1 Gbps) by using more power (60 dBm), whereas the proposed work reached that point with only 17 dBm. Similarly, a data rate of only 1 Mbps is achieved at 20 dBm, where this work achieves 1 Gbps for two users separately, showing the importance of the EH technique as a valuable contribution.

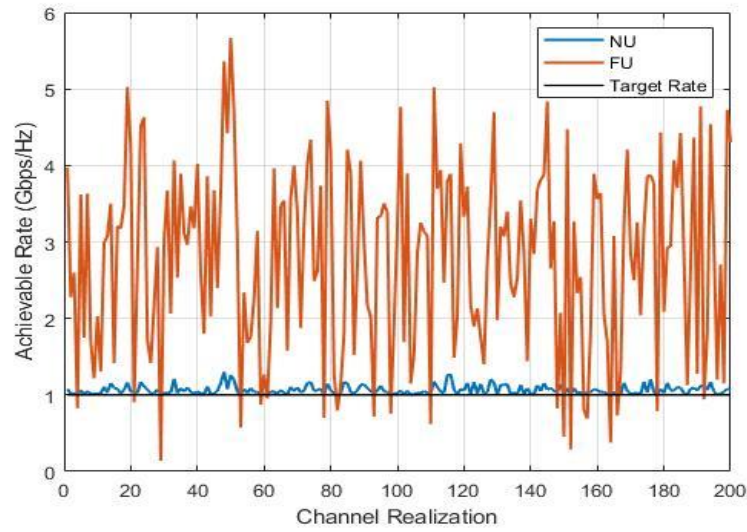


Figure 3.7 Instantaneous rate vs. channel realization.

3.4.4. Scenario1 vs. Scenario2

This section presents the simulation of the main system model Scenario1 versus Scenario 2 with its two cases in three subsections based on the parameters of Scenario1 and Scenario2 in Sections 4 and 5.

3.4.5. Average Achievable Rate against Transmit Power

Figure 3.8 illustrates an observable difference between the two scenarios and how the main Scenario1 outperforms Scenario2 at NU and FU despite setting better parameters' values to Scenario2 (lower frequency, wider BW, and much power). On the one hand, in Scenario1, NU is saturated at the target rate immediately, and FU is met at the NU at 17 dBm power, where the NU with a longer BS-NU distance is saturated using 1.4 dBm power, and the FUs of Scenario2 are met at their NUs using 31 dBm power. All Scenarios' FUs data rates still increase exactly as explained in Figure 9. On the other hand, the enlarged BS-NU distance case shows more transmission effect than the enlarged NU-FU distance case by comparing the two cases in Scenario2.

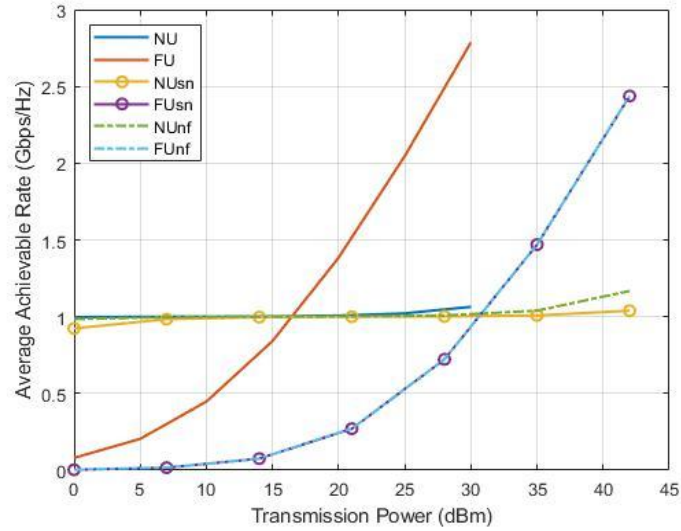


Figure 3.8 Achievable rate vs. transmit power.

3.4.6. OP against Transmit Power

In OP comparison, Figure 3.9 depicts how the main scenario outperforms Scenario2 in NU and FU despite setting better parameters' values to Scenario2 (lower frequency, wider BW, and much power). On the one hand, in Scenario1, NU and FU show better outage performance than NU and FUs of Scenario2. On the other hand, the enlarged BS-NU distance case shows more transmission effect than the enlarged NU-FU distance case, regarding NUs' outage performance by comparing the two cases in Scenario2. This condition is because the NU with a longer BS-NU distance OP is longer than that of a longer NU-FU distance.

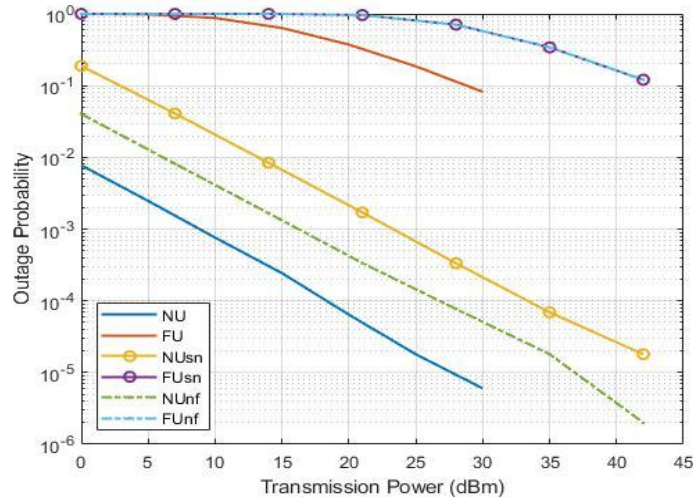


Figure 3.9 OP vs. transmit power.

3.4.6.1. Instantaneous Achievable Rates

To study users' performance accurately in all scenarios, instantaneous achievable rates under channel realization are simulated.

As shown in Figure 3.10, the main scenario outperforms Scenario2 in the NU and the FU despite setting better parameters' values to Scenario2 (lower frequency, wider BW, and much power) in terms of NU's stability and FU's fluctuation spikes. On the one hand, in Scenario1, NU and FU show better performance than NU and FUs of Scenario2. On the other hand, similar to the results in Figure 3.7, the enlarged BS-NU distance case shows more transmission effect than the enlarged NU-FU distance case, regarding NUs' stability and FUs' fluctuating spikes below the target rate by comparing the two cases in Scenario2.

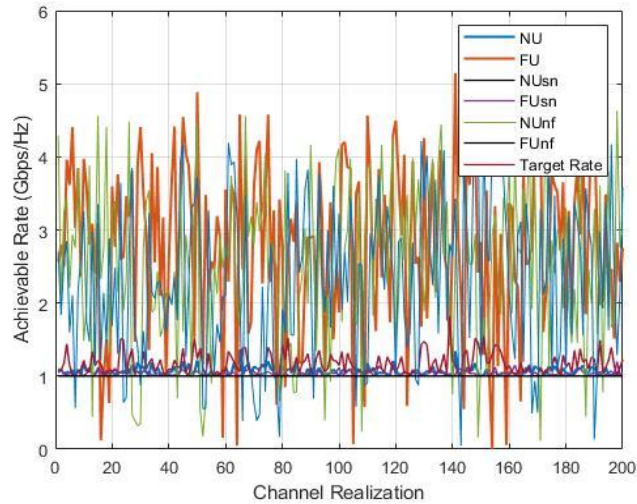


Figure 3.10 OP vs. transmit power.

The results of Section 5.4. demonstrate the importance of selecting the nearest user to the Bs to be a DF relay because the BS signal is logically the dominant controller in NOMA power allocation, unlike the signal that is transmitted by any DF relay while it harvests energy from BS and other surrounding sources, using that power for data retransmission for longer distance.

3.5. Summary

The work centered on the cooperative THz-NOMA system, exploring the application of the EH technique. The study derived optimal EH coefficients, achieving targeted Signal-to-Interference-plus-Noise Ratio (SINR), data rates, and SE. The comparative analysis demonstrated a 70% improvement in SE and EE over existing systems (i.e., [26], [53], [69], [94]–[96]), emphasizing the importance of proximity in DF relaying.

Chapter 4: Cooperative SWIPT MIMO-NOMA for Reliable THz 6G Communications

4.1. Introduction

This chapter provides a comprehensive explanation of the verification process for Cooperative SWIPT MIMO-NOMA for reliable 6G communications. It begins with outlining the system model design, followed by a discussion of the simulation scenarios, and concludes with an in-depth analysis of the simulation results.

4.2. System Model Design

Recent academic and industrial research stated the assumption of deploying UDHNs, with a large number of distributed base stations, access points, relays, and repeaters to the expected 6G densified infrastructure. The presented simple system in Figure 4.1 is suggested to solve the problems of the THz communications' lack of a coverage area, connection failures, and SIC complexity. Particular use cases are studied, e.g., rural areas, countryside, or any other place where IRS and other supporting equipment cannot be deployed, providing dynamic path selectivity in the case of the user's link failure. The system considers a small cell with MIMO-NOMA-based downlink transmission and two SWIPT-paired clustered users. The BS sends the superimposed signal simultaneously to both NOMA-served users, NU and FU. At a certain moment, the BS to FU path is blocked by an obstruction, resulting in significant shadowing. As a result, the FU is unable to identify its obstructed signal. The NU, on the other hand, establishes a strong connection with the BS.

According to NOMA principles, the NU is supposed to first decode the FU's signal before removing it by the SIC process, and then decode its intended signal. Hence, NU receives a copy of the FU's data, such that FU can rely on NU to connect to the BS by exploiting it as a DF relay. For relays, the energy in the NU's battery is insufficient to convey the data to the FU. To this end, it is recommended that NU makes use of EH's power-splitting protocol (SWIPT) to harvest energy from the surrounding radiofrequency energy to use it for this retransmission (relaying process). The transmission procedure is divided into two parts. The NU receives the BS superposed signal at the first phase, whereas the power-splitting procedure captures a portion of the NU's harvested power; however, the remaining power is used for data decoding. The captured energy is then used by NU to convey the FU's information to FU in the second phase.

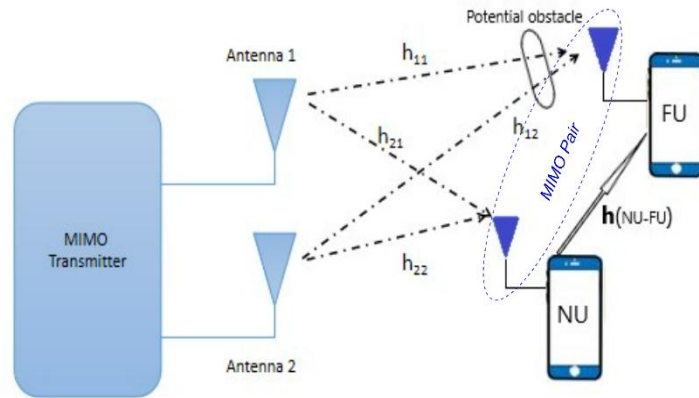


Figure 4.1 Cooperative SWIPT MIMO-NOMA in THz model.

A Rayleigh fading channel with mean = 0 and variance = Transmission Distance^{-THz total losses} was conducted in this analysis for all cases. AWGN with mean = 0 and variance of σ^2 is set, representing the added noise. PDF for point z is given by Equation (3.1).

As space attenuation and molecule absorption are considered in the cooperative SWIPT NOMA signal, the path loss of the NLOS link is

greater than that of the LOS link. If the LOS link prevails, then the NLOS impact can be ignored [95]. In free space, the THz total losses η is set as extraordinarily large. For the users k , the channel gain is given by Equation (3.2).

Where A denotes the MIMO antennas, G denotes the gain of the antenna, and η represents the source–destination THz total losses, given by Equation (3.3).

Where f denotes the THz, d denotes the source-destination distance, $a(f)$ represents the absorbing coefficient, and C denotes the velocity of light.

According to the proposed case, the closed-form derivations are presented below.

Stage 1, BS to NU transmission:

The BS superimposed signal is given by Equation (3.4).

Where P denotes the transmit power, α_n and α_f denote the NU and FU powers, respectively, and x_n and x_f denote the NU and FU signals, respectively. However, FU cannot detect its signal due to obstruction. The NU signal is given by.

$$h_{sn} = (h_{11} + h_{12}), \quad (4.1)$$

$$y_n = \sqrt{P}(\sqrt{\alpha_n} x_n + \sqrt{\alpha_f} x_f)(h_{11} + h_{12}) + w_n, \quad (4.2)$$

Where $h_{sn} (h_{11} + h_{12})$ is the base station to the near user (BS-NU) Rayleigh fading coefficient with mean = 0 and variance of $d_{sn}^{-\eta}$, d_{sn} denotes the BS-NU distance, and w_n is the AWGN with mean = 0 and variance of σ^2 . Using y_n , NU captures a portion of energy named the EH coefficient (ψ). The remaining energy portion ($1 - \psi$) is allocated to data decoding. With EH, the data decoded signal is given by Equation (3.6).

Where W_{eh} denotes thermal noise (zero mean and variance of σ^2). For the mathematical process, the W_n harvested energy is abandoned; consequently, y_D is given by Equation (3.7).

As a function of y_D , NU decodes X_f straightaway. The NU rate to decode FU's data is calculated as:

$$R_{nf} = \frac{1}{2} \log_2 \left(1 + \frac{(1-\psi)P \alpha_f |h_{11} + h_{12}|^2}{(1-\psi)P \alpha_n |h_{11} + h_{12}|^2 + \sigma^2} \right). \quad (4.3)$$

With SIC, the NU rate of NU information decoding is calculated as:

$$R_{nf} = \frac{1}{2} \log_2 \left(1 + \frac{(1-\psi)P \alpha_n |h_{11} + h_{12}|^2}{\sigma^2} \right), \quad (4.4)$$

where ψ is the captured EH coefficient during the first phase. EH is calculated as:

$$P_H = P |h_{11} + h_{12}|^2 \zeta \psi, \quad (4.5)$$

where ζ denotes the circuitry EH efficiency.

Stage 2, NU to FU DF-relaying:

Using the gathered energy, NU conveys the data to FU (PH). As a result, the NU's sent signal is given by Equation (3.11).

The detected signal at FU is given by Equations (3.12) and (3.4).

$$H_f = \min\{(H_{21} + H_{22}), H_{nf}\}, \quad (4.6)$$

where h_f denotes the minimal Rayleigh fading channel of the selected path between the BS and FU (i. e., $(H_{21} + H_{22})$ or H_{nf}), and H_{nf} is the NU-to-FU Rayleigh channel. The rate of the FU is given by Equation (3.13).

In the first stage, NU is supposed to decode the FU's information to determine the ideal power-splitting coefficient, allowing it to properly retransmit FU's data. To do so, the constraint $R_{nf} > R_f^*$ was set.

The FU target rate is R_f^* . This criterion implies that the NU rate for decoding FU data must be higher than the FU intended rate. To derive ψ , R_{nf} in Equation (4.4) is substituted into the assumed constraint presented in Equations (3.14, 3.15, and 3.16).

The term $2^{2R_f^*} - 1$ is represented by τ_f to denote the FU-targeted SINR, given by Equations (3.17, 3.18, 3.19, 3.20, and 3.21).

To guarantee a smaller value of ψ , the above Equation can be reshaped as given in Equation (3.22).

where δ is represented by a very small value (i.e., 10^{-6}); then, ψ guarantees the needed energy to decode the data, achieving the FU targeted rate.

Outage Probability:

It is every user's chance that the data rate will drop beneath the target. R_n^* and R_f^* (bits/s/Hz) are the NU and FU targeted rates, respectively.

FU is considered to fail whenever R_f in Equation (3.16) is smaller than the targeted rate, represented in Equation (3.23).

The NU must accurately decode both signals: the FU signal and its signal. The NU and FU targeted rates must be equal to the NU rate. When using SIC, if the NU or FU targeted rates in Equations (3.11) and (3.16) are not sufficient, NU experiences an outage, which is represented in Equation (3.24).

Following up on the first mode described in the PHY section of [109] of the THz single carrier frequency. This idea is recommended for high-speed transmission links aimed at BW-based cases, e.g., links of backhaul/backhaul, fronthaul/backhaul, and between data center racks [110]. Due to atmosphere and impact, the accessible spectrum is divided into multiple channels on the basis of the spectral windows of THz frequencies (from 252.72 to 321.84) GHz, with each channel having its own features [110]. There are multiple cases of 2.16 GHz within the THz spectrum, whereby six channels and eight bands (from 2.16 to 69 GHz) are discovered. According to some criteria and constraints, these spectral windows can be determined.

Despite the variety of available modulation types in THz-SC PHY (BPSK and QPSK are required), BPSK is utilized as the simplest scheme among the different supported modulations. Transmission distance and system performance are the critical measures that must be balanced on the basis of system metrics, considering a range-to-rate tradeoff strategy [66].

4.3. Implementation

The first implementation is to show that the simulation is valid when compared to the mathematical analysis. The simulation described below compares the recent similar system equipped with the SISO scheme as a baseline to this work's scenario of cooperative SWIPT THz MIMO-NOMA, utilizing moderated parameter settings for transmit frequency, allocated BW, transmit power, and transmit distance.

- (1) Transmit power, frequency, distance, and BW can be adjusted.
- (2) Targeted rates are 1 Gbps for the FU and 3 Gbps for the NU.
- (3) A power of -30 to 30 dBm is dedicated to cover a wider area if the FU goes farther. Hence, transmit power can be reduced.
- (4) A relatively high path-loss exponent $\eta=4$ is set; hence, it can be reduced.

The absorption coefficient can be found in [96]. The simulations were implemented using *MATLAB*[®].

4.4. Simulation Results

This section includes the implementation of simulations and numerical analysis to verify the validation of data rates and OP. The simulation findings confirm the obtained closed forms of the optimized model, and they are compared to earlier research. By existing an obstruction in the link to the BS, the presented mechanism should allow the obstructed user to maintain continuous communication. The sections below explain how the proposed system and mechanism can enhance EE, SE, reliability, and system performance by addressing the distance-limited

communications of THz frequencies. Table 4.2 shows the simulation parameters.

Table 4.2 Simulation parameters.

Notation	Parameters	Value
f	Frequency	311.04 GHz
BW	Bandwidth	12.96 GHz
P	Transmission power	30 dBm
D	Transmission distance	Phase 1 = 20 m
		Phase 2 = 30 m
α_n	NU power coefficient	0.25 of total power
α_f	FU power coefficient	0.75 of total power
G	Antenna gain	25 dB
eta	Path loss exponent	4
	Target data rate	3, 1 Gbps for NU, FU

4.4.1. System Validity Analysis

In contrast, mathematical analysis and simulation were carried out to compare the system sum throughput and OP, using a transmission power of 20 dBm for system validation, verifying the intended objectives.

Figures 4.2 and 4.3 exhibit the striking match between the mathematical analysis of the derived close forms and simulation results. They confirm the analysis accuracy and system validity, including the uniqueness of new values. System metrics are thoroughly studied throughout the remaining parts of this work.

4.4.1.1. Sum Throughput Versus Transmit Power

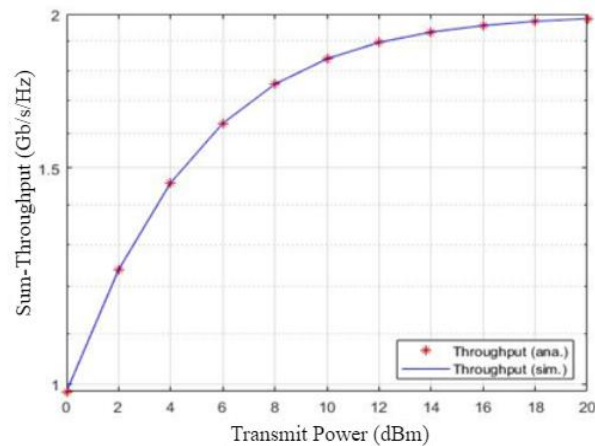


Figure 4.2 Throughput vs. transmit power.

4.4.1.2. Users' OP versus Transmit Power

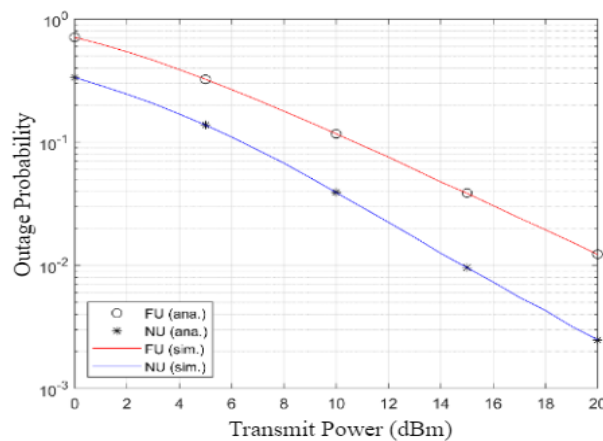


Figure 4.3 OP vs. Transmit Power.

4.4.2. System Simulation

First, the performance of the system's served users was individually implemented, and then the entire system's sum rate was examined. The performance was compared with the previous similar SISO-based system model (as a baseline) to explain how the presented system provides a remarkable improvement of the current wireless communication systems, by employing the edge of technologies mentioned in this work.

4.4.2.1. Achievable Users' Rates versus Transmit Power

Figure 4.4 demonstrates the system users' performance versus the dedicated power. For the two users, the MIMO technique provides

remarkable leverage to system performance compared to the SISO scheme. The NU performs much better than the FU, despite the EH technique allocating the essential energy to achieve the target rate and harvesting the remainder for retransmission, thus clarifying the impact of comparative THz losses. However, the FU still achieves a data rate greater than the target despite the interference it experiences (as the FU does not perform the SIC process). Furthermore, the harvested power could be utilized for further EH processes.

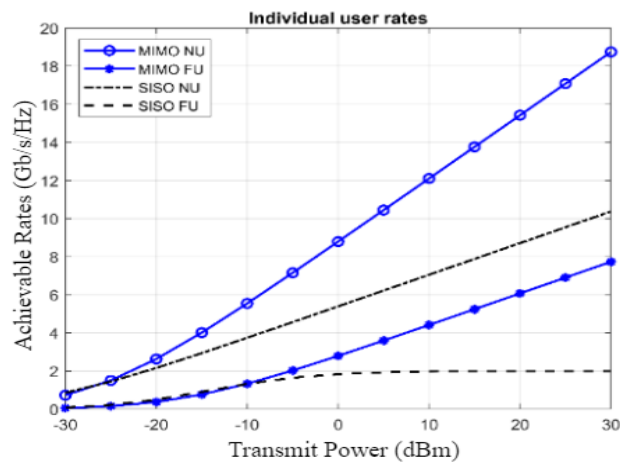


Figure 4.4 Rates vs. transmit power.

4.4.2.2. OP versus Transmit Power

Similarly, for both NOMA users, the MIMO technique provides a notable enhancement of system performance compared to the SISO scheme, as shown in Figure 4.5. Despite having more dedicated power than the NU, the FU has a higher outage. This reflects the expected performance given their distinct channel variations.

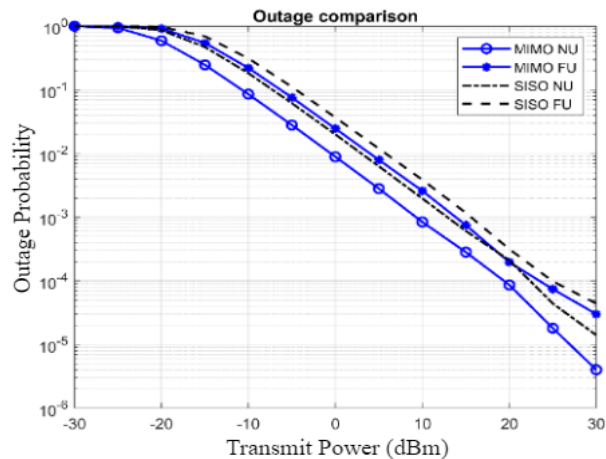


Figure 4.5 OP vs. transmit power.

4.4.2.3. Achievable Sum Rates versus Transmit Power

In Figure 4.6, it is proven that the MIMO technique provides added value through a remarkable impact on the system performance compared to the SISO scheme. Moreover, the presented system outperforms the state of the art considering the previously proposed simpler and cost-effective model, which has lower complexity and achieves higher EE and SE. Hence, this system achieves the same target for the two users using relatively less power than allocated in previous research (e.g., [96]). This demonstrates the significance of using the energy-harvesting technique with the proposed strategy, representing additional gain and a significant contribution.

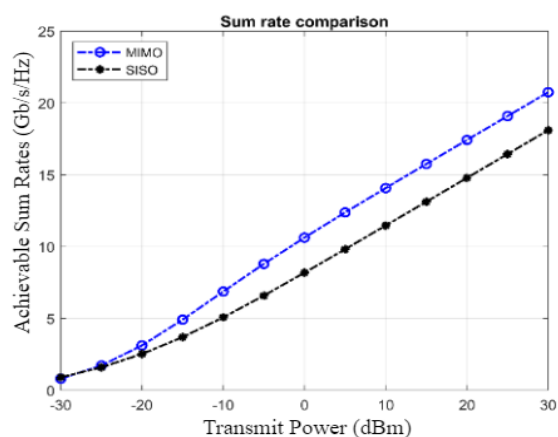


Figure 4.6 Sum rates vs. transmit power.

In contrast, MIMO-NOMA systems might face some drawbacks, e.g., the computational complications of MIMO and procedural complexity of SIC-dependent NOMA, as SIC is widely thought to be implemented flawlessly, notwithstanding the possibility of procedural errors. Thus, it is critical to keep the number of users per cluster as low as possible, as user CSI acquisition has a significant impact on SIC implementation.

4.5. Summary

The work delved into applying the EH technique in a cooperative MIMO-NOMA system for THz communications. This research surpassed comparable studies (i.e., [26], [41], [53], [69], [94]–[96]) , achieving over 50% gains in reliability, OP, SE, and EE compared to basic NOMA. The findings highlighted the success of defined strategies in preserving communication between the BS and potentially obstructed users, offering a dynamic path-selection mechanism for enhanced reliability.

Chapter 5: A Cooperative SWIPT-Hybrid-NOMA Pairing Scheme considering SIC imperfection for THz Communications

5.1. Introduction

This chapter provides a comprehensive explanation of the verification process for A Cooperative SWIPT-Hybrid-NOMA Pairing Scheme considering SIC imperfection for THz Communications. It begins with outlining the system model design, followed by implementation, and concludes with an in-depth analysis of the simulation results.

5.2. System Model

The proposed system (shown in Figure 5.1) operates in large open areas where downlink THz-NOMA small-cell with four users cluster is considered, using a SISO scheme equipped with high-directional antennas. The BS superimposes signals to the served users, near users (NUs), and far users (FUs), where pairing is assumed for every two SWIPT-based users in a cluster, but an obstacle keeps the far two users (U1 and U2) shadowing from the BS at a given time. As a result, far-away users are unable to detect their signals effectively, however, the channel gains of the nearby users (U4 and U3) are sufficient. According to NOMA principles, all FU signals must first be decoded by NUs before SIC can be used to remove them and consequently decode NUs' data. As a result, NUs already hold copies of the FUs' data. Therefore, NUs can assist FUs in connectivity by acting as a DF relay. The energy in the NUs batteries, on the other hand, is insufficient to convey the information to the FUs. It is proposed that NUs use the EH power-splitting protocol (SWIPT) to capture power from BS and radiofrequency energy surrounding them for this purpose during the next level. The entire transmission procedure is split into two parts. NUs

receive the transmitted signal from BS at the first step. The power-splitting mechanism will collect a portion of NUs' received powers, while the left power will be used to decode their data. The NUs then use the captured energy to convey FUs' information to them in the second step.

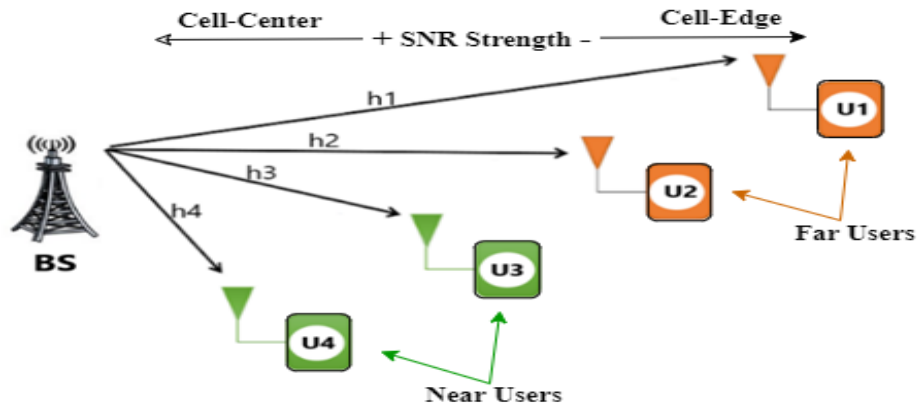


Figure 5.1 SWIPT-paired H-NOMA system.

The channel model and mathematical analysis of cooperative SWIPT NOMA-THz can be found in the previous work [66].

Figure 5.2 explains the concept of H-NOMA as a combination of NOMA and OMA (e.g., TDMA) schemes. It clarifies the probable pairs for the served users assumed in the proposed system model.

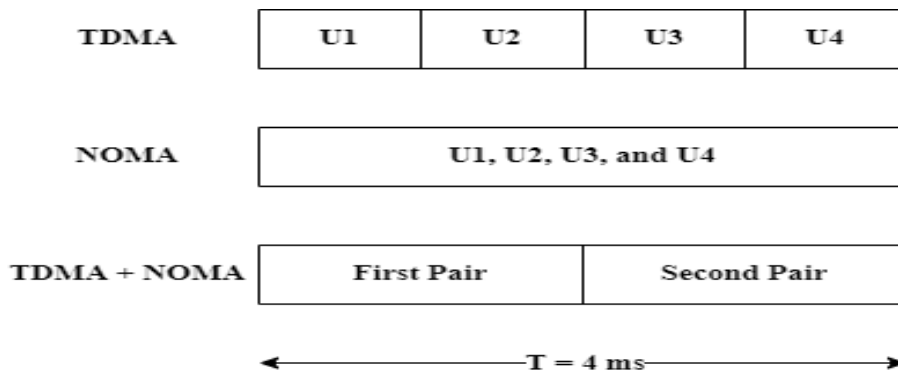


Figure 5.2 Hybrid-NOMA strategies.

Based on Figure 5.1 and Figure 5.2, the two pairing techniques suggested are:

- (1) Near-Far (N-F) pairing technique:

The N-F technique pairs BS's closest user (U4) with BS's farthest user (U1). The second closer user (U3) of BS is paired with the second

farther user of BS (U2). Thus, in the first resource block, the N-F pairing method pairs U4 with U1, and in the second resource block, U3 with U2.

U4 is a NOMA near user (NU) and U1 is a NOMA far user (FU) in the first pair, but power fractions must be allotted using the constraint $\alpha_4 < \alpha_1$. As a result, U4 must perform SIC before decoding its signal, but U1 can simply decode its signal. U3 is NOMA NU and U2 is FU in the second pair, however, power fractions must be distributed using the constraint $\alpha_3 < \alpha_2$. As a result, U3 must execute SIC while U2 directly decodes its signal.

Within the first pair, users' achievable rates are:

$$R_{4,nf} = \frac{1}{2} \log_2 \left(1 + \frac{P\alpha_4|h_4|^2}{\sigma^2} \right) \quad (5.1)$$

$$R_{1,nf} = \frac{1}{2} \log_2 \left(1 + \frac{P\alpha_1|h_1|^2}{P\alpha_4|h_1|^2 + \sigma^2} \right) \quad (5.2)$$

Similarly, for the second pair:

$$R_{3,nf} = \frac{1}{2} \log_2 \left(1 + \frac{P\alpha_3|h_3|^2}{\sigma^2} \right) \quad (5.3)$$

$$R_{2,nf} = \frac{1}{2} \log_2 \left(1 + \frac{P\alpha_2|h_2|^2}{P\alpha_3|h_2|^2 + \sigma^2} \right) \quad (5.4)$$

The sum rate is calculated as:

$$R_{nf} = R_{1,nf} + R_{2,nf} + R_{3,nf} + R_{4,nf} \quad (5.5)$$

(2) Near-Near, Far-Far (N-N, F-F) pairing technique:

In this technique, the nearest user (U4) is paired with a second nearer user (U3), while the distant user (U2) is matched with a second farther user

(U1). Thus, in the first resource block, the N-N, F-F pairing approach pairs U4 with U3, and in the second resource block, U2 with U1.

When compared to U3, U4 is a NOMA NU. As a result, it is needed to allot $\alpha_4 < \alpha_3$. Before decoding its signal, U4 must execute SIC, whereas U3 decodes it directly. In comparison to U1, U2 is a NOMA NU within the opposite pair. As a result, it requires allotting $\alpha_2 < \alpha_1$, while U2 must execute SIC while U1 directly decodes its signal. Within the first pair, users' achievable rates are:

$$R_{4, \text{nn}} = \frac{1}{2} \log_2 \left(1 + \frac{P\alpha_4|h_4|^2}{\sigma^2} \right) \quad (5.6)$$

$$R_{3, \text{nn}} = \frac{1}{2} \log_2 \left(1 + \frac{P\alpha_3|h_3|^2}{P\alpha_4|h_3|^2 + \sigma^2} \right) \quad (5.7)$$

Similarly, for the second pair: 1 and 2

$$R_{2, \text{nn}} = \frac{1}{2} \log_2 \left(1 + \frac{P\alpha_2|h_2|^2}{\sigma^2} \right) \quad (5.8)$$

$$R_{1, \text{nn}} = \frac{1}{2} \log_2 \left(1 + \frac{P\alpha_1|h_1|^2}{P\alpha_2|h_1|^2 + \sigma^2} \right) \quad (5.9)$$

The sum rate is calculated as:

$$R_{\text{nn}} = R_{1, \text{nn}} + R_{2, \text{nn}} + R_{3, \text{nn}} + R_{4, \text{nn}} \quad (5.10)$$

THz atmospheric attenuation and molecular absorption are taken into consideration in signal modeling of cooperative SWIPT H-NOMA [112]. As the path loss of NLOS is significantly greater than that of the LOS path, NLoS impact may be neglected if the LOS path takes precedence [65]. Hence, THz total loss value is set very high.

Based on the Physical layer section THz for high-data-rate communications aimed at BW-demanding applications such as wireless backhaul/backhaul, fronthaul/backhaul, or data center links [111]. Due to free-space effects, [110] split the THz spectrum into 69 overlapping channels with 8 BWs (2.16 - 69 GHz) based on THz spectral windows (252.72 – 321.84) GHz. BPSK and quadrature phase shift keying (QPSK) modulations are required; therefore, the simplest scheme (BPSK) is applied to achieve the trade-off between scale and efficiency [111].

5.3. Implementation

The impact of the SWIPT-pairing strategy in conventional NOMA, OMA (TDMA), and H-NOMA schemes based on Figure 5.2 were studied. For the four users, distant users (i.e., U1 and U2) and the near users (i.e., U3 and U4), the users' associated transmission channels (i.e., h_1 , h_2 , h_3 , and h_4). The approach serves the farthest blocked users (or distant users in the cell edge with weak SNR).

5.3.1. NOMA Users' Capacities

The first system implementation examines the performance of all the served users in Figure 5.1, considering them as SWIPT-based NOMA relaying users (near users). The achievable capacities of individual users will be studied when performing SIC to explore the procedural complexity and the influence of SIC imperfection on SIC-dependent signal detection.

5.3.2. H-NOMA Vs. Other multiple-access schemes

The second system implementation examines each possible SWIPT-pairs of users in Figure 5.1 using the H-NOMA concept in Figure 5.2, e.g., (N-F) and (N-N, F-F) techniques. It investigates the feasibility of applying H-NOMA (studying the best SWIPT-pairing strategy) to the proposed system to achieve the best performance, overcoming conventional NOMA and OMA challenges. This Utilizes all the possible SWIPT pairs with the

available LOS users to specify the best pairing, achieving the best performance.

The simulation scenarios are as follows (parameters can be found in [66]):

The first simulation is to prove the validity of using H-NOMA instead of NOMA for the same purpose to gain the utmost benefits as compared to conventional NOMA or TDMA, comparing the sum-throughput with the mathematical analysis. Then simulate the work's main scenario to investigate the three possible SWIPT pairs with the blocked user (U1), using parameters' values of frequency, BW, power, and distance to compare the system performance of every pair.

Hence:

- 1) Transmit Power, frequency, BW, and distance are adjustable.
- 2) High Path loss is assumed $\eta = 4$ (adjustable depending on the use case). the absorption coefficient is found in [96]. The simulations were implemented by the MATLAB program. Figure 5.2 shows H-NOMA pairing strategies.

5.4. Simulation Results

The simulation of the proposed system model is carried out to prove the validity of system compatibility. All possible SWIPT pairs for the two far users (U1 and U2) are studied (i.e., pairing techniques). Accordingly, system performance is examined considering some factors that THz communication provides. When the far nodes' links fail to connect to the BS due to an obstruction, the proposed solution should allow them to keep communicating. Investigating how this simple and scalable system may be used to control THz transmission restrictions demonstrates how it can increase SE, EE, reliability, and overall performance. In comparison to traditional systems, the simulation results validate the derived closed-form of the optimized system.

5.4.1. NOMA Users' Capacities

The first implementation shown in Figure 5.3 represents the achievable rates of SWIPT-based individual users as NUs when performing SIC the farthest user is assumed as a relaying user for a default far user (i.e., assumed perfect-SIC).

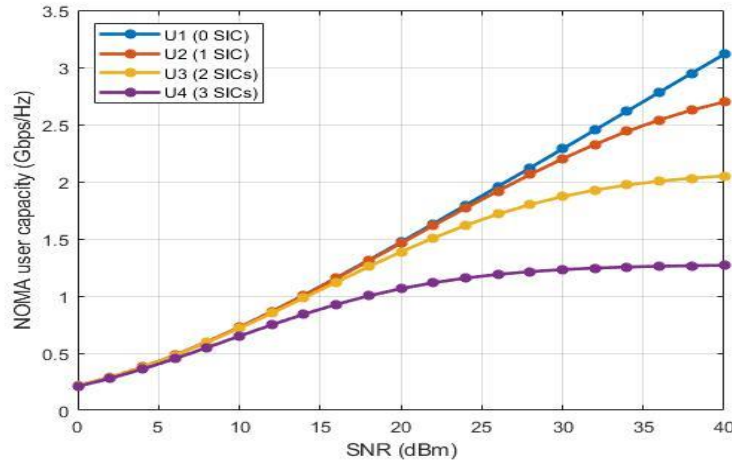


Figure 5.3 NOMA Users' Capacities Vs SNR.

Figure 5.3 depicts users' performance individually performing as NOMA relaying NUs. The farthest user (U1) shows the best performance as SIC is perfectly implemented (i.e., there is not any interference from other users' signals or sequential SIC errors propagated from previous SIC operations) and ultimately, SIC imperfection does not affect its capacity. However, the users U2, U3, and U4 show a gradual degradation in the rates because of the interference of the far users' remaining signal that will be considered as an additional noise to them in case of imperfect SIC. That demonstrates the detrimental impact of SIC accuracy on signal detection due to the interference of the farther users' residues with the SIC-dependent decoded signal. It clarifies the fact that achievable rates' degradation is proportional to SIC error propagation.

5.4.2. H-NOMA Vs. Other multiple-access schemes

This section includes simulating H-NOMA strategies of Conventional Single-Carrier NOMA (SC-NOMA) and OMA (TDMA) in

Figure 5.4 to validate the idea behind using the best scheme and pairing strategy compared to other multiple-access schemes based on the scenario shown in Figure 5.1 and Figure 5.2.

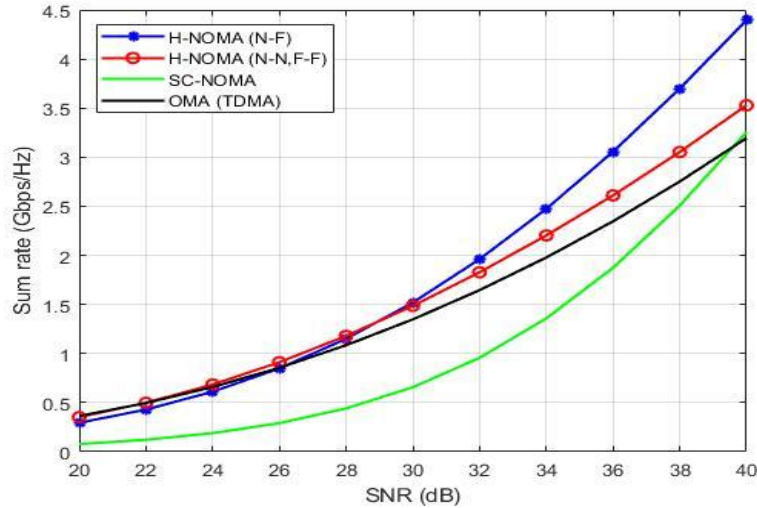


Figure 5.4 System SE Vs. SNR of H-NOMA strategies, NOMA, and OMA.

According to the comparison in Figure 5.4, it could be noticed that NOMA (N-F) strategy outperforms the other strategies in certain cases, meaningfully with THz. It confirms the possibility of taking full advantage of NOMA when the channel conditions difference between NUs and FUs are distinct. With (N-N, F-F) strategy, NOMA still performs better than TDMA, but without a significant improvement. The performance of SC-NOMA is not sufficient because of the interference due to the overloading of users sharing one carrier and the complex error propagating SICs, which accordingly cause interference and complexity issues. Therefore, it is not preferable to increase the number of served users within a single cluster while using a single carrier. However, the SWIPT-paired (two-user clustering) strategy shows a noticeable enhancement of SE and accordingly EE, the harvested power in the SWIPT-based NU is entirely allocated to the FU throughout the relaying stage.

5.5. Summary

The work explored the cost implications of promising technologies, especially those involving complex power-consuming systems. This research addressed the impact of NOMA SIC-imperfection and proposed the best THz H-NOMA SWIPT-paired strategy, enhancing overall performance by 75% over the conventional work (i.e., [66], [67], [94]–[100]). The study emphasized the significance of selecting SWIPT pairing based on the nearest user to the BS, considering location and channel conditions.

Chapter 6: SWIPT-Pairing Mechanism for Channel-Aware Cooperative H-NOMA in 6G Terahertz Communications

6.1. Introduction

This chapter provides a comprehensive explanation of the verification process for the SWIPT-Pairing Mechanism for Channel-Aware Cooperative H-NOMA in 6G Terahertz Communications. It begins with outlining the methodology, followed by implementation, and concludes with an in-depth analysis of the results and discussion. As well as the Optimal SWIPT-Pairing Mechanism and System Numerical Analysis and Simulation.

6.2. Methodology

This section is divided into two sub-sections; the first section studies H-NOMA pairing possibilities and optimizes the optimal pair to the associated users within the cell, whereas the second section studies the best SWIPT-pairing for the farthest blocked user (or distant cell-edge users). The main system model is shown in Figure 6.1; hence, some of the mathematical derivations were developed from the previous analysis conducted in [57], [64], [66].

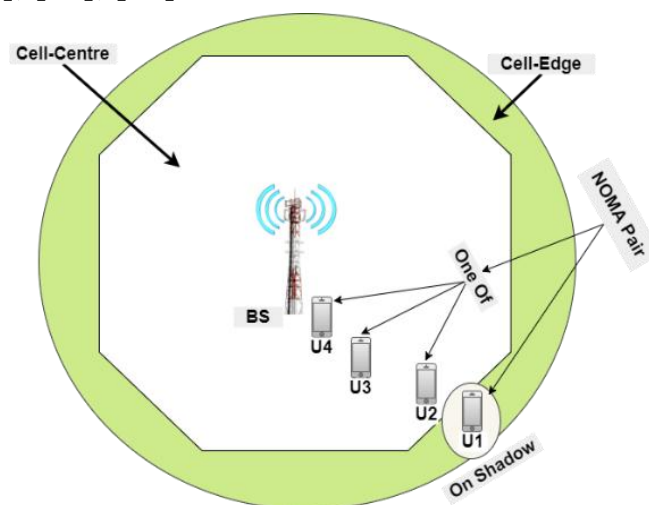


Figure 6.1 Main system model.

The transmission is considered over the Rayleigh channel (mean = 0, variance = Transmission Distance^{-THz losses}) with AWGN (mean = 0, variance = σ^2). PDF of a certain point is given by Equation (3.1).

6.2.1. The Best Hybrid-NOMA Strategy:

This sub-section includes the study of the impact of the user-pairing scheme in NOMA–OMA multiple access (Figure 6.2) to be adopted for the next SWIPT-pairing sub-section.

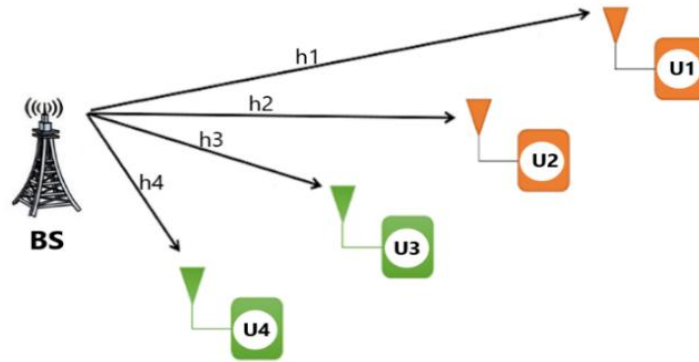


Figure 6.2 Hybrid-NOMA pairing strategy.

6.2.2. Near–Far pairing (N–F)

With the N–F strategy, the nearest user to the BS (User4) pairs with the farthest user (User1). BS’s nearer user (User3) pairs with the second farther user (User2). Thus, in this strategy, User4 and User1 are paired in the first block, whereas User3 and User2 are paired in the second block.

Within the first pair, User4 represents the NU, while User1 is the FU; however, power coefficients are required to be allocated by setting $\alpha_4 < \alpha_1$. Thus, User4 requires SIC implementation before detecting its intended signal, while User1 decodes its intended signal directly without SIC. Within the second pair, User3 represents NU, whereas User2 represents the FU; however, power coefficients must be allocated by setting $\alpha_3 < \alpha_2$. Thus, User3 implements SIC, whereas User2 detects its intended signal directly.

In pair 1, the rates of the users are given by Equations (5.1) and (5.2). Similarly, for the second pair, given by Equations (5.3) and (5.4)

Hence, P denotes transmit power, α_n and α_f are power coefficients of the near user and far user, respectively, and x_n and x_f denote the signals of the near user and far user, respectively.

The far user is not able to detect its signal because of the blockage; however, for the signal of the near user, NU's rate is given by Equation (5.5).

6.2.3. Near–Near, Far–Far pairing (N–N, F–F)

The N–N, F–F strategy addresses that User4 pairs to User3, whereas User2 pairs to User1. This strategy pairs User4 to User3 and User2 to User1 for the two blocks.

In this strategy, U4 is NOMA NU as compared to U3. Therefore, it must allocate $\alpha_4 < \alpha_3$. User4 requires SIC implementation before detecting its intended signal, while User3 decodes its intended signal directly without SIC. In the other block, U2 is NOMA NU as compared to U1. Accordingly, allocate $\alpha_2 < \alpha_1$. Thus, User2 performs SIC and User1 decodes directly. The rates in the first block are given by Equations (5.6) and (5.7). Similarly, for the second pair, given by Equations (5.8) and (5.9). The NU rate is given by Equation (5.10).

6.2.4. The Best SWIPT-Pairing Mechanism

In this sub-section, SWIPT-pairing is studied with three scenarios of pairing using one of the three available LOS near users (U4, U3, or U2) to be the DF relay pairing user with the targeted far user (U1), and then developing a suitable mechanism to select the best SWIPT-pairing user using the minimum (min) function to find the lowest (nearest) channel fading of the available LOS users to be paired with the blocked farthest user to achieve the highest channel gain difference for the optimal NOMA

pair. Otherwise, the mechanism selects the second-lowest fading (second-near) user, and so on.

Based on the Rayleigh fading Equation, a mechanism of selecting the best pairing user is proposed to act as a relay to the user1 and set the minimal Rayleigh fading channel.

$$R=\min\{H^k\} \quad (6.1)$$

Where R is the selected relaying user, and H is a vector of Rayleigh channels for k-number of users; however, propose $k = 4$.

Based on NOMA principles, the selected user is the NU (DF relay user), whereas the blocked user is the FU.

In the proposed system model, as there are 3 LOS available users with FU, the NU selection mechanism is expressed as:

$$NU=\min\{h2,h3,h4\} \quad (6.2)$$

Where h_2 , h_3 , and h_4 denote the Rayleigh fading channels of user2, user3, and user4, respectively, (each with its distance with the BS).

The proposed mechanism (shown in Figure 6.3) works in spacious open areas such as rural territories or the countryside (i.e., it is not possible to deploy other network equipment to aid THz communications). The system considers a downlink THz NOMA-based single-cell serving 4 users, where all the parties are provided with single highly directed antennas. The Tx party (BS) combines users' signals to broadcast them to the Rxs (i.e., various channel-conditioned users) including the paired user (NU and FU), assuming that there is an existing obstacle blocking the BS-U1 link. Accordingly, U1 cannot receive the signal efficiently. The potential NU (U4, U3, or U2) has a sufficient channel gain. Based on NOMA, the signal of the FU is decoded and canceled by the NU implementing SIC before decoding the NU information signal. It is worth noticing that NU receives and decodes FU's signal. Therefore, NU could

aid FU's connection as a DF-relay. To this end, the NU's device power does not suffice to retransmit FU's signal. Thus, NU is suggested to perform SWIPT to harvest energy from radiofrequency energy surrounding it. The communication process is carried out in two phases; the sender's combined signal is received by NU in the initial phase. By adopting the power splitting technique, a portion of the received power will be captured, and the remaining power will be used for information decoding. The captured power is then used by NU to retransmit the signal to the FU.

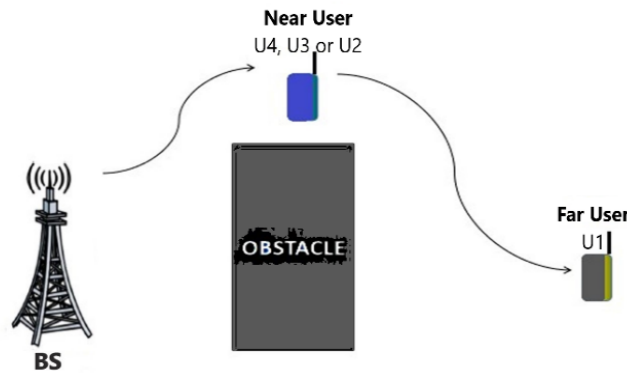


Figure 6.3 Cooperative SWIPT hybrid THz NOMA model.

The proposed system takes into consideration THz frequency characteristics and losses. Transmission link loss in the path NLOS is much more than link loss in LOS; thus, the NLOS impact could be neglected when LOS governs [66]. In this work, THz losses (η) are presumed to be very high. The channel gain can be calculated as given by Equation (3.2).

Hence, A denotes antenna number, G refers to antenna gain, and η denotes THz source-to-destination losses, given by Equation (3.3).

Hence, f denotes frequency, d denotes source-to-destination distance, $a(f)$ denotes absorption coefficient, and c denotes light speed.

The derived closed form according to the proposed scenario is:

Stage 1: The transmission of the superimposed signal in the first stage is shown in Equation (3.4).

Where P denotes transmit power, α_n and α_f are the power coefficients of NU and FU, respectively, and x_n and X_f are the power signal of NU and FU, respectively. Due to the blockage, FU is not able to receive its signal, whereas the received signal at the NU is given by Equation (3.5).

Hence, H_{sn} represents the BS-to-NU Rayleigh channel (mean = 0, variance = $d_{sn}^{-\eta}$), d_{sn} denotes the BS-to-NU transmission distance, and W_n refers to AWGN (mean = 0, variance = σ^2). Out of y_n , NU extracts a portion of power as the EH coefficient (ψ). The rest of the energy ($1-\psi$) is allocated to decode its data, which is represented by Equation (3.6).

Hence, w_n refers to thermal noise (zero mean, variance= σ^2). The tiny EH value of w_n can be neglected; thereby y_D is given by Equation (3.7):

From (17), NU decodes X_f directly first. The achievable rate of the decoded FU's data by the NU is given by Equation (3.8). By implementing SIC, NU's rate is given by Equation (3.9). The harvested energy during phase 1 is represented by Equation (3.10). Hence, ζ denotes the electronic circuits' EH efficiency.

Phase 2: In the next phase, by allocating the harvested energy (PH), NU retransmits the data meant for FU. Consequently, NU's sent signal is given by Equation (11).

Accordingly, the signal at FU is given by Equation (3.12).

Where h_{nf} denotes the NU–FU Rayleigh fading channel. The achievable rate at the FU is given by Equation (3.13).

In order to evaluate the ideal value of the EH-coefficient, NU requires FU information decoding. Next, it can effectively convey the FU signal. Thus, the constraint $R_{nf} > R_f^*$ is set.

Hence, R_f^* represents the targeted rate of FU. Addressing that the NU rate to decode the FU signal must be greater than that of F. $R_{nf} > R_f^*$

(3.21) with the set condition swapped to produce ψ , given by Equations (3.14), (3.15), and (3.16).

Denote $2^{2R_f^*} - 1$ to be τ_f , representing the targeted value of FU's signal to interference plus the noise ratio, given by Equations (3.17), (3.18), (3.19), (3.20), and (3.21).

Verifying the constraint of ψ in (3.21), the Equation is reformed as given by Equation (3.22).

Hence, δ refers to a very small value of 10^{-6} ; however, ψ represents the energy needed to decode information to attain the intended rate of FU.

The outage probability (OP) is the possibility of the data rate of the user falling below the targeted value. Assume R_n^*/R_f^* as the target rates of NU/FU, respectively.

FU is in OP when the R_f rate of (4.1) falls underneath the targeted value, given by Equation (3.23).

NU decodes both signals accurately. Hence, both targeted levels must be equal to or greater than that of NU. By performing SIC, NU faces OP when both values in (3.21) and (4.1) do not meet that value of NU, mathematically given by Equation (3.24).

Based on the IEEE standard in [109], and according to the available THz spectral bands, [110] divided the gap into certain channels and BWs (approved globally), allocated BW depending on the system compatibility, application requirements, hardware limitation, and transmission conditions.

In THz-SC PHY, BPSK and QPSK modulation schemes are mandatory; thus, the simplest scheme (i.e., BPSK) is adopted to improve system performance and mitigate the complexity, as increasing the modulation index, i.e., signal levels, leads to a greater bit error rate (BER) in addition to increasing the processing time and latency (this work achieves higher SE depending on the integrated technologies' capabilities

without the need for high-order modulation schemes). Moreover, the planner must utilize coverage distance with system performance to gain the trade-off between range and rate [109].

6.2.5. Optimal SWIPT-Pairing

The mechanism of the best SWIPT-pairing adopts the principle of the best channel-conditions difference between the targeted blocked user and the paired user. A higher distance between them causes a higher channel condition difference, which means better NOMA performance, especially when the available relaying NU is located at the closest point with regards to Tx. To gain an ideal channel difference, the farthest targeted user requires pairing with the nearest user to the BS, which is preferred to SWIPT; if that is not achievable, then the second nearest user to the BS must be tried, and so on. Then for the next pairing, the targeted user does the same procedure to find its pair starting from the nearest possible user to BS and farthest from itself. The blocked user will find the best available user for the optimal cooperative SWIPT scenario.

6.3. Implementation Environment

This work was simulated as the following (parameters of [58]): Firstly, the simulation and comparison of the performance with mathematical analysis demonstrate the viability of employing H-NOMA to replace NOMA to achieve the intended objectives to gain the most advantages in comparison with NOMA and OMA. After that, an evaluation of the work's core case is processed to examine the three potential SWIPT pairs to the obstructed user (User1) and analyze each pair's performance using parameter settings for frequency, BW, transmit power, and transmission distance. Then the development of a suitable mechanism is proposed to select the optimal DF relaying user (NU) to the intended U1's

pairing. The system was simulated using MATLAB. Table 6.1 shows the simulation parameters.

Table 6.1 Simulation parameters.

Symbol	Parameter	V.A	V.B
f	Frequency	311.04 GHz	311.04 GHz
BW	Bandwidth	12.96 GHz	12.96 GHz
P	Transmission power	20-40 dBm	30 dBm
d	Transmission distance	U1, U2, U3, U4 = (10, 9, 4, 3) m	
α_n	NU power coefficient	0.2 of total power	
α_f	FU power coefficient	0.8 of total power	
G	Antenna gain	25 dB	
eta	Path loss exponent	4	
	Targeted data rate	1 Gbps	
	EH conversion efficiency	0.7	

Based on the influential THz factors, the system performance is investigated. The suggested technique should make it possible for the obstructed user to continue communicating while being shadowed, failing to connect to BS. The ability to regulate THz shortfalls was then explored, demonstrating how this could enhance SE, EE, stability, and the entire efficiency. The modeling findings supported the optimized system's obtained closed form and were compared to that of previous work. Table 6.2 describes H-NOMA strategies.

Table 6.2 H-NOMA strategies.

Users/Time	Multiple Access Technique	Strategy				Time Slots
U1, U2, U3, and U4	TDMA	U1	U2	U3	U4	4
	NOMA	U1, U2, U3, and U4				1
	NOMA \ TDMA	First Pair	Second Pair			2
Time						4 ms.

6.4. Results and Discussion

The system simulation and analysis were carried out to prove the validity of the enhanced achievable rates and outage probability. All possible SWIPT pairs were studied.

6.4.1. H-NOMA, NOMA, and OMA Performance Comparison

The simulation of H-NOMA strategies was carried out in comparison to traditional SC-NOMA and TDMA (Figure 6.4) in order to verify the rationale for selecting the optimal scheme among the MA techniques according to Figure 6.2 and Table 6.2.

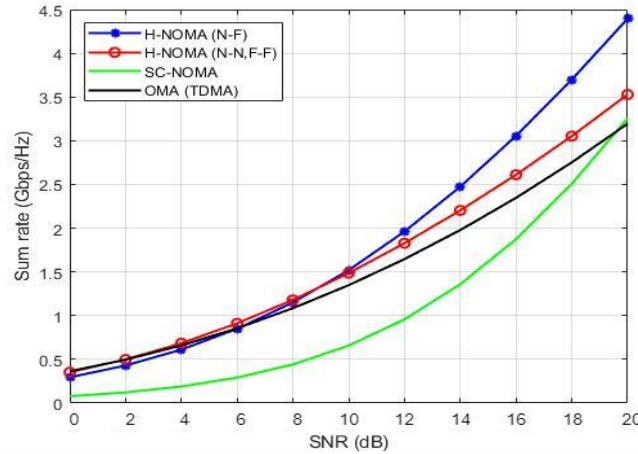


Figure 6.4 H-NOMA techniques vs. NOMA/OMA

Based on Figure 6.4, whenever the channel-condition divergence of NOMA users is distinctive, it can be observed that the (N–F) approach works better than other methods in some circumstances, significantly with THz, confirming that it can fully utilize NOMA in those situations. NOMA still outperforms TDMA with the (N–N, F–F) method, although not significantly better. Due to interference brought on by too many users using the same carrier, SC-NOMA's performance is still insufficient. This leads to problems with complexity and interference. Consequently, employing a single carrier while increasing the number of people served is not recommended.

6.4.2. Proposal Simulation

To analyze system performance and compare it to the related work, and to show how this proposal presents an important improvement to wireless communications by utilizing the key-enabling techniques, it simulates the proposal for each potential relaying user through 3 sections.

Figure 6.5 shows the average achievable rate of near and far users for the three possible SWIPT pairs, namely, U2–U1 (a), U3–U1 (b), and U4–U1 (c). It is noticed that as a result of the EH mechanism, which utilized only the necessary power to achieve the required rate, capturing all the remaining power, NU peaked at 1 Gbps/Hz. Increasingly, in (a), (b), and more in (c), NU achieved a better data rate, exceeding the target for the same power splitting ratio because of the lower distance (better SINR) from the BS, achieving better sum-throughput and SE accordingly. The FU rate increased without affecting NU stability by using the available harvested power in all cases; however, it is possible to make use of the overused FU available energy for more EH operations. The best overall performance resulted in the U4–U1 SWIPT pair (c).

6.4.2.1. Average Rate Versus Transmission Power

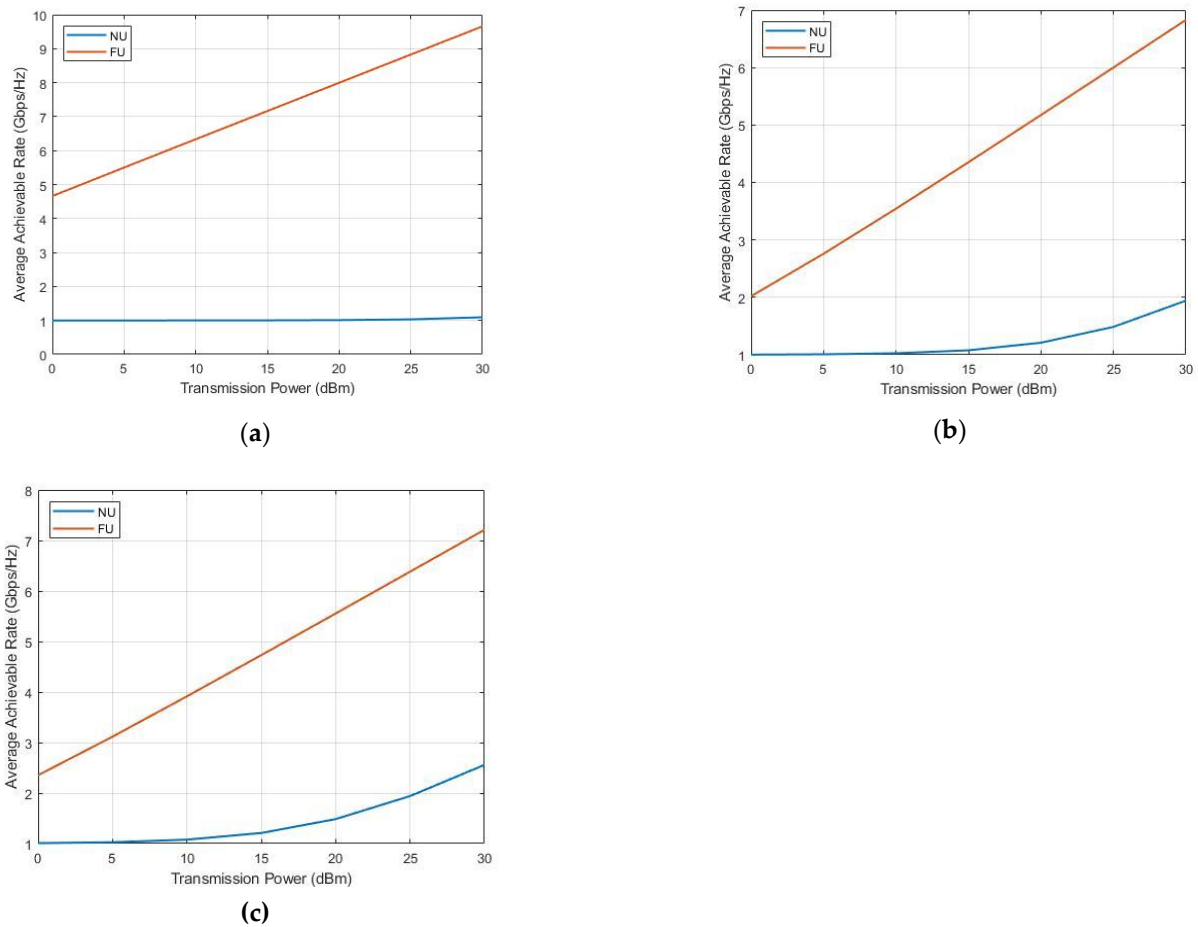


Figure 6.5 Average rate versus transmission power.

6.4.2.2. OP Versus Transmission Power

It is obvious from Figure 6.6 that FU showed higher OP than that of NU in all cases, although having higher rates of FUs as compared with NU. The best overall performance resulted in the U4–U1 SWIPT pair (c) as compared to those of (a) and (b) due to the greater channel difference between the NOMA near and far users (preferable). This supports the idea behind this work to assist the distant, the weak-conditioned, and the path-blocked users.

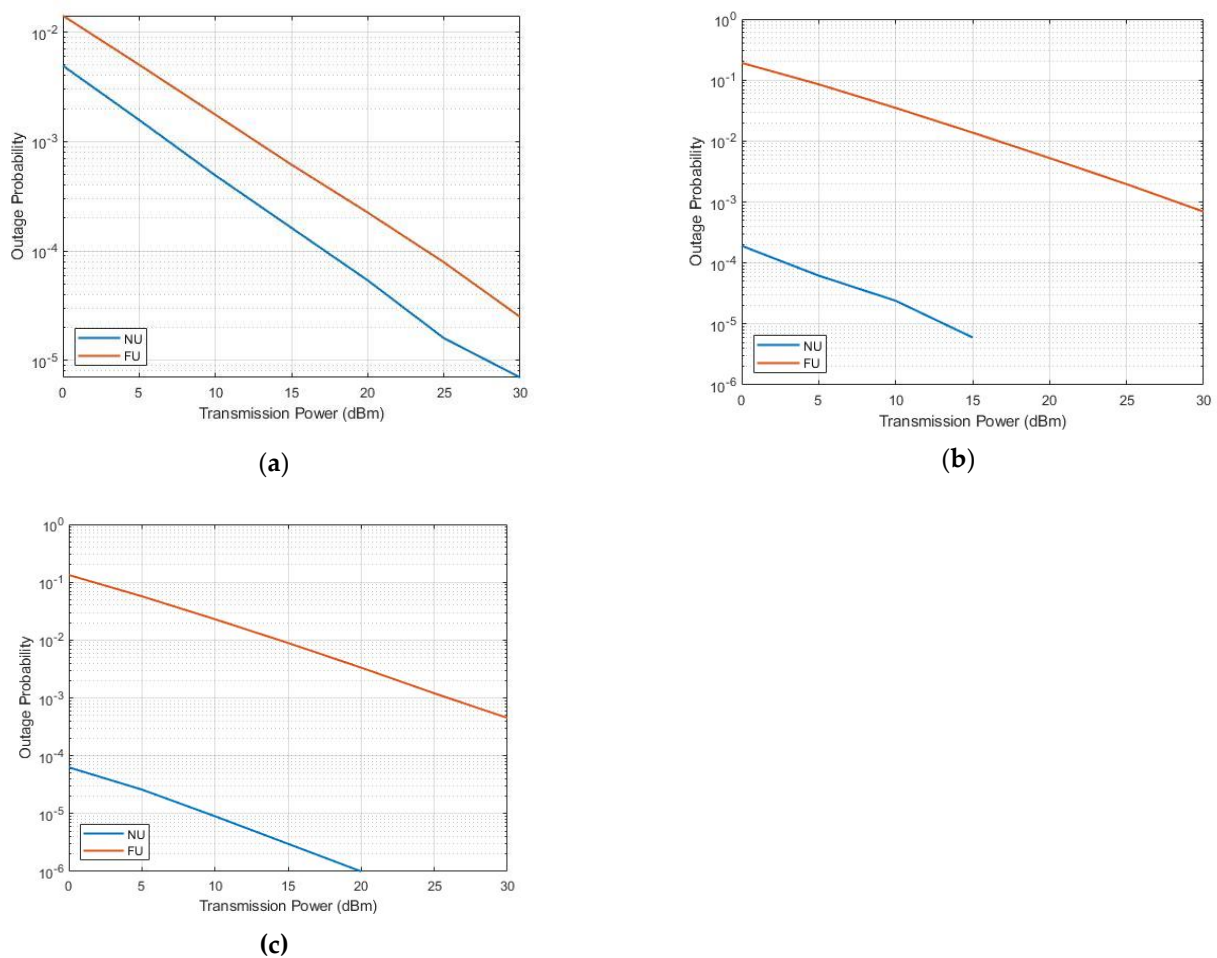


Figure 6.6 OP versus transmission power.

6.4.2.3. Instantaneous-Rate Versus Channel-Realization.

It studies the performance of the SWIPT pairs accurately and examines the instantaneous rates under channel realization.

In Figure 6.7, it is still observable that FU did not show better stability compared to NU in all the cases despite the larger power and data rate;

FU's instantaneous rate was gaining the same level as that in Figure 6.5 and some variations below the targeted level, which explains the variety of users' performance. The best overall performance resulted in the U4–U1 SWIPT pair (c).

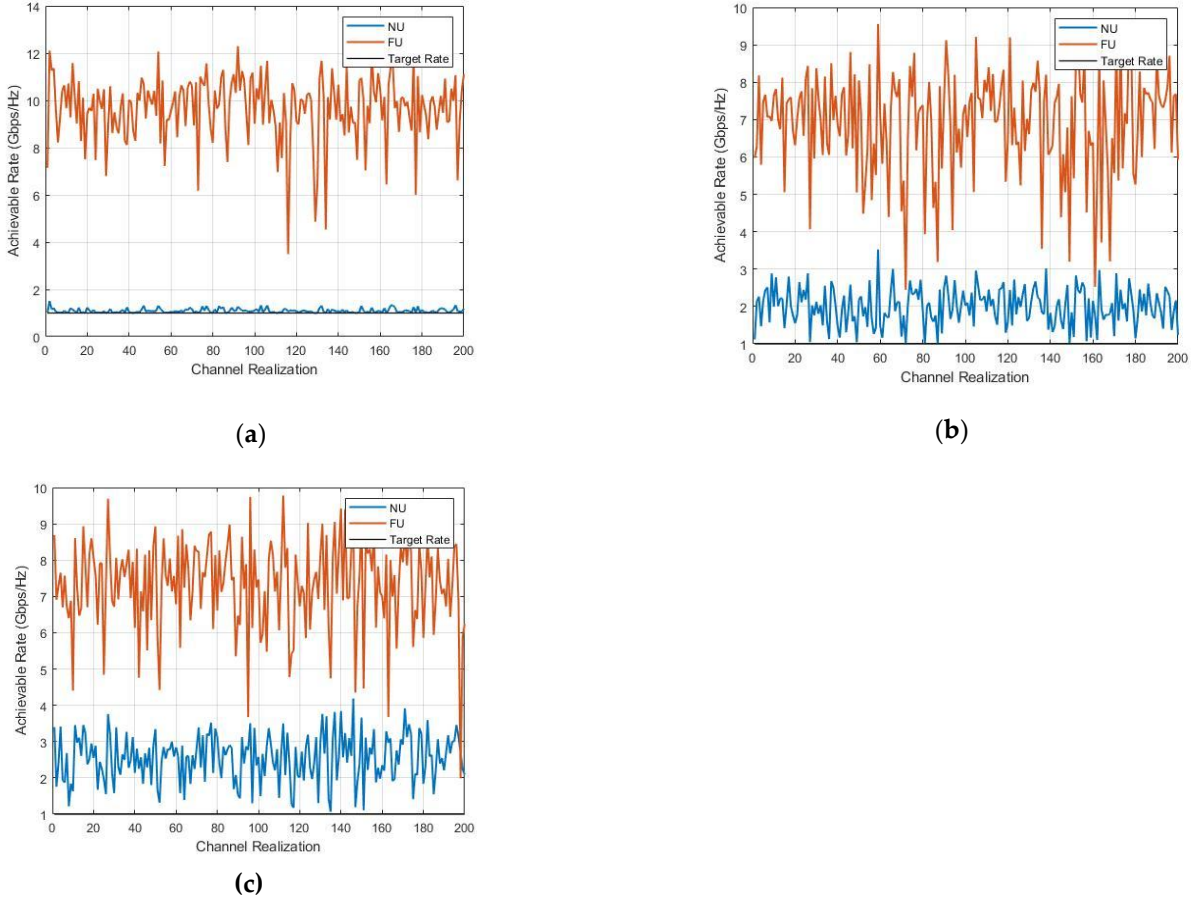


Figure 6.7 Instantaneous rate versus channel realization.

It is worth noting that the proposed system delivered a remarkable enhancement over that of [35] using simpler requirements and lower power/cost, and it gained higher SE and EE. It achieved better performance, showing the importance of EH and emerging techniques.

6.5. Optimal SWIPT-Pairing Mechanism

This section includes simulating the system model using the mechanism in (3.12) to select the best SWIPT partner to act as a DF relay to U1 out of the available LOS users, using the same parameters as in Sections 4 and 5.

6.5.1. Average Rate Versus Transmission Power

Figure 6.8 illustrates how the aforementioned mechanism ran the best SWIPT pair with the best performance, resulting in U4–U1 pair selection. This describes the importance of the channel condition difference between the paired NOMA users (NU and FU); the greater the channel difference, the better the NOMA performance. The privilege of selection dynamism was obtained by the proposed mechanism.

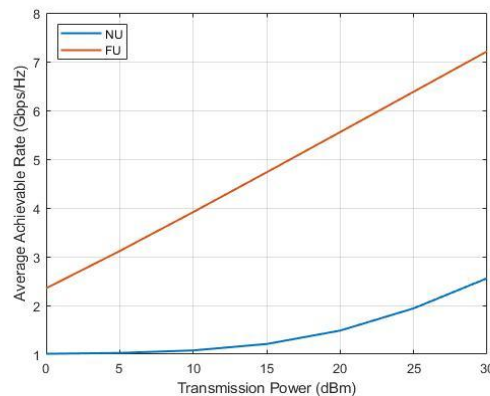


Figure 6.8 Average rate versus transmission power.

6.5.2. OP Versus Transmission Power

Similarly, Figure 6.9 shows how the same mechanism managed to select the best SWIPT pair with the best outage probability, resulting in the selection of the U4–U1 pair. It improved overall system reliability and OP by aiding the targeted user to opt for the best NU to pair within terms of NU location and, accordingly, channel condition difference.

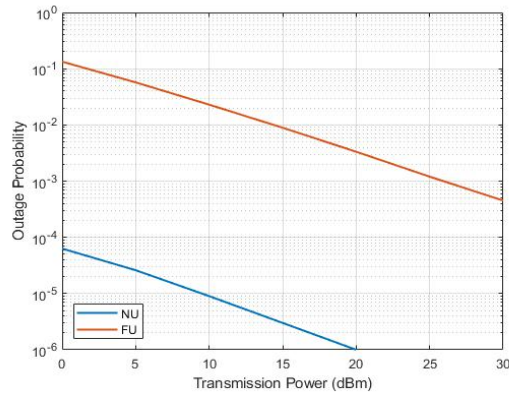


Figure 6.9 OP versus transmission power

6.5.3. Instantaneous Achievable Rate Versus Channel Realization

To make sure that the proposed mechanism achieves accurately the best performance for users, Figure 6.10 above illustrates the simulation of the instantaneous achievable rates under channel realization. Once again, it is clearly shown that the proposed mechanism leads to the best user and overall performance accordingly by selecting the best pair to achieve the intended goal.

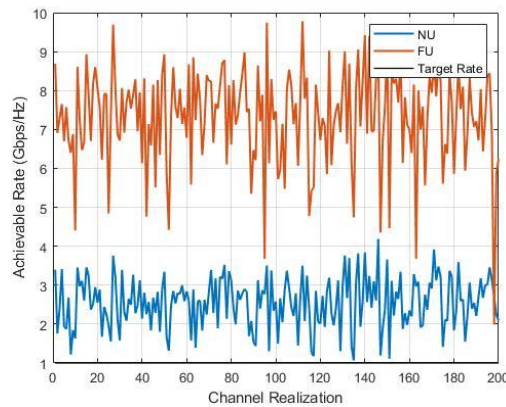


Figure 6.10 Instantaneous rate versus channel realization.

6.6. System Numerical Analysis and Simulation

This section compares the proposal's sum throughput and OP using simulations and analysis to prove the validity of the closed-form of the

system model, leading to the preplanned objectives, utilizing similar input parameters, and setting a transmission power of 20 dBm.

6.6.1. Sum Throughput Versus Transmission Power

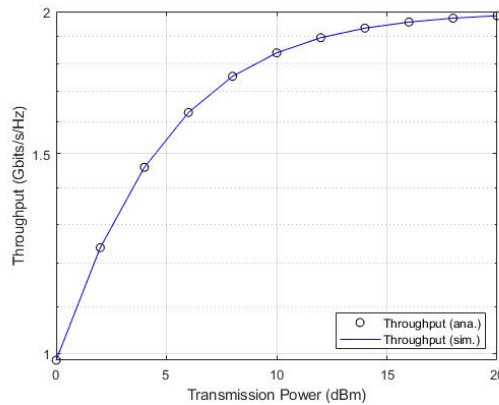


Figure 6.11 Sum throughput versus transmission power

Based on the same parameters used to examine the validity of mathematical derivations, Figure 6.11 shows considerable matching with the system simulation.

6.6.2. User OP Versus Transmission Power

Similarly, Figure 6.12 verifies the feasibility of mathematical analysis by conducting a point-to-point comparison and setting the exact parameters. It shows noticeable matching.

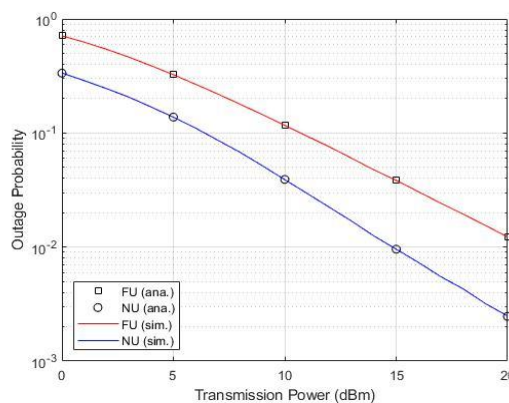


Figure 6.12 User OP versus transmission power.

Remarkably, Figure 6.11 and Figure 6.12 depict clear consistency of both results, which confirm the accuracy of the analyses and system model validity of achieving the objectivity and novelty of the proven added values.

6.7. Summary

In this work, the focus shifted to meeting the stringent specifications of 6G by overcoming the challenges posed by SC-NOMA and THz limitations. An optimal THz H-NOMA pairing approach was proposed, showing a 75% improvement in EE and SE over the conventional work (i.e., [65], [67], [69], [70], [94]–[96]). The study validated the proposed mechanism's effectiveness in achieving the best overall performance, with results matching numerical and simulation outcomes.

Chapter 7: A Secure Deep Autoencoder-based 6G Channel Estimation to Detect/Mitigate Adversarial Attacks

7.1. Introduction

This chapter introduces a secure CE method using a deep autoencoder to detect and mitigate AA. The technique is explained in detail, covering the methodology, programming of the DAE-based CE, its implementation, and a discussion of the results.

7.2. Methodology

Figure 7.1 shows the DAE-based CE general structure to track suspicious activity traffic over the 6G entire network.

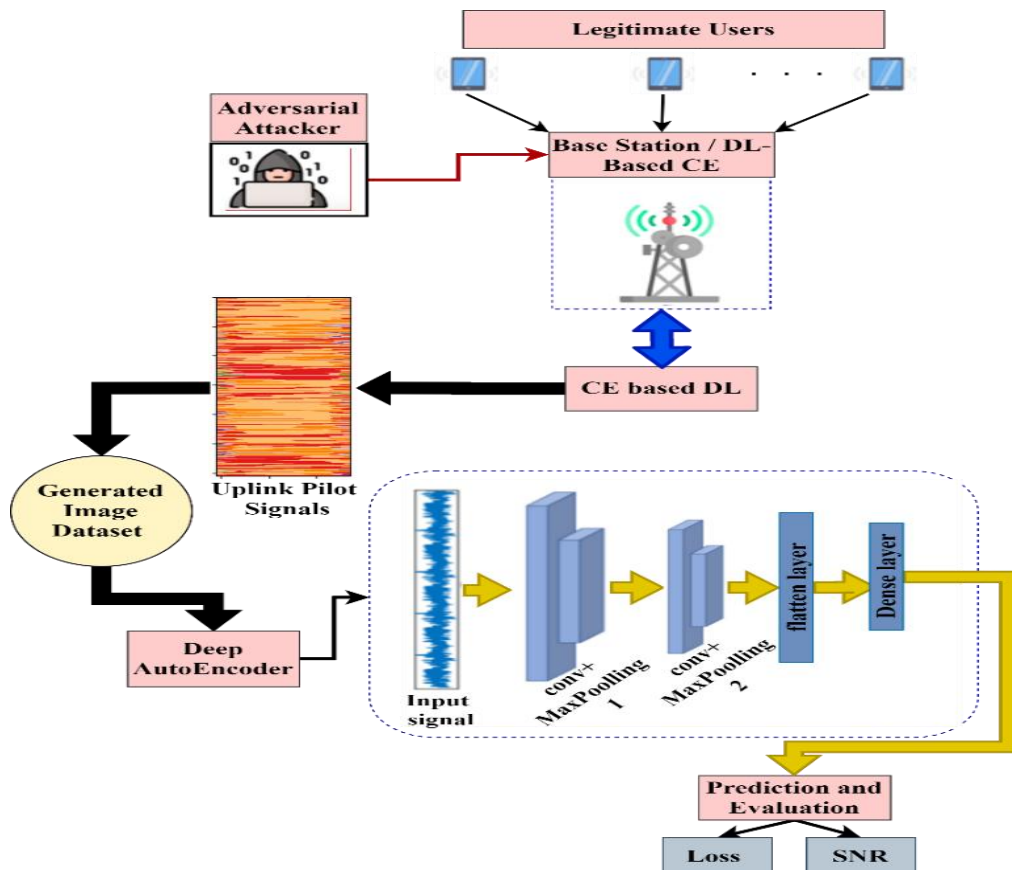


Figure 7.1 The General Structure of DAE-Based CE

Figure 7.1 illustrates all processes made at the BS to detect AA and legitimate users using the DAE model. This model starts with pilots' uplink

signals using MATLAB tools to generate an image dataset to evaluate system performance and robustness. The generated dataset and programming DAE model are:

7.2.1. Dataset Descriptions and Scenario

Many reference cases are available in Toolbox and other next-generation network communication systems. Collecting datasets for DL-based models enables customization and the generation of various waveforms, antennas, and channel models. A reference example in the MATLAB Toolbox is utilized to generate the training dataset for DAE-based CE. Table 7.1 illustrates a sample of this dataset.

Table 7.1 Original dataset description.

Feature 1	Feature 2	Feature 3	Feature 4
0.15+0.89j		0.17+0.91j	0.11+0.88j
-	0.14+0.9j	-	-
0.39+0.84j	0j	0.37+0.89j	0.41+0.89j
-	-	-	-
0.56+0.78j	0.26+0.8j	0.55+0.79j	0.26+0.72j
-	3j	-	-
0.26+0.89j	-	0.44+0.84j	0.32+0.80j
-	0.41+0.8j	.	.
0.86+0.43j	2j	.	.
-	-	.	.
0.88+0.1j	0.32+0.8j	.	.
-	7j	-	-
-	.	0.33+0.23j	0.89+0.21j
-	.		
-	.		
-	.		
0.86+0.43j	-		
-	0.88+0.1j		
-	5j		

A new channel characteristic is generated for every set of training datasets based on different parameters.

Table 7.2 lists channel characteristics with associated values.

Table 7.2 CE parameters.

Channel Parameters	Values
Doppler-Shift	0.0004-100 MHz

Delay Spread	0.001-0.25 ns
Sample Rate	32950000
NFFT	1024
Windows	36
Symbols/Slot	14
Slots/Frame	20
Slots/Sub-frame	2
Polarity	CoPolar
Transmit Antennas no.	64
Receive Antennas no.	64
Fading Distribution	Rayleigh
Modulation	16QAM

7.2.2. Programming Deep Autoencoder-Based Channel Estimation

The DAE model can provide several advantages when used for CE in 6G wireless communication systems:

- **Improving Accuracy:** DAEs can learn complex features of a wireless channel, e.g., multipath propagation, noise, and interference, which can improve the accuracy of CE compared to traditional methods.
- **Robustness:** DAEs are robust to noise and interference, which can improve the reliability of CE in practical wireless communication scenarios.
- **Reducing Training Data Requirements:** DAEs can learn from fewer training samples than traditional methods, which can be especially advantageous in low SNR scenarios where collecting large amounts of training data is difficult.
- **Low Complexity:** DAEs have a relatively low computational complexity compared to other ML algorithms, which makes them suitable for implementation in real-time wireless communication systems.
- **Adaptability:** DAEs can adapt to changes in the wireless channel over time, which enables enhanced CE performance in dynamic wireless communication scenarios.

The AE-based DL model's hyper-parameters are shown in Table 7.3.

Table 5.3 DAE parameters.

DAE Parameters	Values
Activation Function	ReLu
Batch size	128
Testing samples	30%
Training samples	70%
Loss function	MSR
Learning rate	0.001
Number of epochs	1000
Optimizer	Adam
Momentum	0.9
Input/output size	612 x 14

The DAE model for the CE employed is depicted in Figure 7.2.

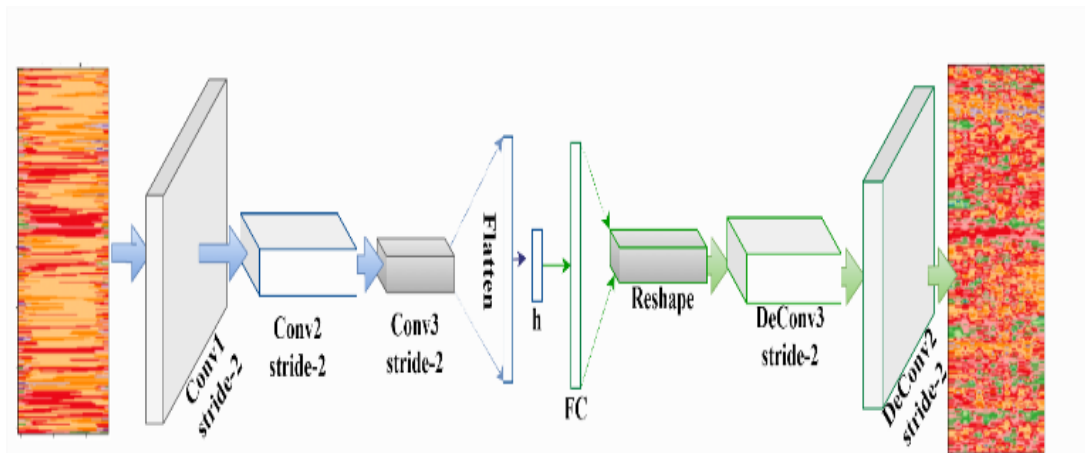


Figure 7.2 The DAE-Based CE.

In Figure 7.2, DAE works when the dataset is generated then the first stage of AE, i.e., convolution 1 (Conv.1) layer with a stride-2 can be used for features extraction of the input signal. The Conv.1 layer architecture is a set of filters that slide over the input signal to generate a set of feature maps. The basic idea behind using a Conv.1 layer with a stride is performing a local feature extraction, where each filter extracts features

from a local region of the input signal. The stride ensures that the filter covers every possible local region of the input signal. To program a DAE using a Conv.1 layer with a stride, the following steps can be followed:

Define the Conv.1 layer: it specifies the filters' number, filter size, and stride.

Feed the input signal into the Conv.1 layer: it produces a set of feature maps. For example, assuming the input signal is an image of size 128x128 with 3 color channels as follows:

Use the feature maps for further processing: it is produced by the Conv.1 layer and can be used as input for further processing in the AE architecture.

By using a Conv.1 layer with a stride-2 in a DAE model, the model can learn to extract local features from the input signal. The local features can be used to reconstruct the input signal in a lower-dimensional feature space, which can be used for various applications, significantly for CE in wireless communication systems. Deconvolution (DeConv.) layers with a stride-2 and flattening layers are often used for various applications, e.g., image dataset processing. These layers help to increase the spatial resolution of the feature maps and convert them into a vector form, respectively. These layers work in a DAE as:

DeConv. layer with stride-2 (so-called a transpose convolutional layer or a fractionally-strides convolutional layer): it can be used to increase the spatial resolution of the feature maps produced by the previous layers. The DeConv layer performs the opposite operation of a Conv.1 layer, and it can be used to reconstruct the input signal or to up-sample the feature maps.

Flattening layer: it is used to convert the 3D feature maps into a 1D vector format. This is typically done before passing the feature vectors through a dense layer for classification or regression tasks, defined as:

Using these layers in a deep autoencoder: in a deep autoencoder, a DeConv. layer with stride-2 can be used to up-sample the feature maps, and a flattening layer can be used to convert the feature maps into a 1D vector format. The model is assessed and contrasted using MSE. The MSE scores are used to analyze the model further. It is calculated by:

$$MSE = \frac{\sum(Y_t - \hat{Y}_t)^2}{n} \quad (7.1)$$

Where Y_t means the actual attribute and \hat{Y}_t means forecasted attribute.

The MSE between the real and predicted scales is measured. Whenever a model is perfect that means the MSE measurement is zero. It is proportional to model error. Algorithm 1 with pseudo-code demonstrates the main steps of DAE for CE.

Algorithm 1: DAE-based CE

Input: Generated and Load the dataset: Load the dataset which consists of input signals and corresponding CEs. /*Preprocess the input data: Normalize the input data by dividing each element by the maximum value*/.

Output: Training dataset, MSR.

Begin:

Define the AE /*the encoder and decoder architecture using Conv. and DeConv. layers, respectively in Table III*/.

Define the CE parameters using Table II a dense layer.

Concatenate the input signal and CE.

Define the DAE-based CE model: with the following Pseudocode.

AE-model=Model (concatenated-input, decoded-signal).

CE-model=Model (channel-input, channel-estimate).

Combined-input = Input (shape= (64, 64, 1)).

Channel-output=CE-model (CE).

Combined-output=concatenate ([combined-input, channel-output]).

AE-output = AE-model (combined-output)

Full-model=Model (inputs= [combined-input, channel-input], outputs= [AE-output, channel-output])

Compile and train the model: Compile the full model and train it on the input data and channel estimates. As follows:

```
Full model. Compile(optimizer=Adam(lr=0.001),  
loss= ['MSE', MSE], metrics=['accuracy']).  
history = full-model. Fit ([input-data, CE], [input-data, CE], epochs=50,  
batch-size=32, shuffle=True, validation-split=0.2)  
Return MSR (accuracy).
```

End.

The model examinations of the AA's five attacks (FGSM, BIM, MIM, PGD, and C&W) trained and tested the effectiveness of the suggested mitigation measures to achieve the highest performance (i.e., the lowest possible MSE).

7.3. Implementation Environment

MATLAB tools, Python, and Collaborator (Colab) are general-purpose programming languages, which are simple to use and learn. They are compatible with numerous operating systems i.e., Windows, Linux, and Mac. TensorFlow and Keras are two open-source DL libraries created to expand the Python library. As a result, this paper uses these languages and libraries to put the suggestions into practice. The DAE is carried out using MATLAB Toolbox to generate the dataset. Furthermore; the DAE model is implemented using Python 3.8 in colab, using TensorFlow and Keras libraries. The laptop used is equipped with a Core i7 CPU, 10th Generation, and 64-bit Operating System Win. 11.

7.4. Results, Evaluation, and Discussion

7.4.1. Performance Results and Evaluation

To assess the effectiveness of DAE-based channel estimate models in the 6G Network, attack success ratio (ASR) was used for evaluation statistics as:

$$ASR = \frac{1}{m} \sum_{i=0}^m \frac{MSE(X_{(i)}^{adv}, y(i)) - MSE(X(i), y(i))}{MSE(X_{(i)}^{adv}, y(i))} \quad (7.2)$$

ASR represents the test-samples proportion, which the attacker may incorrectly forecast to all test samples. An attack is more effective if the ASR is higher. Table 7.4 shows the experimental findings for the suggested AA-based mitigation techniques.

Table 7.4 Experimental test results of DAE-based CE for AA.

Attacks Names	Epsilon	MSE		ASR
		Normal	Attacks	
FGSM	0.1	0.02812	0.02848	0.018932
	0.5	0.02812	0.03676	0.218932
	1.0	0.02810	0.07848	0.618932
	2.0	0.02822	0.19284	0.818932
	3.0	0.02783	0.30651	0.918932
BIM	0.1	0.02812	0.02848	0.018932
	0.5	0.02812	0.03676	0.218932
	1.0	0.02810	0.07848	0.618932
	2.0	0.02822	0.19284	0.818932
	3.0	0.02783	0.30651	0.918932
MIM	0.1	0.02812	0.02848	0.018932
	0.5	0.02812	0.03676	0.218932
	1.0	0.02810	0.07848	0.618932
	2.0	0.02822	0.19284	0.818932
	3.0	0.02783	0.30651	0.918932
C&W	–	0.02831	0.02980	0.066435
PGD	0.1	0.02812	0.02848	0.018932
	0.5	0.02812	0.03676	0.218932
	1.0	0.02810	0.07848	0.618932
	2.0	0.02822	0.19284	0.818932
	3.0	0.02783	0.30651	0.918932

In Table 7.4, epsilon values typically refer to the maximum amount of perturbation or distortion allowed to be added to the AA original input data (the epsilon value refers to a small perturbation value that is added to the input data to create AA. The objective of AA is to cause an ML model to misclassify an input by making small modifications to the input data. It determines the magnitude of these modifications). That generates more aggressive AA to fool intelligent systems. For example, in the popular Fast

Gradient Sign Method (FGSM) attack, the perturbation added to the input image is scaled by a small value of epsilon, which controls the amount of distortion introduced to the original image. By adjusting the value of epsilon, an attacker can control the trade-off between the degree of distortion introduced to the input and the likelihood of AA successfully, fooling the model. The experiment results demonstrate that the suggested approach can increase the CE model's accuracy. The findings depict that the approach can deliver superior outcomes for AA (FGSM, BIM, MIM, PGD, and C&W).

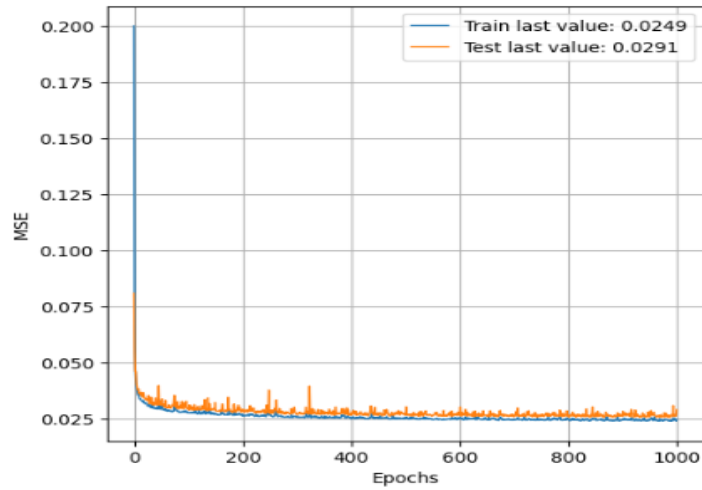


Figure 7.3 demonstrates the training and testing dataset's MSE with epochs 1000.

7.4.2. MSE for Training and Testing Datasets.

The effectiveness of the CE model can be increased by the outcomes of the suggested DAE model. Figure 7.4 shows the MSE values change before and after applying a DAE model. The MSE values before the model (left-sided Fig.) are virtually identical to the attacks and the values are maximum. However, when the DAE model is applied, the values of MSE of all attacks are minimal.

The experimental results of DAE-based CE between MSE and epsilon.

Figure 40 shows that DEA-based CE is efficient at predicting and detecting the AA with the epsilon values added to the original data. Table 7.5 demonstrates the details about all the AA.

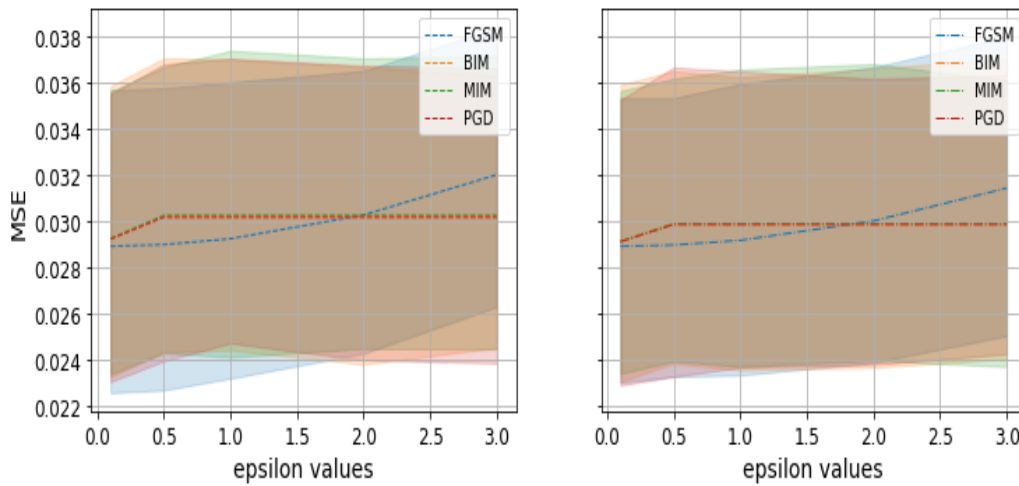


Figure 7.4 malicious distance with real and predicted MSE for each attack.

Table 7.5 Demonstrates the details about all the AA.

Index	Malicious Distance	Real Predicted MSE	Malicious Predicted MSE	Attacks	epsilon
377	2.7999999	0.0118651	0.0129488	BIM	3.0
179	2.8000023	0.0329317	0.0329508		2.0
301	0.7000001	0.0100393	0.0100881	FGSM	0.5
290	1.4000003	0.0537686	0.0534277		1.0
490	1.4000003	0.0382549	0.0385098		1.0
510	1.4000003	0.0077401	0.0080595	MIM	1.0
529	2.8000063	0.0344316	0.0354635		2.0
66	2.8000068	0.0269185	0.0276220	PGD	1.0
142	2.8000023	0.0296083	0.0299384		2.0
131	2.8000068	0.0411919	0.0422248	C&W	0.5
366	2.8000020	0.0319317	0.0319400		0.5

Table 7.5 shows various forms of attacks. The index-based attacks focus on finding the closest AA, whereas distance-based attacks focus on maximizing the distance between the original data point and AA. The experimental results are consistent across all types of AA (BIM, FGSM,

MIM, C&W, and PGD). Furthermore, the epsilon values range was expanded to (0.5-3.0), whereas the MSE values of real and predicted malicious are still similar or close to each other across the different combinations of attack, epsilon value, and distance metrics. These findings prove that the model is highly susceptible to a wide range of adversarial perturbations. Hence, small changes in the perturbation parameters do not significantly affect the quality of AA detection concerning the MSE metric.

7.5. Summary

This study proposed a secure DAE-based 6G CE model to detect and mitigate potential AA. It demonstrated promising results in improving the robustness and effectiveness of CE against AA in 6G networks throughout comprehensive experimental evaluations. The results proved the system's outperformance over traditional CEs per simplicity, accuracy, and resilience against AA (a high accuracy to detect AA (FGSM, BIM, PGD, MIM, and C&W) with minimum MSE of real and predicted malicious) when the epsilon values ranged (0.5-3.0) with various attacks' distances.

Chapter 8: Conclusion, Challenges, and Recommendations for Future Work

8.1. Introduction

To advance wireless communications for the next era, this chapter concludes the investigation of the potentials of THz communications, NOMA, H-NOMA, and other integrated technologies, and the improved system performance. While significant progress was made, certain challenges persisted, such as the limited transmission distance in THz due to its characteristics, e.g., high path loss and susceptibility to blockage. This research addressed these challenges and proposed innovative solutions. Moreover, security concerns in the 6G context were considered and improved concerning updated AI-based daily attacks.

8.2. Conclusions

- ❖ The first conclusion centered on the cooperative THz-NOMA system, exploring the application of the EH technique. The study derived optimal EH coefficients, achieving targeted Signal-to-Interference-plus-Noise Ratio (SINR), data rates, and SE. Comparative analysis demonstrated a 70% improvement in SE and EE over existing systems, emphasizing the importance of proximity in DF relaying.
- ❖ The second conclusion delved into applying the EH technique in a cooperative MIMO-NOMA system for THz communications. This research surpassed comparable studies, achieving over 50% gains in reliability, OP, SE, and EE compared to basic NOMA. The findings highlighted the success of defined strategies in preserving communication between the BS and potentially obstructed users, offering a dynamic path-selection mechanism for enhanced reliability.

- ❖ The third conclusion explored the cost implications of promising technologies, especially those involving complex power-consuming systems. This research addressed the impact of NOMA SIC-imperfection and proposed the best THz H-NOMA SWIPT-paired strategy, enhancing overall performance by 75%. The study emphasized the significance of selecting SWIPT pairing based on the nearest user to the BS, considering location and channel conditions.
- ❖ In the fourth conclusion, the focus shifted to meeting the stringent specifications of 6G by overcoming the challenges posed by SC-NOMA and THz limitations. An optimal THz H-NOMA pairing approach was proposed, showing a 75% improvement in EE and SE. The study validated the proposed mechanism's effectiveness in achieving the best overall performance, with results matching numerical and simulation outcomes.
- ❖ In a nutshell, this study proposed a secure DAE-based 6G CE model to detect and mitigate potential AA. It demonstrated promising results in improving the robustness and effectiveness of CE against AA in 6G networks throughout comprehensive experimental evaluations. The results proved the system's outperformance over traditional CEs per simplicity, accuracy, and resilience against AA (a high accuracy to detect AA (FGSM, BIM, PGD, MIM, and C&W) with minimum MSE of real and predicted malicious) when the epsilon values ranged (0.5-3.0) with various attacks' distances.

8.3. Challenges

The lack of THz equipment and resources is the biggest challenge that prevents researchers from conducting further verifications which the author hopes to provide as soon as possible. Moreover, despite the several advantages of the cooperative SWIPT THz-NOMA system over conventional systems, some challenges still need to be reconsidered. The

most important one is mobility, especially with the increasing number of served users; hence, other metrics are affected by mobility such as CSI, power allocation, hardware limitation, beam steering, interference cancelation, and other related parameters; however, incorporating AI will improve CSI, localization, tracking, power allocation, and system performance. On the other hand, it is worth noticing that AI-based work requires updated and accurate 6G datasets, which are still unavailable.

8.4. Recommendations for Future Work

Some recommendations for refining and enhancing the conclusions:

- Emphasizing the practical implications of the improvement in SE and EE, such as potential energy savings and increased data rate with transmission reliability.
- Suggesting future research directions, e.g., exploring different EH techniques or investigating the scalability of the proposed system.
- Discussing the practical implications of achieving gains in reliability, Outage Probability, SE, and EE in a cooperative MIMO-NOMA system.
- Proposing avenues for further research, such as investigating the impact of varying environmental conditions on the proposed techniques.
- Highlighting the improvement in overall performance and discussing potential cost savings or EE gains in deploying the proposed THz H-NOMA SWIPT-paired strategy.
- Suggesting potential research areas, such as optimizing the SWIPT-paired strategy for different network scenarios.
- Emphasizing on how the proposed THz H-NOMA pairing approach addresses the challenges of SC-NOMA and THz limitations, potentially paving the way for 6G network advancements.

- Recommending further investigations into the scalability and adaptability of the proposed pairing approach in diverse 6G deployment scenarios.
- Automating procedural and computational operations using AI algorithms.
- Highlighting the significance of the proposed secure DAE-based 6G CE model in improving the robustness and effectiveness of CE against AA.
- Recommending practical applications, such as integrating the proposed model into real-world 6G networks and exploring its compatibility with other security mechanisms.
- The proposed security approach paves the way for the development of more advanced and effective security mechanisms in 6G networks to ensure the reliability and availability of 6G communications. In the future, further developments might be made in several directions. Validating this model performance upon the deployment of 6G networks in real-world practice, integrating it with other defense mechanisms and response systems, or extending it to address other types of attacks in 6G networks, e.g., jamming, poisoning, dark net, and spoofing attacks.

In all conclusions, it is recommended to consider reinforcing the real-world applications and impact of the research, and to encourage further studies in certain directions that make a remarkable contribution to the field. Additionally, it is recommended to maintain collaborations or interdisciplinary approaches for future research endeavors.

REFERENCES

- [1] F. Yang, P. Pitchappa, and N. Wang, “Terahertz Reconfigurable Intelligent Surfaces (RISs) for 6G Communication Links,” *Micromachines*, vol. 13, no. 2, 2022, doi: 10.3390/mi13020285.
- [2] M. Ardanuc, M. Basaran, Y. Hmamouche, L. Durak-Ata, and H. Yanikomeroglu, “Energy Efficiency Analysis in Heterogeneous Networks: A Stochastic Geometry Perspective,” *IEEE Open J Veh Technol*, vol. 4, no. March, pp. 438–443, 2023, doi: 10.1109/OJVT.2023.3269890.
- [3] T. Hossfeld, S. Wunderer, F. Loh, and D. Schien, “Analysis of Energy Intensity and Generic Energy Efficiency Metrics in Communication Networks: Limits, Practical Applications, and Case Studies,” *IEEE Access*, vol. 12, no. August, pp. 105527–105549, 2024, doi: 10.1109/ACCESS.2024.3435716.
- [4] D. Wu, W. Wei, J. Bai, and S. Mei, “Energy and Exergy Efficiency Analysis of Advanced Adiabatic Compressed Air Energy Storage Based Trigeneration Energy Hub,” *CSEE J Power Energy Syst*, vol. 9, no. 6, pp. 2409–2422, 2023, doi: 10.17775/CSEEJPES.2022.00720.
- [5] M. Rubina Aktar *et al.*, “Energy-Efficient Hybrid Powered Cloud Radio Access Network (C-RAN) for 5G,” *IEEE Access*, vol. 11, no. December 2022, pp. 3208–3220, 2023, doi: 10.1109/ACCESS.2023.3234190.
- [6] M. Ahmed, S. Genevey, M. Ali, Y. Savaria, and Y. Audet, “Recent Start-Up Techniques Intended for TEG Energy Harvesting: A Review,” *IEEE Access*, vol. 12, no. February, pp. 34116–34130, 2024, doi: 10.1109/ACCESS.2024.3372849.
- [7] K. Niotaki *et al.*, “RF Energy Harvesting and Wireless Power Transfer for Energy Autonomous Wireless Devices and RFIDs,” *IEEE J Microwaves*, vol. 3, no. 2, pp. 763–782, 2023, doi: 10.1109/JMW.2023.3255581.
- [8] S. M. Hosseini, M. Soleymani, S. Kelouwani, and A. A. Amamou, “Energy Recovery and Energy Harvesting in Electric and Fuel Cell Vehicles, a Review of Recent Advances,” *IEEE Access*, vol. 11, no. August, pp. 83107–83135, 2023, doi: 10.1109/ACCESS.2023.3301329.
- [9] J. Wu *et al.*, “A Simultaneous Wireless Information and Power Transfer System with Independent Channel for Information Transfer,” *IEEE Access*, vol. 8, pp. 125610–125619, 2020, doi: 10.1109/ACCESS.2020.3007888.

References

- [10] A. Esse, K. Abdullah, M. H. Habaebi, and H. A. M. Ramli, “Dynamic Power Splitting Simultaneous Wireless Information and Power Transfer Split Receiver for Wireless Sensor Networks,” *IEEE Access*, vol. 9, pp. 129407–129416, 2021, doi: 10.1109/ACCESS.2021.3113330.
- [11] N. Ashraf, S. A. Sheikh, S. A. Khan, I. Shayea, and M. Jalal, “Simultaneous Wireless Information and Power Transfer with Cooperative Relaying for Next-Generation Wireless Networks: A Review,” *IEEE Access*, vol. 9, pp. 71482–71504, 2021, doi: 10.1109/ACCESS.2021.3078703.
- [12] K. B. Ofori-Amanfo, D. K. P. Asiedu, R. K. Ahiadormey, and K. J. Lee, “Multi-Hop MIMO Relaying Based on Simultaneous Wireless Information and Power Transfer,” *IEEE Access*, vol. 9, pp. 144857–144870, 2021, doi: 10.1109/ACCESS.2021.3122375.
- [13] I. Ishteyaq, K. Muzaffar, N. Shafi, and M. A. Alathbah, “Unleashing the Power of Tomorrow: Exploration of Next Frontier with 6G Networks and Cutting Edge Technologies,” *IEEE Access*, vol. 12, no. February, pp. 29445–29463, 2024, doi: 10.1109/ACCESS.2024.3367976.
- [14] N. A. Alhaj *et al.*, “Integration of Hybrid Networks, AI, Ultra Massive-MIMO, THz Frequency, and FBMC Modulation Toward 6G Requirements: A Review,” *IEEE Access*, vol. 12, no. December 2023, pp. 483–513, 2024, doi: 10.1109/ACCESS.2023.3345453.
- [15] W. Zhou *et al.*, “Channel Scenario Extensions, Identifications, and Adaptive Modeling for 6G Wireless Communications,” *IEEE Internet Things J*, vol. 11, no. 5, pp. 7285–7308, 2023, doi: 10.1109/JIOT.2023.3315296.
- [16] N. A. Khan and S. Schmid, “AI-RAN in 6G Networks: State-of-the-Art and Challenges,” *IEEE Open J Commun Soc*, vol. 5, no. December 2023, pp. 294–311, 2024, doi: 10.1109/OJCOMS.2023.3343069.
- [17] Y. Zeng *et al.*, “A Tutorial On Environment-Aware Communications via Channel Knowledge Map for 6G,” *IEEE Commun Surv Tutor*, no. cm, pp. 1–1, 2024, doi: 10.1109/comst.2024.3364508.
- [18] R. Kamran, S. Kiran, P. Jha, A. Karandikar’t, and P. Chaporkar, “Green 6G: Energy Awareness in Design,” *2024 16th Int Conf Commun Syst NETWORKS, COMSNETS 2024*, pp. 1122–1125, 2024, doi: 10.1109/COMSNETS59351.2024.10427334.
- [19] W. Jiang, B. Han, M. A. Habibi, and H. D. Schotten, “The road towards 6G: A comprehensive survey,” *IEEE Open Journal of the Communications Society*, vol. 2, pp.

References

- 334–366, 2021, doi: 10.1109/OJCOMS.2021.3057679.
- [20] M. Alsabah *et al.*, “6G Wireless Communications Networks: A Comprehensive Survey,” *IEEE Access*, vol. 9, pp. 148191–148243, 2021, doi: 10.1109/ACCESS.2021.3124812.
- [21] J. Wang, C. X. Wang, J. Huang, and Y. Chen, “6G THz Propagation Channel Characteristics and Modeling: Recent Developments and Future Challenges,” *IEEE Commun Mag*, vol. 62, no. February, pp. 56–62, 2022, doi: 10.1109/MCOM.001.2200403.
- [22] X. Cai, X. Cheng, and F. Tufvesson, “Toward 6G with Terahertz Communications: Understanding the Propagation Channels,” *IEEE Commun Mag*, vol. 62, no. February, pp. 32–38, 2022, doi: 10.1109/MCOM.001.2200386.
- [23] J. Zhang *et al.*, “Deterministic ray tracing: A promising approach to THz channel modeling in 6G deployment scenarios,” *IEEE Commun Mag*, vol. 62, no. February, pp. 48–54, 2023, doi: 10.1109/MCOM.001.2200486.
- [24] T. Mao, L. Zhang, Z. Xiao, Z. Han, and X. G. Xia, “Terahertz-Band Near-Space Communications: From a Physical-Layer Perspective,” *IEEE Commun Mag*, vol. 62, no. February, pp. 110–116, 2022, doi: 10.1109/MCOM.004.2200429.
- [25] D. Jung *et al.*, “Terahertz Antenna-in-Package Design and Measurement for 6G Communications System,” *IEEE Trans Antennas Propag*, vol. 72, no. 2, pp. 1085–1096, 2023, doi: 10.1109/TAP.2023.3320276.
- [26] H. Tataria, M. Shafi, A. F. Molisch, M. Dohler, H. Sjoland, and F. Tufvesson, “6G Wireless Systems: Vision, Requirements, Challenges, Insights, and Opportunities,” *Proc IEEE*, vol. 109, no. 7, pp. 1166–1199, 2021, doi: 10.1109/JPROC.2021.3061701.
- [27] V. Petrov, H. Guerboukha, D. M. Mittleman, and A. Singh, “Wavefront Hopping: An Enabler for Reliable and Secure Near Field Terahertz Communications in 6G and Beyond,” *IEEE Wirel Commun*, vol. 31, no. 1, pp. 48–55, 2024, doi: 10.1109/mwc.003.2300310.
- [28] N. Yang and A. Shafie, “Terahertz Communications for Massive Connectivity and Security in 6G and Beyond Era,” *IEEE Commun Mag*, vol. 62, no. February, pp. 72–78, 2022, doi: 10.1109/MCOM.001.2200421.
- [29] O. Maraqa, S. Al-Ahmadi, A. S. Rajasekaran, H. U. Sokun, H. Yanikomeroğlu, and S. M. Sait, “Energy-Efficient Optimization of Multi-User NOMA-Assisted Cooperative THz-SIMO MEC Systems,” *IEEE Trans Commun*, vol. 71, no. 6, pp. 3763–3779, 2023,

References

- doi: 10.1109/TCOMM.2023.3265123.
- [30] Y. Liu, W. Yi, Z. Ding, X. Liu, O. A. Dobre, and N. Al-Dhahir, “Developing NOMA to Next Generation Multiple Access: Future Vision and Research Opportunities,” *IEEE Wirel Commun*, vol. 29, no. 6, pp. 120–127, 2022, doi: 10.1109/MWC.007.2100553.
- [31] X. Mu, Z. Wang, and Y. Liu, “NOMA for Integrating Sensing and Communications towards 6G: A Multiple Access Perspective,” *IEEE Wirel Commun*, vol. PP, pp. 1–8, 2023, doi: 10.1109/MWC.015.2200559.
- [32] A. Al-Dweik, A. Bedoui, and Y. Iraqi, “On the BER Analysis of NOMA Systems,” *IEEE Wirel Commun Lett*, vol. 13, no. 3, pp. 786–790, 2023, doi: 10.1109/LWC.2023.3343813.
- [33] Z. Ding, R. Schober, and H. V. Poor, “NOMA-Assisted Grant-Free Transmission: How to Design Pre-Configured SNR Levels?,” *IEEE Wirel Commun Lett*, vol. 13, no. 2, pp. 412–416, 2024, doi: 10.1109/LWC.2023.3330785.
- [34] Y. Sun and B. Cyr, “Sampling for data freshness optimization: Non-linear age functions,” in *Journal of Communications and Networks*, 2019, vol. 21, no. 3, pp. 204–219, doi: 10.1109/JCN.2019.000035.
- [35] M. Liaqat, K. A. Noordin, T. Abdul Latef, and K. Dimiyati, “Power-domain non orthogonal multiple access (PD-NOMA) in cooperative networks: an overview,” *Wirel Networks*, vol. 26, no. 1, pp. 181–203, 2020, doi: 10.1007/s11276-018-1807-z.
- [36] O. Ozdogan, E. Bjornson, and E. G. Larsson, “Intelligent Reflecting Surfaces: Physics, Propagation, and Pathloss Modeling,” *IEEE Wirel Commun Lett*, vol. 9, no. 5, pp. 581–585, 2020, doi: 10.1109/LWC.2019.2960779.
- [37] A. Krishnamoorthy and R. Schober, “Uplink and Downlink MIMO-NOMA with Simultaneous Triangularization,” *IEEE Trans Wirel Commun*, vol. 20, no. 6, pp. 3381–3396, 2021, doi: 10.1109/TWC.2021.3049594.
- [38] A. Damnjanovic *et al.*, “UE cooperative communications for future cellular networks,” *IEEE Veh Technol Conf*, vol. 2023-June, pp. 1–6, 2023, doi: 10.1109/VTC2023-Spring57618.2023.10199976.
- [39] Y. Yu, Z. Yang, Y. Wu, J. A. Hussein, W. K. Jia, and Z. Dong, “Outage Performance of NOMA in Cooperative Cognitive Radio Networks with SWIPT,” *IEEE Access*, vol. 7, pp. 117308–117317, 2019, doi: 10.1109/ACCESS.2019.2936321.
- [40] N. Sachdeva, V. B. Kumaravelu, P. Selvaprabhu, J. Helen Sheeba, C. S. Evangeline, and A. L. Imoize, “Probability of Error Analysis of Decode-and-Forward Cooperative

References

- Relaying System with Maximal Ratio Combining,” *ViTECoN 2023 - 2nd IEEE Int Conf Vis Towar Emerg Trends Commun Netw Technol Proc*, pp. 1–5, 2023, doi: 10.1109/ViTECoN58111.2023.10157570.
- [41] S. Han, T. Xie, and I. Chih-Lin, “Greener Physical Layer Technologies for 6G Mobile Communications,” *IEEE Commun Mag*, vol. 59, no. 4, pp. 68–74, 2021, doi: 10.1109/MCOM.001.2000484.
- [42] F. R. Ghadi and F. J. Lopez-Martinez, “Performance Analysis of SWIPT Relay Networks over Arbitrary Dependent Fading Channels,” *IEEE Trans Commun*, pp. 1–13, 2024, doi: 10.1109/TCOMM.2024.3359034.
- [43] T. B. Doan and T. H. Nguyen, “Exploiting SWIPT for Coordinated-NOMA Systems under Nakagami-m Fading,” *IEEE Access*, vol. 12, no. February, pp. 19216–19228, 2024, doi: 10.1109/ACCESS.2024.3361319.
- [44] S. Fan, S. Tao, W. Ni, and H. Tian, “Convergence Analysis and Optimization of SWIPT-Based Over-the-Air Federated Learning,” *IEEE Commun Lett*, vol. PP, p. 1, 2024, doi: 10.1109/LCOMM.2024.3371216.
- [45] C. De Alwis *et al.*, “Survey on 6G Frontiers: Trends, Applications, Requirements, Technologies and Future Research,” *IEEE Open J Commun Soc*, vol. 2, pp. 836–886, 2021, doi: 10.1109/OJCOMS.2021.3071496.
- [46] T. S. Rappaport *et al.*, “Wireless communications and applications above 100 GHz: Opportunities and challenges for 6g and beyond,” *IEEE Access*, vol. 7, pp. 78729–78757, 2019, doi: 10.1109/ACCESS.2019.2921522.
- [47] Y. Liu, F. Liu, G. Zhu, X. Wang, and Y. Jiao, “Dynamic power optimization of pilot and data for downlink OFDMA systems,” *J Commun Networks*, vol. 23, no. 4, pp. 250–259, 2021, doi: 10.23919/jcn.2021.000023.
- [48] P. Chatzimisios, D. Soldani, A. Jamalipour, A. Manzalini, and S. K. Das, “Special issue on 6G wireless systems,” *Journal of Communications and Networks*, vol. 22, no. 6, pp. 440–443, 2020, doi: 10.23919/JCN.2020.100039.
- [49] D. Darsena, G. Gelli, and F. Verde, “Design and performance analysis of multiple-relay cooperative MIMO networks,” *J Commun Networks*, vol. 21, no. 1, pp. 25–32, 2019, doi: 10.1109/JCN.2019.0000003.
- [50] I. F. Akyildiz, A. Kak, and S. Nie, “6G and Beyond: The Future of Wireless Communications Systems,” *IEEE Access*, vol. 8, pp. 133995–134030, 2020, doi: 10.1109/ACCESS.2020.3010896.

References

- [51] G. Gür, “Expansive networks: Exploiting spectrum sharing for capacity boost and 6G vision,” *J Commun Networks*, vol. 22, no. 6, pp. 444–454, 2020, doi: 10.23919/JCN.2020.000037.
- [52] H. Elayan, O. Amin, B. Shihada, R. M. Shubair, and M. S. Alouini, “Terahertz band: The last piece of rf spectrum puzzle for communication systems,” *IEEE Open J Commun Soc*, vol. 1, pp. 1–32, 2020, doi: 10.1109/OJCOMS.2019.2953633.
- [53] D. W. K. Ng, T. Q. Duong, C. Zhong, and R. Schober, *Wireless information and power transfer: Theory and practice*. 2018.
- [54] R. Chataut and R. Akl, “Massive MIMO systems for 5G and beyond networks—overview, recent trends, challenges, and future research direction,” *Sensors (Switzerland)*, vol. 20, no. 10. 2020, doi: 10.3390/s20102753.
- [55] Y. Liu *et al.*, “Evolution of NOMA Toward Next Generation Multiple Access (NGMA) for 6G,” *IEEE J Sel Areas Commun*, vol. 40, no. 4, 2022, doi: 10.1109/JSAC.2022.3145234.
- [56] I. F. Akyildiz, A. Kak, and S. Nie, “6G and Beyond: The Future of Wireless Communications Systems,” *IEEE Access*, vol. 8, 2020, doi: 10.1109/ACCESS.2020.3010896.
- [57] H. W. Oleiwi, H. L. Al-Taie, N. Saeed, and D. N. Mhawi, “A Comparative Investigation on Different QoS Mechanisms in Multi-Homed Networks,” *Iraqi J Ind Res*, vol. 9, no. 1, pp. 1–11, 2022, doi: 10.53523/ijoirvol9i1id141.
- [58] H. Oleiwi, N. Saeed, H. Al-Taie, and D. Mhawi, “An Enhanced Interface Selectivity Technique to Improve the QoS for the Multi-homed Node,” *Eng Technol J*, vol. 40, no. 8, pp. 101–109, 2022, doi: 10.30684/etj.2022.133066.1165.
- [59] H. Sareddeen, M. S. Alouini, and T. Y. Al-Naffouri, “An Overview of Signal Processing Techniques for Terahertz Communications,” *Proceedings of the IEEE*, vol. 109, no. 10. pp. 1628–1665, 2021, doi: 10.1109/JPROC.2021.3100811.
- [60] I. Sim *et al.*, “Deep learning based successive interference cancellation scheme in nonorthogonal multiple access downlink network,” *Energies*, vol. 13, no. 23, 2020, doi: 10.3390/en13236237.
- [61] O. Maraqa, A. S. Rajasekaran, S. Al-Ahmadi, H. Yanikomeroglu, and S. M. Sait, “A Survey of Rate-Optimal Power Domain NOMA with Enabling Technologies of Future Wireless Networks,” *IEEE Commun Surv Tutor*, vol. 22, no. 4, pp. 2192–2235, 2020, doi: 10.1109/COMST.2020.3013514.

References

- [62] F. Tanaka, H. Suganuma, and F. Maehara, “Hybrid Multiple Access Scheme Using NOMA and OMA Simultaneously Considering User Request,” *Int Symp Wirel Pers Multimed Commun WPMC*, vol. 2021-Decem, pp. 19–20, 2021, doi: 10.1109/WPMC52694.2021.9700453.
- [63] Y. Liu and M. ElKashlan, “On the application of SWIPT in NOMA networks,” in *Wireless Information and Power Transfer: Theory and Practice*, 2018.
- [64] H. W. Oleiwi and H. Al-Raweshidy, “Cooperative Hybrid-NOMA / Dynamic SWIPT - Pairing Mechanism for 6G THz Communications,” *Proc - 2023 IEEE 5th Glob Power, Energy Commun Conf GPECOM 2023*, pp. 524–529, 2023, doi: 10.1109/GPECOM58364.2023.10175775.
- [65] T. N. Do and B. An, “Optimal sum-throughput analysis for downlink cooperative SWIPT NOMA systems,” in *Proceedings - 2018 2nd International Conference on Recent Advances in Signal Processing, Telecommunications and Computing, SIGTELCOM 2018*, 2018, vol. 2018-January, doi: 10.1109/SIGTELCOM.2018.8325811.
- [66] H. W. Oleiwi and H. Al-Raweshidy, “Cooperative SWIPT THz-NOMA/6G Performance Analysis,” *Electron*, vol. 11, no. 6, 2022, doi: 10.3390/electronics11060873.
- [67] H. W. Oleiwi, N. Saeed, and H. Al-Raweshidy, “Cooperative SWIPT MIMO-NOMA for Reliable THz 6G Communications,” *Network*, vol. 2, no. 2, pp. 257–269, 2022, doi: 10.3390/network2020017.
- [68] H. W. Oleiwi, N. Saeed, and H. S. Al-Raweshidy, “A Cooperative SWIPT-Hybrid-NOMA Pairing Scheme considering SIC imperfection for THz Communications,” *Proc - 2022 IEEE 4th Glob Power, Energy Commun Conf GPECOM 2022*, no. June, pp. 638–643, 2022, doi: 10.1109/GPECOM55404.2022.9815677.
- [69] E. Bjornson, O. Ozdogan, and E. G. Larsson, “Intelligent Reflecting Surface Versus Decode-and-Forward: How Large Surfaces are Needed to Beat Relaying?,” *IEEE Wirel Commun Lett*, vol. 9, no. 2, pp. 244–248, 2020, doi: 10.1109/LWC.2019.2950624.
- [70] H. W. Oleiwi and H. Al-Raweshidy, “SWIPT-Pairing Mechanism for Channel-Aware Cooperative H-NOMA in 6G Terahertz Communications,” *Sensors*, vol. 22, no. 16, p. 6200, 2022, doi: 10.3390/s22166200.
- [71] U. Mutlu and Y. Kabalci, “Deep Learning Aided Channel Estimation Approach for 5G Communication Systems,” *Proc - 2022 IEEE 4th Glob Power, Energy Commun Conf*

References

- GPECOM* 2022, no. DI, pp. 655–660, 2022, doi: 10.1109/GPECOM55404.2022.9815811.
- [72] B. Ozpoyraz, A. T. Dogukan, Y. Gevez, U. Altun, and E. Basar, “Deep Learning-Aided 6G Wireless Networks: A Comprehensive Survey of Revolutionary PHY Architectures,” *IEEE Open J Commun Soc*, vol. 3, pp. 1749–1809, 2022, doi: 10.1109/OJCOMS.2022.3210648.
- [73] H. W. Oleiwi, N. Saeed, H. L. Al-taie, and D. N. Mhawi, “Evaluation of Differentiated Services Policies in Multihomed Networks Based on an Interface-Selection Mechanism,” *Sustainability*, vol. 14, no. 20, pp. 1–12, 2022, doi: 10.3390/su142013235.
- [74] H. W. Oleiwi, D. N. Mhawi, and H. Al-Raweshidy, “MLTs-ADCNs: Machine Learning Techniques for Anomaly Detection in Communication Networks,” *IEEE Access*, vol. 10, no. August, pp. 91006–91017, 2022, doi: 10.1109/ACCESS.2022.3201869.
- [75] D. N. Mhawi, H. W. Oleiwi, N. H. Saeed, and H. L. Al-Taie, “An Efficient Information Retrieval System Using Evolutionary Algorithms,” *Network*, vol. 2, no. 4, pp. 583–605, 2022, doi: 10.3390/network2040034.
- [76] H. W. Oleiwi, D. N. Mhawi, and H. Al-Raweshidy, “A Meta-Model to Predict and Detect Malicious Activities in 6G-Structured Wireless Communication Networks,” *Electron*, vol. 12, no. 3, 2023, doi: 10.3390/electronics12030643.
- [77] D. Liu *et al.*, “Jacobian norm with Selective Input Gradient Regularization for interpretable adversarial defense,” *Pattern Recognit*, vol. 145, 2024, doi: 10.1016/j.patcog.2023.109902.
- [78] Y. Xu, D. Li, Q. Li, and S. Xu, “Malware Evasion Attacks Against IoT and Other Devices: An Empirical Study,” *Tsinghua Sci Technol*, vol. 29, no. 1, 2024, doi: 10.26599/TST.2023.9010005.
- [79] Y. Qu, S. Huang, X. Chen, X. Wang, and Y. Yao, “Detection of backdoor attacks using targeted universal adversarial perturbations for deep neural networks,” *J Syst Softw*, vol. 207, 2024, doi: 10.1016/j.jss.2023.111859.
- [80] X. Sun, J. Dai, P. Liu, A. Singhal, and J. Yen, “Using Bayesian Networks for Probabilistic Identification of Zero-Day Attack Paths,” *IEEE Trans Inf Forensics Secur*, vol. 13, no. 10, pp. 2506–2521, 2018, doi: 10.1109/TIFS.2018.2821095.
- [81] M. Alazab, “Profiling and classifying the behavior of malicious codes,” *J Syst Softw*, vol. 100, pp. 91–102, 2015, doi: 10.1016/j.jss.2014.10.031.
- [82] I. Sumaiya Thaseen and C. Aswani Kumar, “Intrusion detection model using fusion of

References

- chi-square feature selection and multi class SVM,” *J King Saud Univ - Comput Inf Sci*, vol. 29, no. 4, pp. 462–472, 2017, doi: 10.1016/j.jksuci.2015.12.004.
- [83] W. Liang, L. Xiao, K. Zhang, M. Tang, D. He, and K. C. Li, “Data Fusion Approach for Collaborative Anomaly Intrusion Detection in Blockchain-based Systems,” *IEEE Internet Things J*, 2021, doi: 10.1109/JIOT.2021.3053842.
- [84] M. Shafiq, Z. Tian, A. K. Bashir, X. Du, and M. Guizani, “CorrAUC: A Malicious Bot-IoT Traffic Detection Method in IoT Network Using Machine-Learning Techniques,” *IEEE Internet Things J*, vol. 8, no. 5, pp. 3242–3254, 2021, doi: 10.1109/JIOT.2020.3002255.
- [85] M. A. Khan and J. Kim, “Toward developing efficient Conv-AE-based intrusion detection system using heterogeneous dataset,” *Electron*, vol. 9, no. 11, pp. 1–17, 2020, doi: 10.3390/electronics9111771.
- [86] M. Safaldin, M. Otair, and L. Abualigah, “Improved binary gray wolf optimizer and SVM for intrusion detection system in wireless sensor networks,” *J Ambient Intell Humaniz Comput*, vol. 12, no. 2, pp. 1559–1576, 2021, doi: 10.1007/s12652-020-02228-z.
- [87] A. R. Javed, S. U. Rehman, M. U. Khan, M. Alazab, and T. G. Reddy, “CANintelliIDS: Detecting In-Vehicle Intrusion Attacks on a Controller Area Network Using CNN and Attention-Based GRU,” *IEEE Trans Netw Sci Eng*, vol. 8, no. 2, pp. 1456–1466, 2021, doi: 10.1109/TNSE.2021.3059881.
- [88] D. N. Mhawi and S. H. Hashim, “Proposed Hybrid Ensemble Learning algorithms for an Efficient Intrusion Detection System,” *IJCCE*, vol. 22, no. 2, pp. 73–84, 2022.
- [89] A. Swaroopa, M. Brendha, A. S. P, V. Singh, and S. M. Belgaonkar, “Analysis of Channel Estimation Techniques for MIMO Wireless Channel Models,” *2023 10th Int Conf Electr Eng Comput Sci Informatics*, no. September, pp. 439–445, 2023, doi: 10.1109/EECSI59885.2023.10295603.
- [90] D. N. Mhawi and S. H. Hashem, “Proposed Hybrid Correlation Feature Selection Forest Panalized Attribute Approach to advance IDSs,” *Karbala Int J Mod Sci*, vol. 7, no. 4, pp. 405–420, 2021, doi: 10.33640/2405-609X.3166.
- [91] G. Gui, M. Liu, F. Tang, N. Kato, and F. Adachi, “6G : Opening New Horizons for Integration of Comfort , Security , and Intelligence,” *IEEE Wirel Commun*, vol. 27, no. 5, pp. 126–132, 2020.
- [92] Q. Hu, F. Gao, H. Zhang, S. Jin, and G. Y. Li, “Deep Learning for Channel Estimation:

References

- Interpretation, Performance, and Comparison,” *IEEE Trans Wirel Commun*, vol. 20, no. 4, pp. 2398–2412, 2021, doi: 10.1109/TWC.2020.3042074.
- [93] D. N. Mhawi, A. Aldallal, and S. Hassan, “Advanced Feature-Selection-Based Hybrid Ensemble Learning Algorithms for Network Intrusion Detection Systems,” *Symmetry (Basel)*, vol. 14, no. 7, p. 1461, 2022, doi: 10.3390/sym14071461.
- [94] H. Zhang, H. Zhang, W. Liu, K. Long, J. Dong, and V. C. M. Leung, “Energy Efficient User Clustering, Hybrid Precoding and Power Optimization in Terahertz MIMO-NOMA Systems,” in *IEEE Journal on Selected Areas in Communications*, 2020, vol. 38, no. 9, pp. 2074–2085, doi: 10.1109/JSAC.2020.3000888.
- [95] M. Saad, N. Al Akkad, H. Hijazi, A. C. Al Ghouwayel, F. Bader, and J. Palicot, “Novel MIMO technique for wireless terabits systems in Sub-THz Band,” *IEEE Open J Veh Technol*, vol. 2, pp. 125–139, 2021, doi: 10.1109/OJVT.2021.3054737.
- [96] O. Elkarbotly, E. Maher, A. El-Mahdy, and F. Dressler, “Optimal power allocation in cooperative MIMO-NOMA with FD/HD relaying in THz communications,” 2020, doi: 10.23919/PEMWN50727.2020.9293074.
- [97] A. W. Nazar, S. A. Hassan, H. Jung, A. Mahmood, and M. Gidlund, “BER Analysis of a Backscatter Communication System with Non-Orthogonal Multiple Access,” *IEEE Trans Green Commun Netw*, vol. 5, no. 2, 2021, doi: 10.1109/TGCN.2021.3068105.
- [98] W. U. Khan, X. Li, M. Zeng, and O. A. Dobre, “Backscatter-Enabled NOMA for Future 6G Systems: A New Optimization Framework under Imperfect SIC,” *IEEE Commun Lett*, vol. 25, no. 5, 2021, doi: 10.1109/LCOMM.2021.3052936.
- [99] W. U. Khan, M. A. Javed, T. N. Nguyen, S. Khan, and B. M. Elhalawany, “Energy-Efficient Resource Allocation for 6G Backscatter-Enabled NOMA IoV Networks,” *IEEE Trans Intell Transp Syst*, vol. 23, no. 7, 2022, doi: 10.1109/TITS.2021.3110942.
- [100] M. Ahmed, W. U. Khan, A. Ihsan, X. Li, J. Li, and T. A. Tsiftsis, “Backscatter Sensors Communication for 6G Low-Powered NOMA-Enabled IoT Networks Under Imperfect SIC,” *IEEE Syst J*, vol. 16, no. 4, 2022, doi: 10.1109/JSYST.2022.3194705.
- [101] W. U. Khan *et al.*, “Integration of Backscatter Communication with Multi-cell NOMA: A Spectral Efficiency Optimization under Imperfect SIC,” in *IEEE International Workshop on Computer Aided Modeling and Design of Communication Links and Networks, CAMAD*, 2022, vol. 2022-November, doi: 10.1109/CAMAD55695.2022.9966913.
- [102] K. B. Letaief, W. Chen, Y. Shi, J. Zhang, and Y. J. A. Zhang, “The Roadmap to 6G: AI

References

- Empowered Wireless Networks,” *IEEE Commun Mag*, vol. 57, no. 8, pp. 84–90, 2019, doi: 10.1109/MCOM.2019.1900271.
- [103] Y. Jin, J. Zhang, S. Jin, and B. Ai, “Channel Estimation for Cell-Free mmWave Massive MIMO through Deep Learning,” *IEEE Trans Veh Technol*, vol. 68, no. 10, 2019, doi: 10.1109/TVT.2019.2937543.
- [104] Y. Jin, J. Zhang, B. Ai, and X. Zhang, “Channel Estimation for mmWave Massive MIMO with Convolutional Blind Denoising Network,” *IEEE Commun Lett*, vol. 24, no. 1, 2020, doi: 10.1109/LCOMM.2019.2952845.
- [105] M. Kuzlu, C. Fair, and O. Guler, “Role of Artificial Intelligence in the Internet of Things (IoT) cybersecurity,” *Discov Internet Things*, vol. 1, no. 1, 2021, doi: 10.1007/s43926-020-00001-4.
- [106] P. Porambage, G. Gur, D. P. Moya Osorio, M. Livanage, and M. Ylianttila, “6G security challenges and potential solutions,” 2021, doi: 10.1109/EuCNC/6GSummit51104.2021.9482609.
- [107] Y. Siriwardhana, P. Porambage, M. Liyanage, and M. Ylianttila, “AI and 6G security: Opportunities and challenges,” 2021, doi: 10.1109/EuCNC/6GSummit51104.2021.9482503.
- [108] G. Li, K. Ota, M. Dong, J. Wu, and J. Li, “DeSVig: Decentralized Swift Vigilance against Adversarial Attacks in Industrial Artificial Intelligence Systems,” *IEEE Trans Ind Informatics*, vol. 16, no. 5, pp. 3267–3277, 2020, doi: 10.1109/TII.2019.2951766.
- [109] I. C. Society, *IEEE Standard for High Data Rate Wireless Multi-Media Networks Amendment 3: Extending the Physical Layer (PHY) Specification for Millimeter Wave to Operate from 57.0 GHz to 71 GHz*, vol. 2017. 2018.
- [110] V. Petrov, T. Kurner, and I. Hosako, “IEEE 802.15.3d: First Standardization Efforts for Sub-Terahertz Band Communications toward 6G,” *IEEE Commun Mag*, vol. 58, no. 11, pp. 28–33, 2020, doi: 10.1109/MCOM.001.2000273.
- [111] IEEE, *IEEE Standard for High Data Rate Wireless Multi-Media Networks--Amendment 2: 100 Gb/s Wireless Switched Point-to-Point Physical Layer*, vol. 2017. 2017.
- [112] Z. Ding, P. Fan, and H. V. Poor, “Impact of User Pairing on 5G Nonorthogonal Multiple-Access Downlink Transmissions,” *IEEE Trans Veh Technol*, vol. 65, no. 8, 2016, doi: 10.1109/TVT.2015.2480766.